THESIS

DEVELOPING A METHOD TO SAMPLE POTENTIAL RESUSPENSION OF RADIOACTIVE CONTAMINANTS NEAR THE FORMER ROCKY FLATS TECHNICAL PLANT

Submitted by

Richard V. Alcantar

Department of Environmental and Radiological Health Sciences

In partial fulfillment of the requirements

For the Degree of Master of Science

Colorado State University

Fort Collins, Colorado

Summer 2024

Master's Committee:

Advisor: Ralf Sudowe

Tom Johnson
John Volckens

ABSTRACT

DEVELOPING METHODS TO SAMPLE POTENTIAL RESUSPENSION OF RADIOACTIVE CONTAMINANTS NEAR THE FORMER ROCKY FLATS TECHNICAL PLANT

From 1952 until 1989, the Rocky Flats Technical Plant processed plutonium for use as triggers in nuclear weapons. Throughout the facility's nearly 37 years in operation, several events led to radioactive contamination in areas within and surrounding the site. Since then, multiple cleanup projects have occurred, remediating contamination to acceptable levels. However, an increase in the number, size, and severity of Colorado wildfires in recent years has raised public concern for the potential resuspension of radioactive surface contamination to the now-populous areas surrounding Rocky Flats. Air sampling during specific conditions such as high winds, naturally occurring wildfires, and controlled burns would provide valuable data to determine if resuspension of radioactive contamination may be of concern. Sampling under such circumstances, however, is restricted by situation, permission, and weather. Whereas traditional aerosol sampling collects “total dust” samples to amass particles in the air with equal efficiency, without regard to particle size fraction, the use of a cascade impactor to separate aerosols by size can be utilized to relate how deep varied-sized particles might penetrate the human respiratory tract after inhalation. This would not only indicate the presence of radionuclides but also the deposition location within the human body, an important factor in determining the best dose estimate for the person. This study will compare the efficacy of a 3D-printed cascade impactor in separating particle size fractions to the capability of a commercial Andersen cascade impactor. Methods used in this thesis included radiological analysis with a Mirion LB4200 gas proportional counter. Significant

imperfections of a printed prototype indicate that a stage-to-stage comparison between a commercial and a 3D-printed cascade impactor cannot be justified. Additionally, it is unlikely that current technology is capable of printing the exact same impactor with each subsequent print. The determination of a similar decay curve between stages of both impactors in some instances as well as similar trends in activity fraction by filter, however, indicate that a functional 3D-printed cascade impactor is feasible. Individually, each printed cascade impactor would require proper characterization to determine the particle size fraction that each stage captures. The evidence outlined in this study suggests that a functional cascade impactor can be fabricated by 3D printing. Still, additional studies would be necessary to characterize particle size distribution properly.

ACKNOWLEDGEMENTS

First and foremost, I'd like to express my gratitude to my professors in the Department of Radiological Health Sciences: Dr. Tom "TJ" Johnson, Dr. Alex Brandl, and my thesis advisor, Dr. Ralf Sudowe. You have all challenged me and given me a genuine example of what it is to be a mentor.

The time I committed to doing my research proved to be among the most challenging and rewarding at CSU. A special thanks to Dr. John Volckens and Amber Prebble. Your altruism was consistently the highlight of those days. Without it and your technical expertise, I would never have gotten as far as I did in my research. Thank you.

To my colleagues at CSU, as with any "tour of duty" bonds are forged through the many challenges faced together. I am grateful for the experiences shared and the professional and personal growth we have gained together. I look forward to the contributions I am sure you will make to our field.

To my wife, Michele, I would have never achieved a million things in this life if not for you. You have loved and supported me across thousands of miles and through an eternity of months apart. My education brought me back, but it made me no less absent. I look forward to giving you the world that I one day promised you. I love you forever.

To the Sailors I have served across six commands, if not for your dedication and excellence I would never have reached this point in my career. Thank you for being my purpose.

To the United States Navy for funding this endeavor. Never in my wildest dreams did I think that a start in Navy Nuclear Power would get me here. Finally, to the RHO community, thank you for believing in me.

DEDICATION

For my wife, Michele, you have been my rock through every challenge I have ever faced. With you, anything is possible. I love you forever.

LABOR OMNIA VINCIT.

TABLE OF CONTENTS

DISCLAIMER

THE VIEWS EXPRESSED ARE THOSE OF THE AUTHOR AND DO NOT REFLECT THE OFFICIAL POLICY OR POSITION OF THE UNITED STATES NAVY, DEPARTMENT OF DEFENSE, OR THE US GOVERNMENT.

CHAPTER 1: INTRODUCTION

History of Rocky Flats

Historical Prelude

On August 6th, 1945, Paul Tibbets, a United States Air Force pilot, flew the B-29 bomber *Enola Gay*, named for his mother, 1,900 feet above the city of Hiroshima, Japan. As the crew of the *Enola Gay* approached their target, the first of two atomic bombs used on Japan was released. Nicknamed *Little Boy*, this nuclear bomb exploded with a force of nearly 12,500 tons of TNT at 8:16:02 Hiroshima time, less than a minute after being deployed from the *Enola Gay*. A first-hand account from a fourth-grade boy was later documented (Rhodes, 1968):

> "When I opened my eyes after being blown at least eight yards, it was as dark as though I had come up against a black-painted fence. After that, as if thin paper was being peeled off one piece at a time, it gradually began to grow brighter. The first thing that my eyes lighted upon then was the flat stretch of land with only dust clouds rising from it. Everything had crumbled away in that one moment, and changed into streets of rubble, street after street of ruins."

Three days later, on August 9th, the second atomic bomb, *Fat Man,* was dropped on the Japanese city of Nagasaki. Within a few days, Japan surrendered, ending World War II. In a speech to the people of Japan, Emperor Hirohito referred to "a new and most cruel bomb" as a reason for their surrender under the terms of the Allied Forces (Reed, 2014). If not for the success of the United States (U.S.) Nuclear Program, the atomic bomb would never have been developed, and an Allied victory may not have occurred; it all began with the Manhattan Project.

The Manhattan Project

The U.S. Army-led Manhattan Project was the most complex and costly research and development project of its time (ibid.). Although World War II had ended, the threat of other world powers possessing nuclear weapons was highly concerning. News that the Soviet Union was developing its own atomic bombs further strained relations between the U.S. and the Union of Soviet Socialist Republics (USSR). The arms race to build a nuclear arsenal had begun, and with it, the development of the Cold War (Department of Energy – Office of Legacy Management, 2020).

The National Security Enterprise

The development of the U.S. nuclear weapons complex began in 1942 with the creation of the Manhattan Project, the top-secret mission to build an atomic bomb before Germany. Interrelated and independent facilities were constructed to develop, manufacture, and maintain the country's nuclear arsenal. Three facilities were initially constructed to support this mission: component and subassembly production at Oak Ridge Reservation, Tennessee in September 1942; the Hanford Site in 1943; and laboratories for weapons design and research at Los Alamos National Laboratory (LANL) in 1943. As the Cold War dragged on, additional facilities were warranted. By the 1990s, the complex eventually expanded to include thirteen facilities with various supporting operations as shown in Figure 1.1; one of which was the Rocky Flats Technical Plant. The complex as a whole was initially run by the military during World War II, with ownership transferring to several entities over the years: the Atomic Energy Commission (AEC) in 1947, the Energy Research and Development Administration (ERDA) in 1975, and finally the Department of Energy (DOE) in 1977 (National Park Service, 1998). Within the DOE, the semi-autonomous agency National Nuclear Security Administration (NNSA) is currently responsible for ensuring the U.S.

nuclear weapons stockpile remains safe, secure, effective, and able to meet mission requirements when necessary. Additional agency functions include detecting and preventing the proliferation of weapons of mass destruction (WMDs), securing radiological materials, providing the U.S. Navy with fuel for nuclear plant operation, and providing the nation with nuclear counterterrorism and emergency response capabilities. The Nuclear Security Enterprise, previously the nuclear weapons complex, has since consolidated into eight facilities, as shown in Figure 1.2 (Office of the Deputy Assistant Secretary of Defense for Nuclear Matters, 2020).

Fig 1.1: Nuclear Weapons Complex**.** Reproduced from Historic American Engineering Record, National Park Service, Rocky Flats Plant, sheet 2 of 17, 1998.

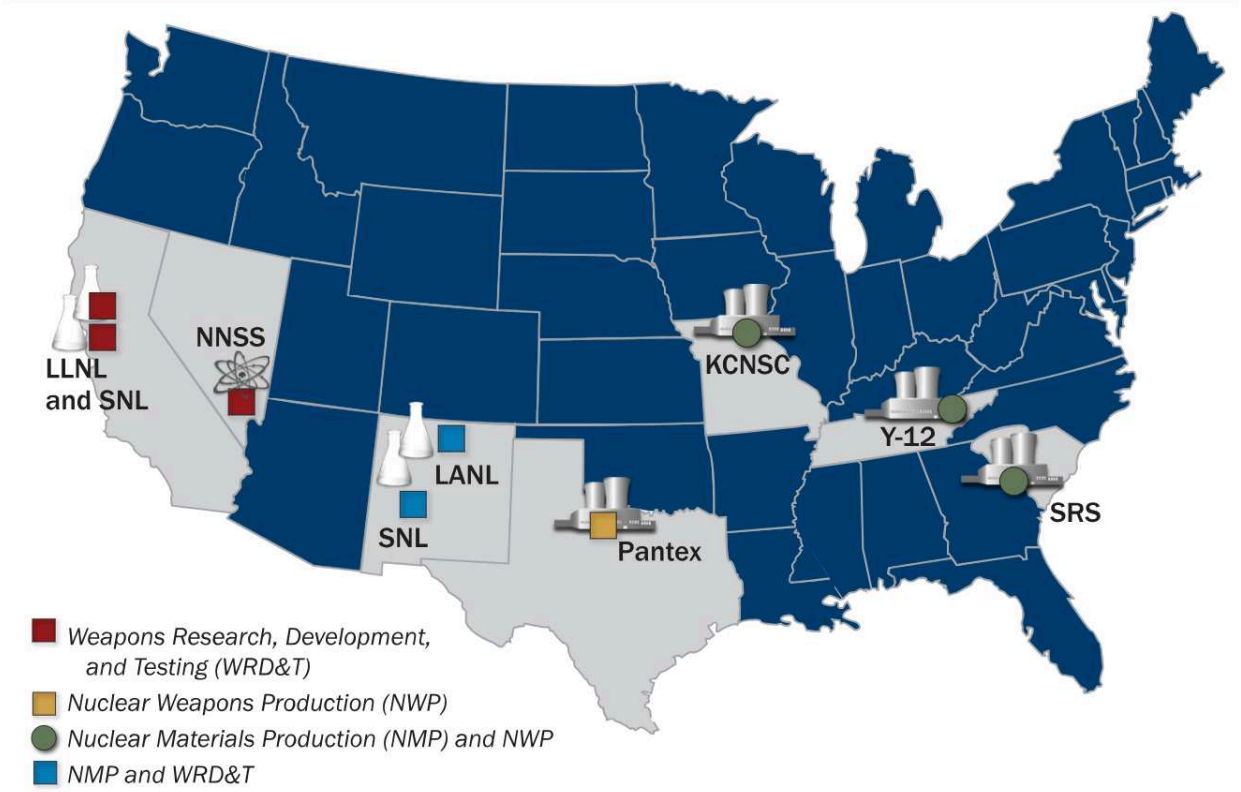

- **National Security Laboratories:** Los Alamos National Laboratory (LANL) in Los Alamos, New Mexico; Lawrence Livermore National Laboratory (LLNL) in Livermore, California; and Sandia National Laboratories (SNL) in both Albuquerque, New Mexico, and Livermore, California.
- **Manufacturing Sites:** Kansas City National Security Campus (KCNSC) in Kansas City, Missouri; Pantex Plant in Amarillo, Texas; Savannah River Site (SRS) in Aiken, South Carolina; and Y-12 National Security Complex in Oak Ridge, Tennessee.
- **Test Site:** Nevada National Security Site (NNSS) in Nye County, Nevada.

Fig 1.2: National Security Enterprise. Reproduced from Office of the Deputy Assistant Secretary of Defense for Nuclear Matters, *Nuclear Matters Handbook*, Chapter 5, 2020.

Rocky Flats Overview

The former Rocky Flats Technical Plant (RFTP) was a 6,500-acre site located in Jefferson County, Colorado. Situated a few kilometers (km) from the Colorado cities of Arvada, Westminster, Broomfield, and 26 km northwest of downtown Denver, the site served as a research, development, and production facility for the nuclear weapons complex from 1952 until 1989

(Colorado Department of Public Health and Environment (CDPHE), Radiological Assessments Corporation, 1999). During this timeframe, the primary mission of the RFTP was to process and machine plutonium, uranium, beryllium, stainless steel, and other materials into detonators or "triggers." Each trigger contained a large portion of the fissile material used in a nuclear weapon and could be used to initiate the self-sustaining fission reaction of an atomic bomb (Department of Energy – Office of Legacy Management, 2020). Throughout its history, the RFTP had a number of weapons programs going on at any given time. These included developing and producing nuclear weapons components from plutonium, beryllium, stainless steel, and depleted uranium; recovery and reprocessing of plutonium from retired weapons and by-product residues from manufacturing and recovery operations; fulfilling DOE and Department of Defense (DOD) new deployment and testing requirements such as for Nevada Test Site triggers and non-nuclear hardware; conducting in-house technology and process development; providing weapons trainers and mockups; disassembly and evaluation of triggers from stockpiles; providing reliability evaluation programs; and fabricating and modifying tractors, rail cars, and trailers for safe and secure transport of nuclear materials and weapons (National Park Service, 1998).

Throughout RFTP's nearly 37 years in operation, the facility had some significant problems. Several events led to the radioactive contamination of areas within and surrounding the site. Specifically, there were two incidents of fires igniting in gloveboxes of plutonium processing facilities and, most notably, leaking waste oil drums at the 903 Area. Due to a high regard for national security, early operations at the RFTP were shrouded in secrecy. Although the first fire and subsequent spread of contamination occurred in 1957, it wasn't until the fire of 1969 that the public became generally aware that radioactive contamination had been released (CDPHE - Historical Public Exposure Studies on Rocky Flats, 2023).

Summary of the September 1957 Fire

At approximately 10:10 p.m. on September 11, 1957, a burning smell emitting from the plutonium processing building, Building 71, led security personnel to discover the fire. The 1957 fire is suspected to have been caused by the spontaneous ignition of alpha-plutonium turnings or skulls (metallic casting residues). This fire would burn for approximately thirteen hours before responders extinguished the flames at 11:28 a.m. on September 12th. Building 71, also called "C Plant" at the time, was later renamed Building 771 and is shown in Figure 1.3. Monitoring surveys were conducted in and around the complex during and following the fire. While only "possible plutonium contamination" on and off site was initially reported, studies eventually concluded that approximately 160 - 510 grams of plutonium was released, equating to 11 - 36 curies (Ci) of activity. There were no serious injuries or deaths that resulted directly from the fire, and the plant's director of health physics reported trace amounts of plutonium in 88 nose and throat swipes. Subsequent tests of personnel found plutonium in one urinalysis, three fecal, and two blood samples. Throughout this thesis, plutonium concerns commonly refer to specific isotopes of plutonium, such as $^{238, 239, 240}$Pu. Plutonium, however, can form compounds with various elements, including plutonium oxide (PuO_2). Although the oxides of plutonium are not expressly stated as the specific source of internal contamination from the 1957 fire, plutonium and its compounds, including PuO_2, can spread throughout the body depending on the mode of intake, inhalation or ingestion (Cochran, 1996). Inhalation would constitute the greater hazard, and Figure 1.4 is included to show possible deposition within the human respiratory tract (Rademacher et al., 2007).

Cleanup costs were estimated at $818,600. Lessons learned included using non-combustible air filters in glovebox ventilation systems and increased provisions for automatic fire detection and controls in AEC facilities. The AEC would later be split into the ERDA and the

Nuclear Regulatory Commission (NRC) by the Energy Reorganization Act in 1974 (DOE Office of Environment, Health, Safety, and Security). The ERDA would eventually dissolve into the DOE by order of the Department of Energy Organization Act in August of 1977 (National Archives, 2023).

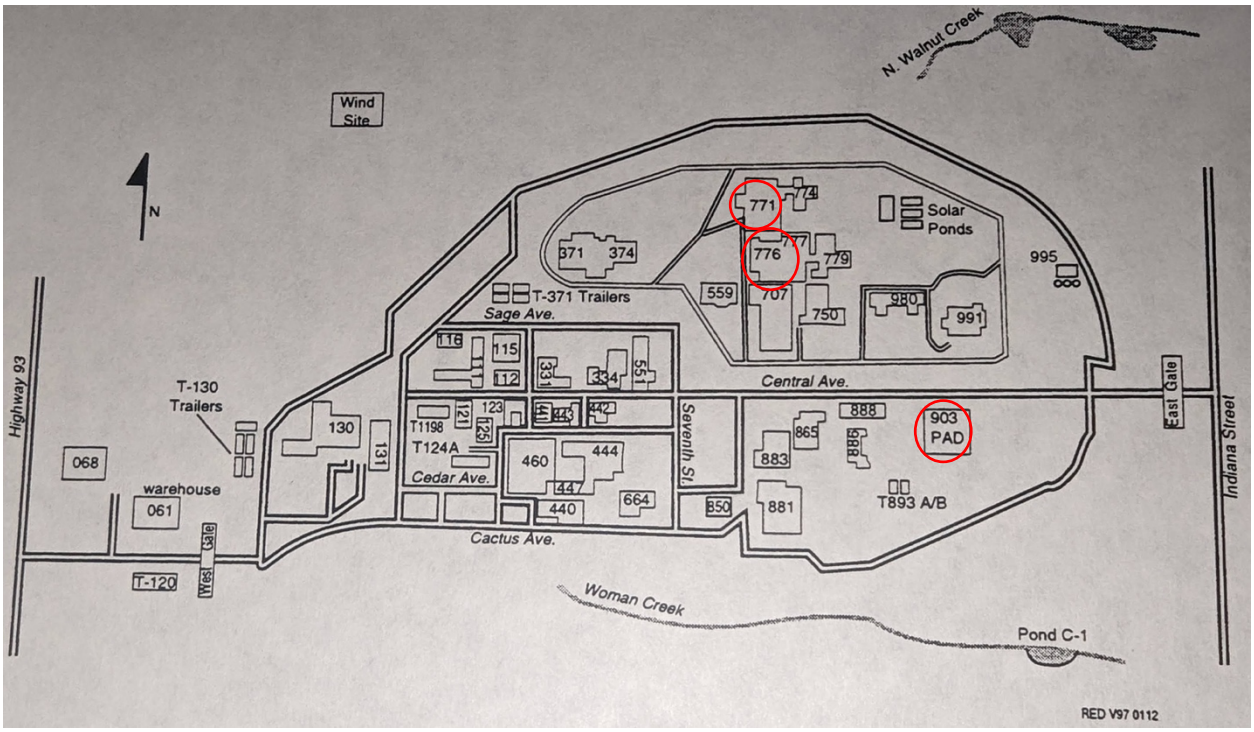

Fig 1.3: Original main production area of RFTP. After the fact, red circles were added to highlight sites of interest to this thesis. Map reproduced from Development of the Rocky Flats Plant 903 Area Plutonium Source Term—Final Report, August 1999.

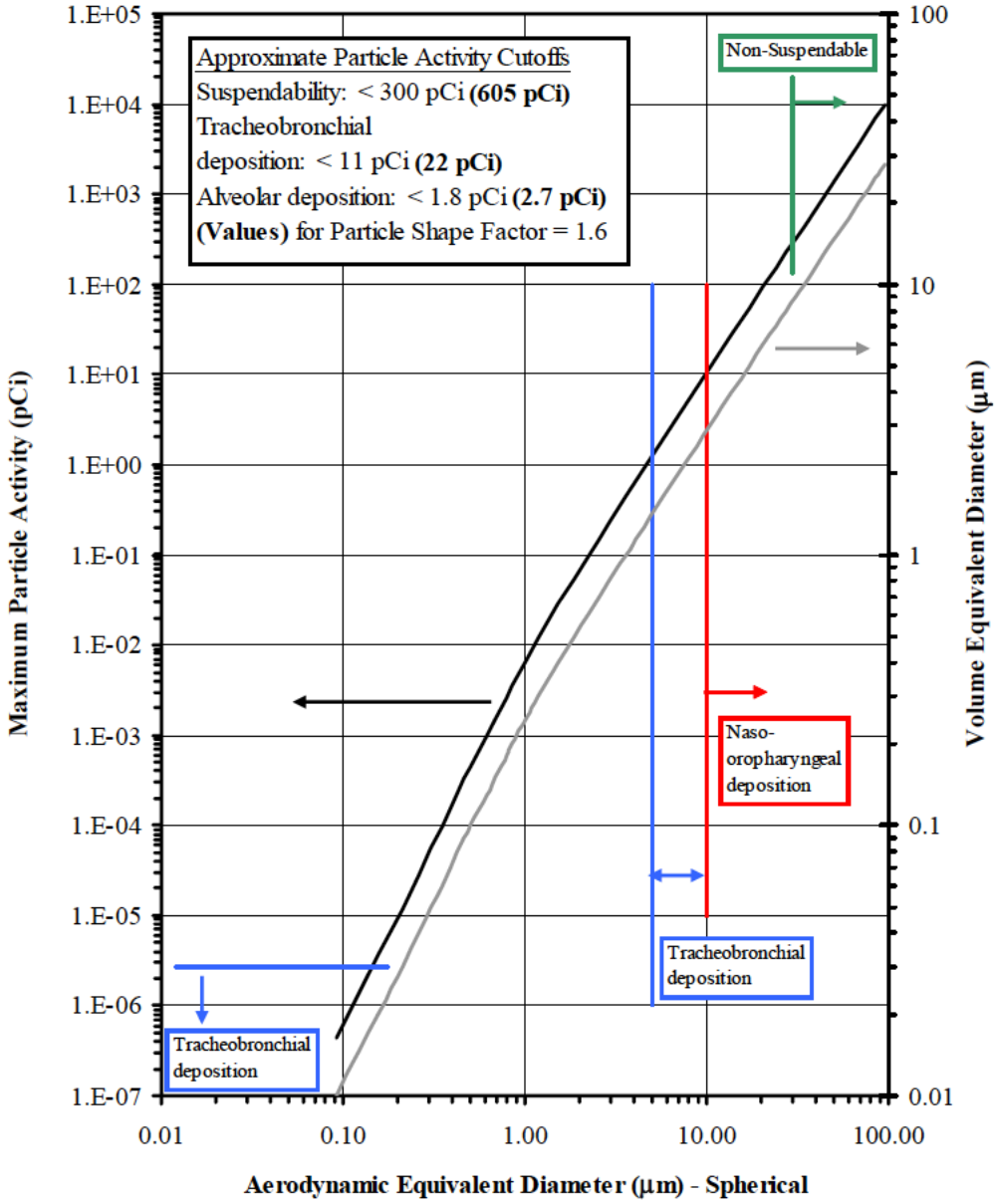

Fig 1.4: Maximum particle activities and volume equivalent diameters for aerodynamic equivalent diameter (spherical) of PuO_2 particles. The black line relates $^{239+240}Pu$ activity to the aerodynamic equivalent diameter, while the gray line relates volume and aerodynamic equivalent diameters. Reproduced from Boeing Michigan Aeronautical Research Center Missile Shelters and Bunkers Scoping Survey Workplan. Rademacher, S. E., Hubbell, J. L., and Cicotte, G.R. 2007.

Summary of the 1969 Fire

At approximately 2 p.m. on 11 May 1969, plutonium within a glovebox in Building 776 began to smolder due to spontaneous combustion. The generated heat caused the plastic storage

chest to catch fire, spreading quickly and burning other flammable materials nearby. The fire was then drawn into the glovebox ventilation system, causing large portions of the building to be affected by the fire. The fire was contained by 6:40 p.m. and fully extinguished by 8 p.m. on the same day. Lessons incorporated following the 1957 fire, such as not using highly flammable High-Efficiency Particulate Air (HEPA) filters in the glovebox ventilation system, contributed to minimal spread of contamination relative to the 1957 fire. It was estimated that between 0.14 and 0.9 grams (or 10 and 60 mCi) of plutonium was released into the atmosphere during this incident. Computer modeling later calculated the assessment of aerosolized plutonium concentrations on- and off-site. Personnel contamination records were not included in this report and were not further investigated (CDPHE - Rocky Flats Historical Public Exposure Studies, 2023).

Computer modeling was necessary since there are periods in the RFTP operational history when useful measurements of $^{239,\ 240}$Pu in air were not available. Actual on- and off-site measurements are always preferred because modeling tends to produce high levels of uncertainty in results due to spatial and temporal averages of meteorological data used. However, available monitoring data and computer models were able to estimate concentrations of $^{239,\ 240}$Pu in air on-site and at site perimeter locations. Model-predicted concentrations represent an average of the 27 computational nodes shown in Figure 1.5. Results of plutonium concentrations in air as a function of time are shown in Figure 1.6. Although not discussed in the subchapter above, Figure 1.6 also shows computational estimates of $^{239,\ 240}$Pu concentrations in air following the 1957 fire (ORAU Team NIOSH, 2004).

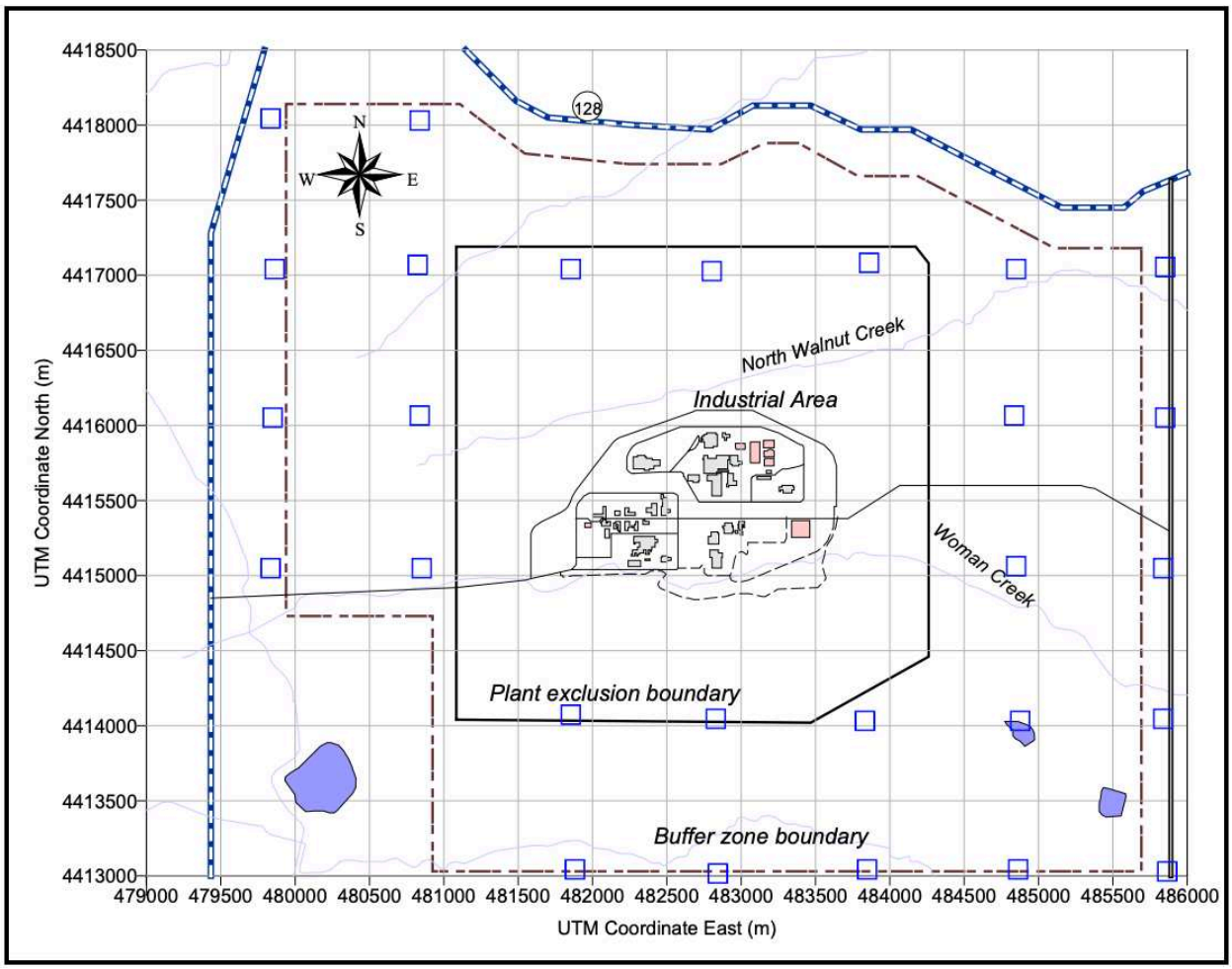

Fig 1.5: Locations of computational nodes (blue squares) used to compute annual average perimeter concentrations. Reproduced, with permission, from ORAU Team NIOSH Dose Reconstruction Project, document number: ORAUT-TKBS-0011-4, 2004.

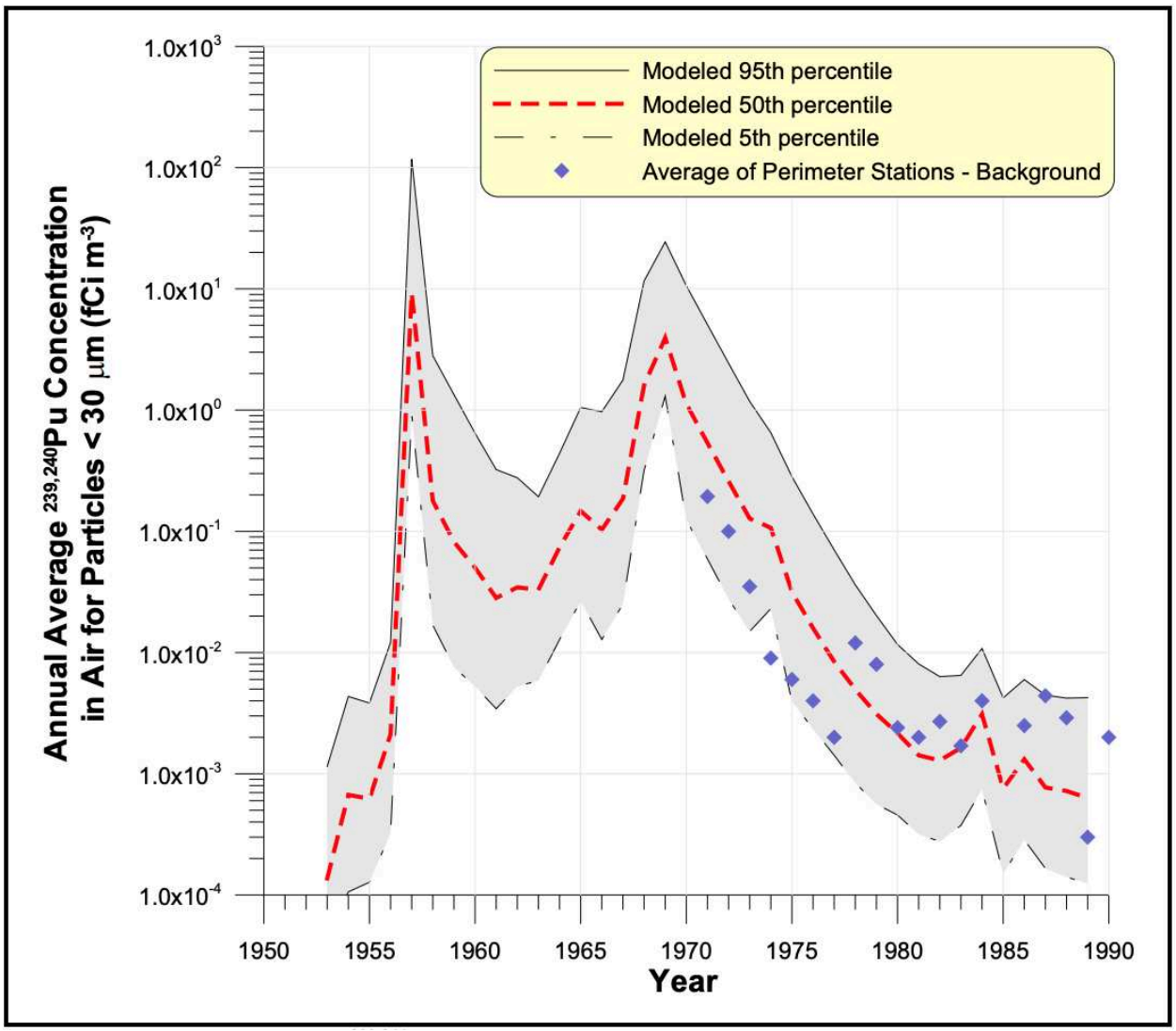

Fig 1.6: Annual average of $^{239, 240}$Pu concentrations in air as a function of time for particles < 30 μm aerodynamic equivalent diameter at the perimeter areas surrounding RFTP. This plot represents the model-predicted concentrations as an average of the 27 computational nodes of Figure 1.5. The model used is described by Rood and Grogan (1999). Reproduced, with permission, from ORAU Team NIOSH Dose Reconstruction Project, document number: ORAUT-TKBS-0011-4, 2004.

Summary of the 903 Pad

Through the late 1950s and 1960s, as many as 5,000 barrels containing over 200,000 gallons of waste oil and solvents contaminated with plutonium and uranium were stored outdoors at the 903 Area, later renamed the 903 Pad, as seen in Figure 1.3, when an asphalt pad was used to cover the most contaminated area. Many barrels corroded over time and leaked plutonium-

contaminated oil onto the surrounding soil. Weeds managed to grow through those barrels with significant corrosion, Figure 1.7. The liquids stored in these drums were a result of the lathe machining of plutonium pits (triggers). Oil was used as a cutting lubricant throughout the machining process. A carbon tetrachloride solvent would then be routinely used to clean the cutting oil from lathe parts and other tools (CDPHE - Rocky Flats Historical Public Exposure Studies, 2023). Early attempts at onsite waste disposal included burning uranium-contaminated oil in a pit and burying barrels containing plutonium-contaminated oil. Although these interim waste-handling methods were used, waste barrels still began to accumulate at the 903 Area. Since no long-term waste disposal methods were available at that time, and no good alternatives to barrels, contaminated liquid waste accumulated at this site (CDPHE, Radiological Assessments Corporation, 1999).

Fig 1.7: Corroded Barrel from 903 Area**.** Reproduced from Citizen Summaries – 903 Area, Colorado Department of Public Health and Environment—Rocky Flats Historical Public Exposure Studies, 2023.

Although concerns were raised by RFTP staff about leaking oil and contaminated wildlife in the mid-1960s, it wasn't until 1967 that the cleanup of damaged barrels began. Oil from the 903 Area barrels was transferred into new 55-gallon drums in preparation for transfer and processing. Of the 5,237 barrels initially delivered to the 903 Area, only 4,826 new barrels were filled with

repackaged oil. The discrepancy in barrels used is assumed to be due to a number of barrels either not initially filled completely or because of leakage; precise records were not maintained, and the exact cause of the discrepancy cannot be determined. Waste oil barrels were transferred to Building 774 for processing or shipped to Idaho National Laboratories (INL) for burial, thereby exposing all contaminated soil at the 903 Area. Dow Engineering initially requested to cover the area with asphalt; however, this request was not acted upon. Instead, the first remediation attempt involved leveling the area with a road grader and covering it with dirt to reduce the potential spread of contamination. Freshly disturbed soil and subsequent high winds resulted in the spread of radioactive contamination, evidenced by local area surveys and perimeter air samples east of the site. This was partly determined using suspension modeling and data from early on-site air samplers. Air samplers are shown in Figure 1.8, denoted by a number with prefix "S." High alpha activity readings at the S-8 air sampler, located near the east gate, are correlated with the high wind events at the RFTP. These high activity readings were then assumed to be due to the suspension of plutonium-contaminated soil from the 903 Area and used to quantify the amount of plutonium contamination distributed. The results of these estimates relative to results from other nearby air samplers are shown in Figure 1.9. Gravel fill and an asphalt pad would eventually be used to cover the 903 Area as a final remediation attempt (ibid.).

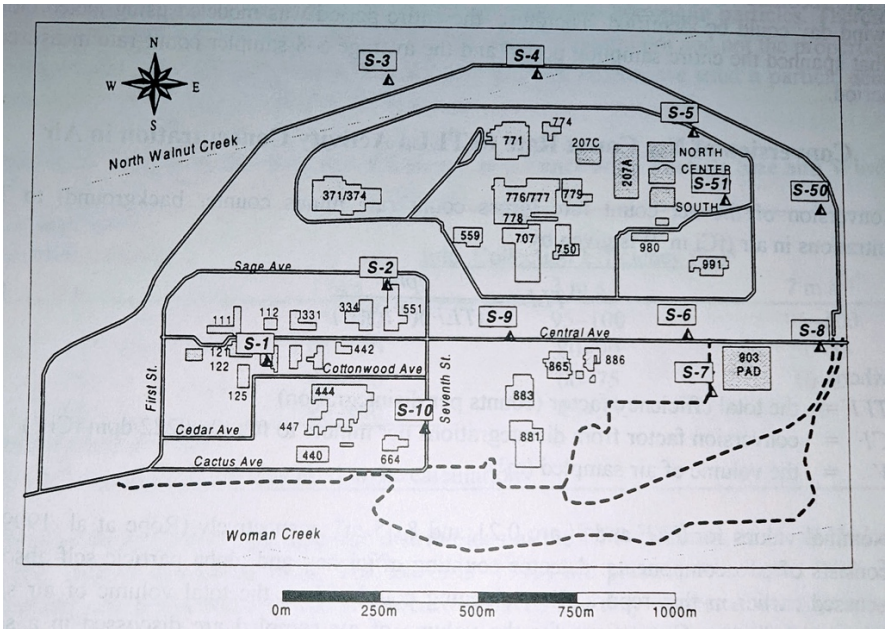

Fig 1.8: Locations of on-site ambient air samplers at RFTP, circa 1971. Alpha activity measurements in the S-8 air sampler were most affected by the 903 Area. Reproduced from Development of the Rocky Flats Plant 903 Area Plutonium Source Term—Final Report, August 1999.

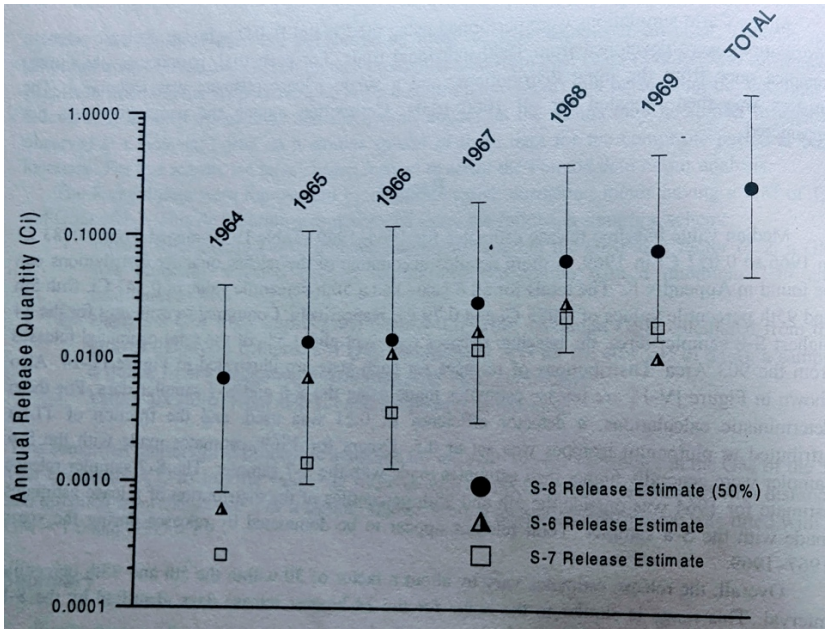

Fig 1.9: Distribution of baseline release estimate quantities by year. The black dot represents the 50th percentile, while the 95th and 5th percentile are the bars extending above and below, respectively. Reproduced from Development of the Rocky Flats Plant 903 Area Plutonium Source Term—Final Report, August 1999.

Rocky Flats Today

From 1952 until 1994, the primary mission of the RFTP was to produce nuclear and nonnuclear weapons components to supply America's nuclear arsenal. Nuclear component production ceased in 1989 following the Federal Bureau of Investigations (FBI) and the U.S. Environmental Protection Agency (EPA) entry into the RFTP alleging environmental crimes. Although work to resume operations in plutonium trigger production buildings began in 1990, the termination of the W88 trident missile warhead program ended the need for mass production of plutonium pits. In February of 1992, the RFTP officially changed its mission from nuclear material production to environmental cleanup. In 1993 the RFTP again changed its mission to decontamination and decommissioning (D & D). Soon thereafter, the last shipment of defense-related materials was transferred out in 1994 (DOE – Office of Legacy Management, CERCLA/RCRA Site Fact Sheet, 2023).

In 1995 the DOE estimated cleaning up Rocky Flats would cost over 37 billion US dollars (USD) and take approximately 65 years. However, in October of 2005, DOE and its contractor completed D & D in only 10 years with a 7 billion USD budget. The DOE Office of Legacy Management (LM) assumed responsibility for site operation in October 2005 and final jurisdiction of the site in 2008. In September of 2006, the former RFTP property was subdivided into two operable units, the Central Operable Unit (COU), approximately 1,309 acres that required continued remedial actions, and the Peripheral Operable Unit (POU), approximately 4,883 acres of generally unaffected property that surrounds the COU. The POU was transferred to the U.S. Department of Interior in July of 2007 to be managed by the U.S. Fish and Wildlife Service as the Rocky Flats National Wildlife Refuge (ibid.). Side-by-side photos of the Rocky Flats site are

shown in Figure 1.10. An overview map of the COU and POU can be viewed in the following subchapter of this thesis.

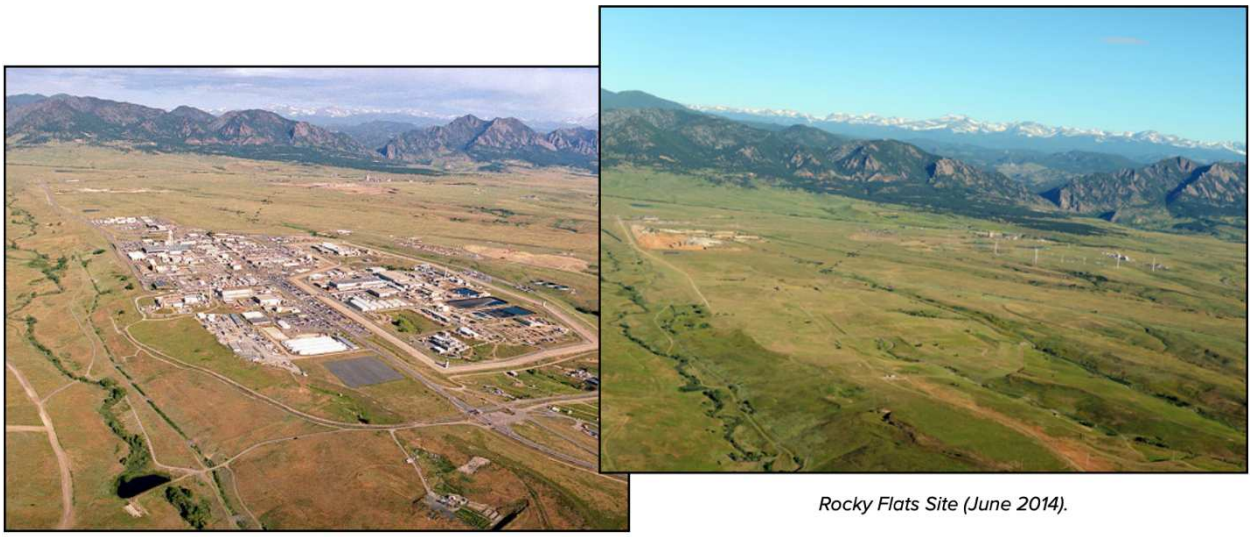

Fig 1.10: Aerial View of Rocky Flats Site – 1995 and 2014. Image reproduced from U.S. Department of Energy – Legacy Management. Rocky Flats Site, Colorado, A CERCLA/RCRA Site Fact Sheet, 2023.

Colorado Wildfires

The Colorado Department of Public Safety – Division of Fire Prevention and Control has reported the following Colorado fire history facts:

- 20 of the 20 largest wildfires have occurred in the last 20 years (since 2001)
- 16 of the top 20 largest wildfires have occurred in the last 13 years (since 2008)
- 15 of the top 20 largest wildfires have occurred in the last 9 years (since 2012)
- 11 of the top 20 largest wildfires have occurred in the last 5 years (since 2016)
- 9 of the top 20 largest wildfires have occurred in the last 3 years (2018 and 2020)
- 4 of the top 5 largest wildfires have occurred in the last 3 years (2018 and 2020)

The most destructive in terms of homes lost was the Marshall fire in 2021, in which 1,084 homes were lost (Colorado Department of Public Safety – Division of Fire Prevention and Control, 2024).

The wind-driven Marshall Fire on 30 December 2021 became the costliest wildfire in Colorado history. Fueled by a snow-free and drought-laden state, the Marshall Fire burned for nearly 11 hours. When combined with extreme local downslope wind gusts that day of over 45 m s^{-1} (100 mph), the fire quickly spread into the Boulder, Colorado suburbs of Louisville and Superior. The Marshall Fire burn area can be seen as the red boundaries of Figure 1.11. Additional points of interest include locations of ignition (cyan), Louisville and Superior town outline (black), approximate zones for maximum wind gusts (white), and four weather stations near the site, numbered 1 – 4 (Benjamin, S. G., et al., 2023). Figure 1.12 is included to show the relative proximity of the Marshall Fire burn area to the current Rocky Flats National Wildlife Refuge. Marshall Lake and Standley Lake, as labeled in Figure 1.11, were circled in red and purple, respectively, in Figure 1.12 to provide reference points. The increase in severity and intensity of Colorado wildfires in recent years, in addition to the relative closeness of the Marshall Fire to the Rocky Flats site, has re-sparked local community concern for the potential resuspension of radioactive contamination from Rocky Flats.

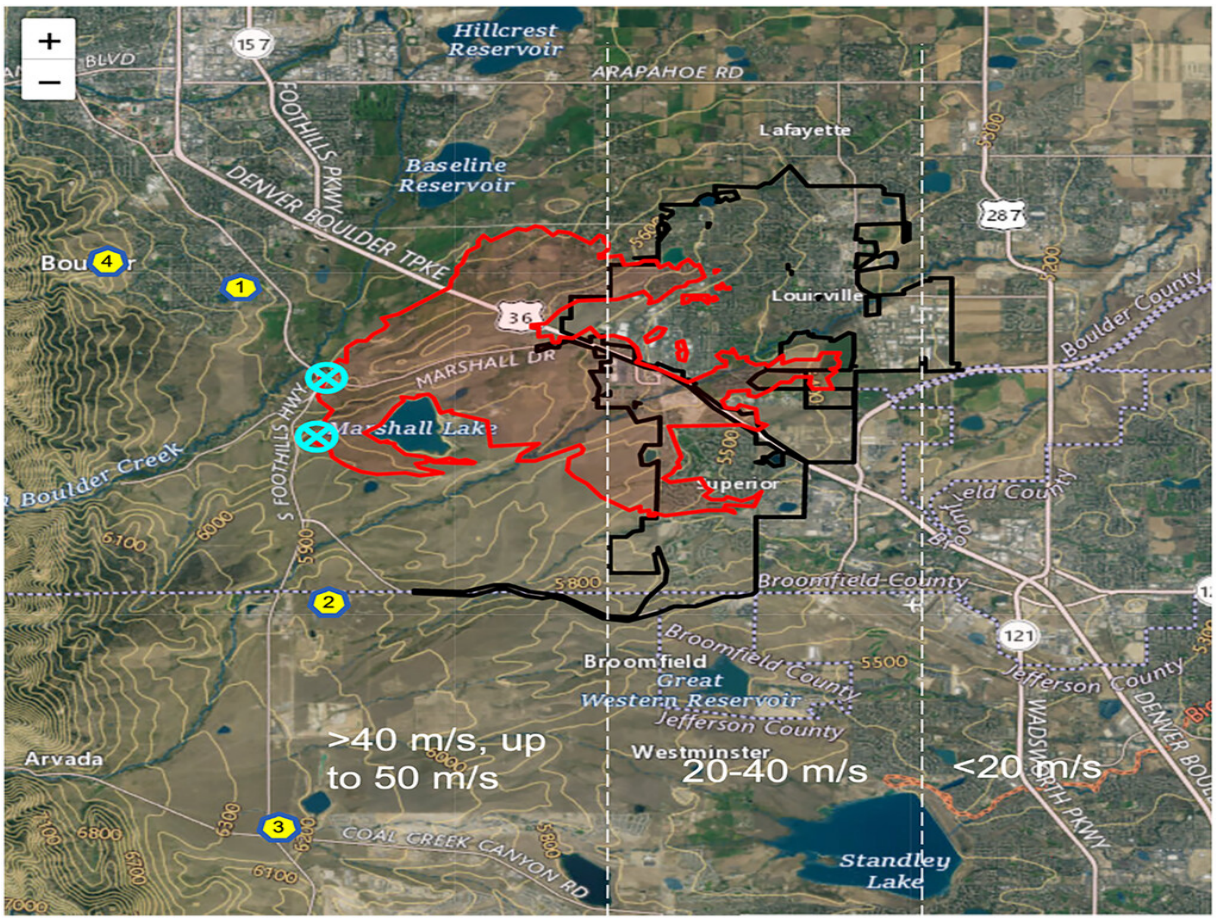

Fig 1.11: Marshall Fire Burn Area. Reproduced from The 30 December 2021 Colorado Front Range Windstorm and Marshall Fire: Evolution of Surface and 3D Structure, NWP Guidance, NWS Forecasts, and Decision Support. *Weather and Forecasting. © American Meteorological Society*. Used with permission. 2023.

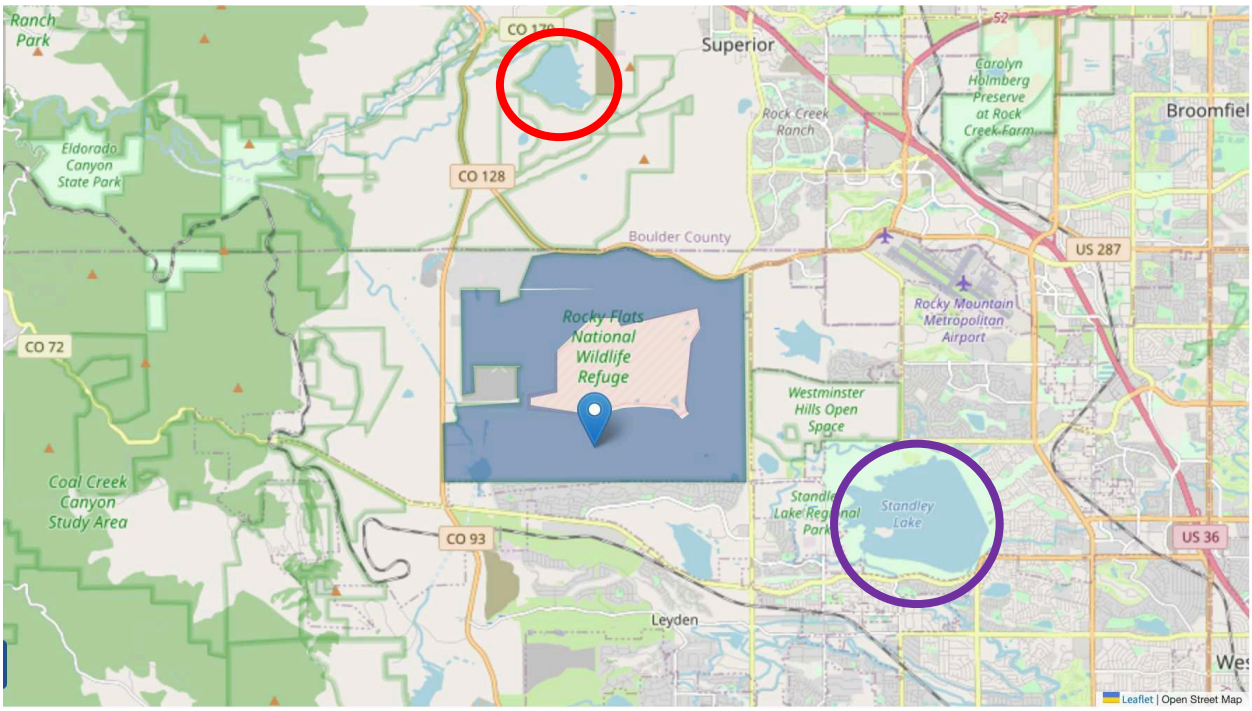

Fig 1.12: Map of Rocky Flats Wildlife Refuge (Blue Shaded Area). Image reproduced from U.S. Fish & Wildlife Service – Rocky Flats National Wildlife Refuge, 2023.The red and purple circles were added after the fact. The blue-shaded area, now the Rocky Flats Wildlife Refuge (previously the POU), surrounds the COU. https://www.fws.gov/refuge/rocky-flats/visit-us.

Public Concern

Soon after the Marshall Fire and early in the stages of rebuilding local communities, public concern for the potential resuspension of radioactive contamination from the Rocky Flats Site due to wildfires was reignited. An internet search for "Rocky Flats wildfire concerns" quickly yields articles such as *Concerns raised about a Marshall-style wildfire on former Rocky Flats nuclear site* (Aguilar, 2022), *Fear of a Marshall Fire at Rocky Flats is real* (Young, 2022), and *Wildfire worries dominate discussion of Rocky Flats refuge* (The Associated Press, 2022). The fear of resuspension of radioactive particles from potentially contaminated land is not new, however. In January 2015, High Country News reported that scheduled prescribed burns used to prevent uncontrolled wildfires were met with resistance by activists, former RFTP workers, and new homeowners who are concerned about the health effects of burning potentially contaminated

grasslands (Zaffos, 2015). The nearest housing developments to Rocky Flats can be seen in Figures 1.13 through 1.15, with the closest being the Candelas housing development, which lies on the southern border of the Rocky Flats National Wildlife Refuge. The following photos, Figures 1.13 through 1.15, were taken from the walking path along the southern border and inside the boundary of the Rocky Flats Wildlife Refuge.

Fig 1.13: Candelas Housing Development. Image by Author. Taken at the southern border of the Rocky Flats Wildlife Refuge (105° 12' 41.868" W Lat 39° 52' 14.43" N) facing south/southwest on 27 June 2023.

Fig 1.14: Trail to Candelas Development. Image by Author. Taken at the southern border of the Rocky Flats Wildlife Refuge (105° 12' 17.622" W 39° 52' 14.562" N) facing southeast on 27 June 2023.

Fig 1.15: View of Arvada, Colorado and Downtown Denver. Image by Author. Taken near the southern border of the Rocky Flats Wildlife Refuge (105° 11' 35.892" W 39° 52' 22.482" N) facing southeast on 27 June 2023. Standley Lake can be seen on the left, and the Welton Reservoir on the right. The buildings of downtown Denver can be seen in the distance between both bodies of water.

The Colorado Department of Public Health and Environment (CDPHE) reports that decades of on- and off-site air monitoring during the life of the facility, when contaminant emissions would have been at their highest, yielded results at or near analytical detection limits for radionuclides. As a result, DOE has discontinued the performance of air sampling as of 2007 (CDPHE – Hazardous Materials & Waste Management Division, 2024). Despite all evidence to the contrary, the general public remains concerned. The Rocky Flats Stewardship Council consists of a board of locally elected officials from counties and cities surrounding Rocky Flats who work with DOE and U.S. Fish & Wildlife Service personnel to provide periodic updates to the

community about issues related to the ongoing management of Rocky Flats. Documentation of the quarterly meeting on 7 February 2022 discusses public concerns for potential plutonium inhalation following a wildfire or high wind events at the Rocky Flats Site. Particular comments worth noting by the DOE's Site Manager for Rocky Flats at that time are "…nothing in existing plans would call for provision of air monitoring following a fire on [the Rocky Flats] site…. air monitoring was conducted during previous fires and did not show any movement of radioactive materials" and "DOE is not equipped to fight fires. They will report any fires to local officials and stay out of the way" (Rocky Flats Stewardship Council, 2022). This project aims to provide accessible resources to the concerned citizen for the collection of air samples that could show respiratory tract deposition and ultimately give the best dose estimate to the person if resuspended radionuclides were present.

Cascade Impactors

Impaction has been analyzed very thoroughly as an aerosol separation process. Through the use of cascade impactors, the principles of impaction can be used to determine particle size distributions. All inertial impactors operate on the same principle. An aerosol is passed through a nozzle or jet and the output stream is directed towards an impact plate. The impact plate deflects the air stream to form an abrupt bend in the streamline. Particles with sufficient inertia are unable to follow the streamline and impact the plate. In the case of single-stage impactors without a final capture mechanism, smaller particles following streamlines can avoid impaction and eventually exit the impactor. This principle is shown in Figure 1.16 (Hinds, 1982).

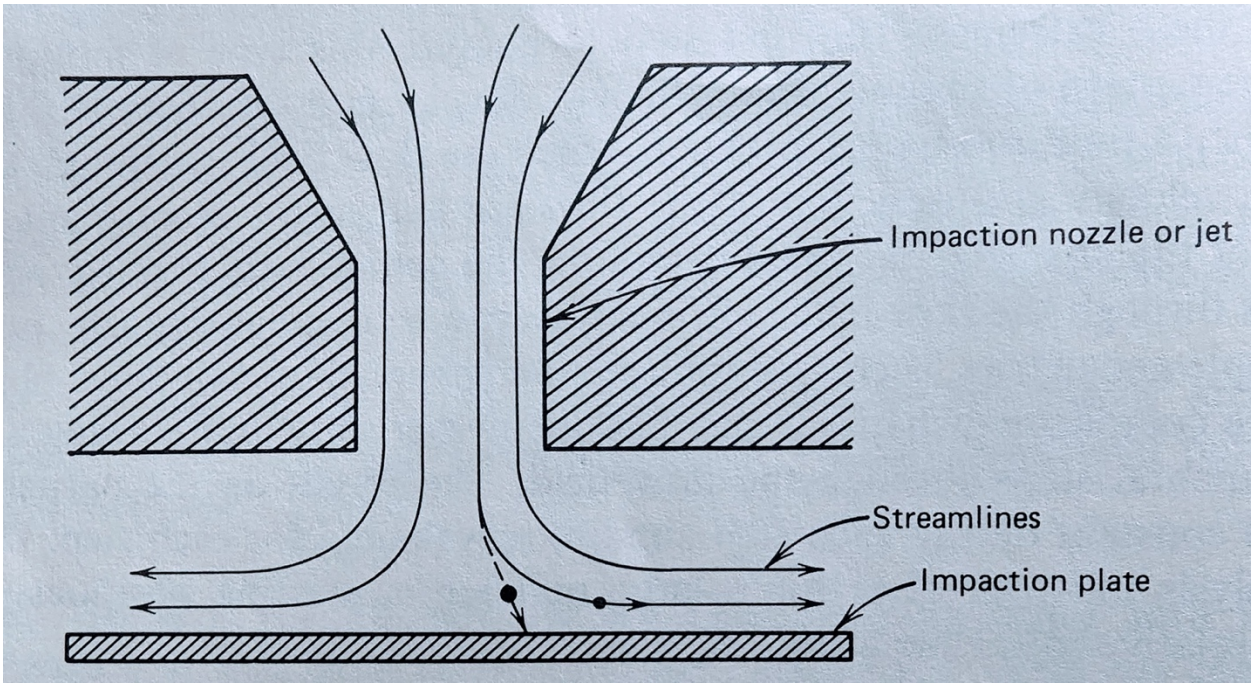

Fig 1.16: Cross-sectional view of an impactor. Reproduced, with permission, from Aerosol Technology – Properties, Behavior, and Measurement of Airborne Particles. Hinds,1982.

Sampling devices that use impaction-type sampling are commonly used for aerosol characterization with regard to particle size. Impaction-based sampling relies on the airborne particle's inertia to carry it onto a collection plate in the path of the sample airstream as demonstrated in Figure 1.16. A multi-stage or cascade impactor uses stages of descending cut size so that the largest particles are removed in the first stage, and sequentially smaller particles are removed in subsequent stages. Commercial cascade impactors can collect a narrow range of particle sizes so that airborne particles can be separated into separate particle size fractions (Anna, 2011). The basic working principles of a cascade impactor can be seen in Figure 1.17. A vacuum pump is used to draw a sample of air through the impactor. Entrained larger particles cannot make the sharp turn and are collected on the impact plate (green). The smaller particles pass through onto the next stage and are similarly collected on the next impact plate. This process continues through subsequent stages as each stage allows smaller and smaller particles to pass through. In

the case of this experiment, filter paper will be used in the final stage to prevent any particles from collecting in the vacuum pump.

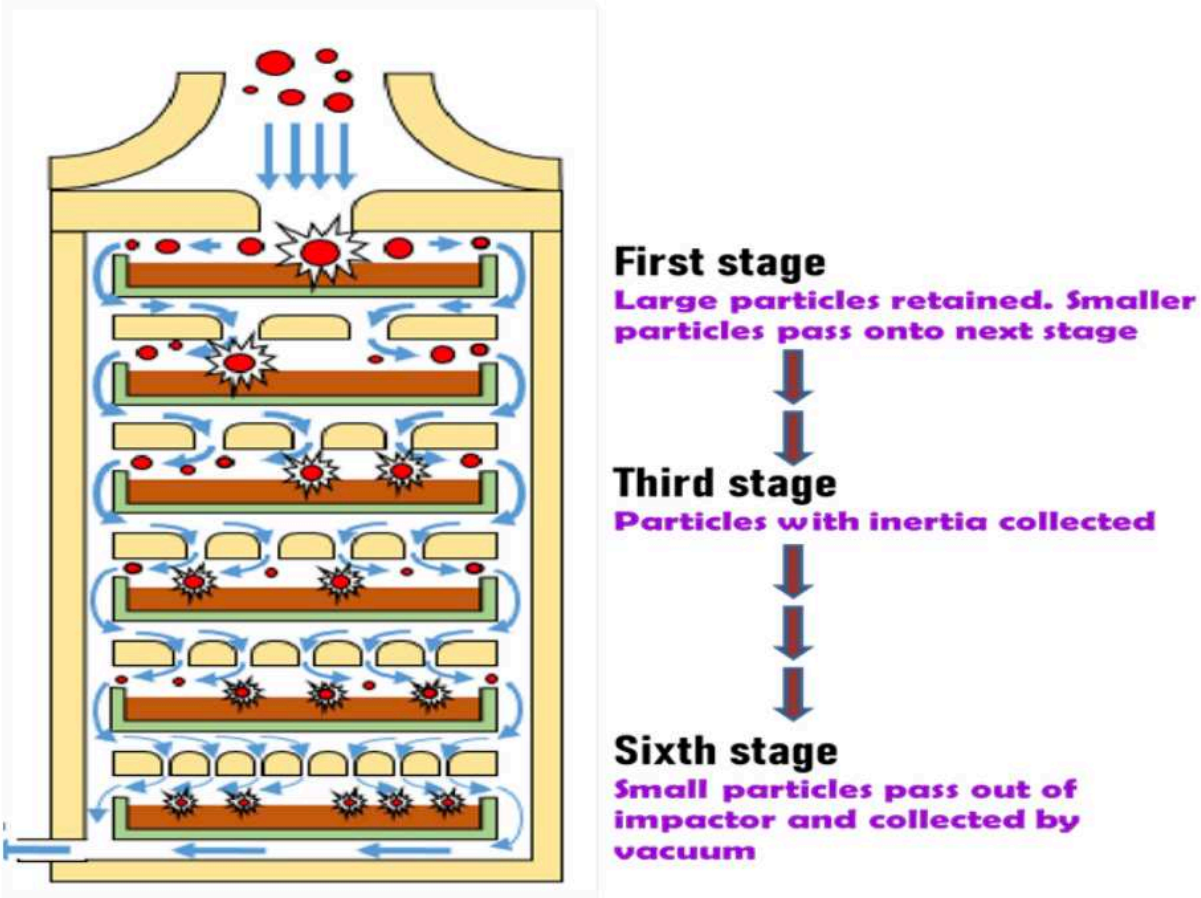

Fig 1.17: Basic Principles of a Cascade Impactor. Diagram reproduced from Evaluation of Aerodynamic Particle Size Distribution of Drugs Used in Inhalation Therapy: A Concise Review. International Journal of Research. Nayak, S., et al., 2020.

It is common to use a substrate on each collection plate to assist in capturing particles in each stage. Particle composition, velocity, and the type of impaction surface will determine if a particle bounces off of the plate and is carried back into the airstream. Although air sample filters provide an optimal substrate for subsequent radiological analysis, they do not provide the best collection surface. Fibrous filters are considered unsatisfactory collection surfaces because some flow goes through the filter, and particles may bounce off their fibers. Particles may also be collected in the passages between stages and can contribute to additional measurement

uncertainties when using cascade impactors. The efficiency of particle collection and interstage losses as a function of particle size is shown in Figures 1.18 and 1.19, respectively. The square root of the stokes number ($\sqrt{Stk}$) in Figure 1.18 is directly proportional to particle size (Hinds, 1982).

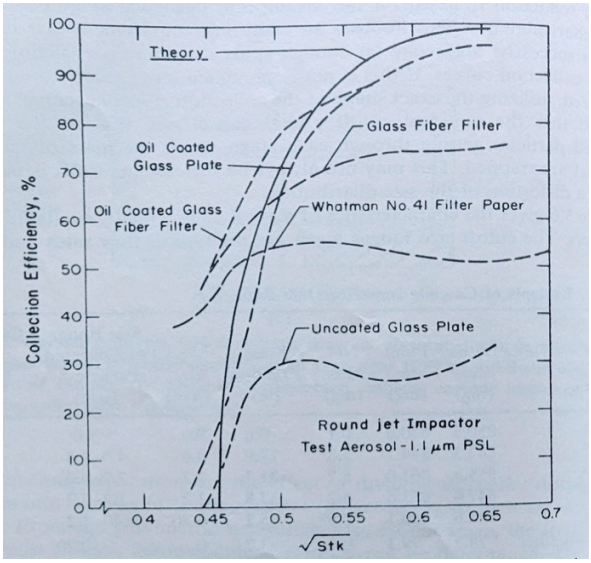

Fig 1.18: Effect of collection surfaces on impactor cutoff curve. Reproduced, with permission, from Aerosol Technology – Properties, Behavior, and Measurement of Airborne Particles. Hinds,1982.

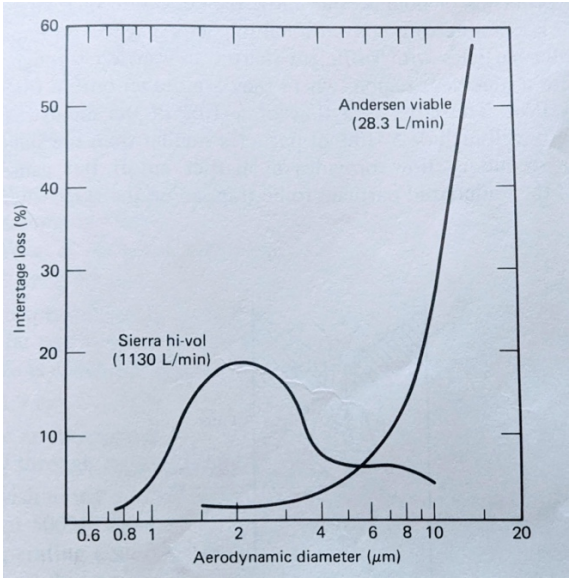

Fig 1.19: Total interstage losses for Andersen and Sierra impactors versus aerodynamic diameter. Reproduced, with permission, from Aerosol Technology. Hinds,1982.

Human Respiratory Tract

When airborne radionuclides are inhaled, parts of the respiratory system, other organs, and body tissues are irradiated by radiation originating from the material deposited in the lungs and from the movement of inhaled material to body tissues from the respiratory system. Following inhalation of airborne radionuclides, doses received by various regions of the respiratory system will significantly differ depending on the size distribution of the inhaled material (ICRP 30, 1979). However, entry into the respiratory tract depends on several factors, such as properties of the inhaled radionuclide, deposition sites, retention times or clearance rates, rates of absorption into the blood, and movement to other tissues. Other physiological factors that will determine respiratory tract entry and deposition include respiratory rate and volume, nose or mouth breathing, and overall health condition of respiratory tissues. When combined with the known radiological properties of the inhaled material and the sensitivity of irradiated tissues, the health risk and radiation dose can be estimated (ICRP 66, 1994).

The depth of penetration of airborne particles into the human respiratory tract largely depends on the airborne particle's size. Relatively large airborne particles exceeding 5 micrometers (μm) will likely be filtered out by nasal hair or by impact on the nasopharyngeal surface. Penetration depth is also affected by gravitational settling. Gravitational settling becomes less prominent as particle size decreases. For reference, a particle with a diameter of 20 μm settles at a velocity of about 1 cm s^{-1}, while a particle with a diameter of 1 μm will settle at a rate of about 0.003 cm s^{-1}. Therefore, all but very large particles may be carried by moving air while small particles tend to remain suspended in the atmosphere. Due to the relatively small air passages of the human respiratory tract, inhaled air and entrained particles may reach relatively high velocities, resulting in any large particles that pass through the hair-filtered nasal passages having high kinetic

energies. Similarly, as shown in Figure 1.17, these large high-velocity particles cannot follow the curvature of the respiratory tree and strike the walls of the upper respiratory tract. Inertial impact decreases as particle size decreases below 5 μm, resulting in a larger fraction of particles being carried into the lung. As these small particles are carried deeper into the lungs, they have a greater chance of gravitational settling, with chances decreasing as size decreases, reaching a minimum at about 0.5 μm. Brownian motion becomes significant at a particle size of about 0.1 μm, and particles become trapped on respiratory tract surfaces as they move about randomly and strike nearby walls. The combination of inertial impact, gravitational settling, and Brownian motion results in a maximum likelihood of deposition deep within the respiratory tract for particles in the size range of 1 – 2 μm and minimum deposition in the respiratory tract for particles in the size range of 0.1 – 0.5 μm (Johnson, 2017). Estimated deposition of inhaled particles in the human respiratory tract as a function of aerodynamic particle size is shown in Figure 1.20. Particle size is expressed as the diameter of an aerodynamically equivalent sphere of unit density. A basic model of the human respiratory tract is included in Figure 1.21.

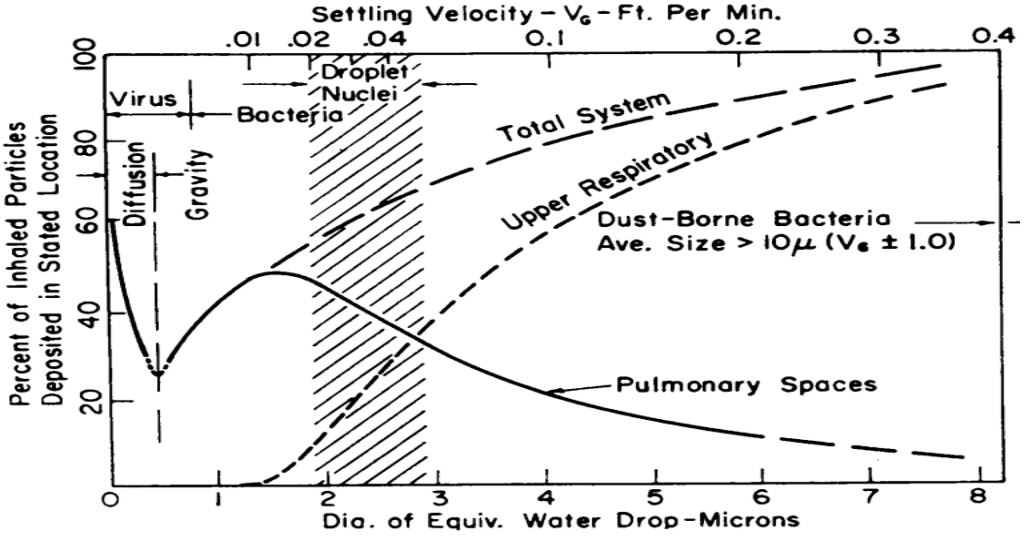

Fig 1.20: Total and regional deposition of inhaled particles in relation to aerodynamic particle size. Reproduced, with permission, from Distribution and Deposition of Inhaled Particles in the respiratory tract, Figure 1, 1961.

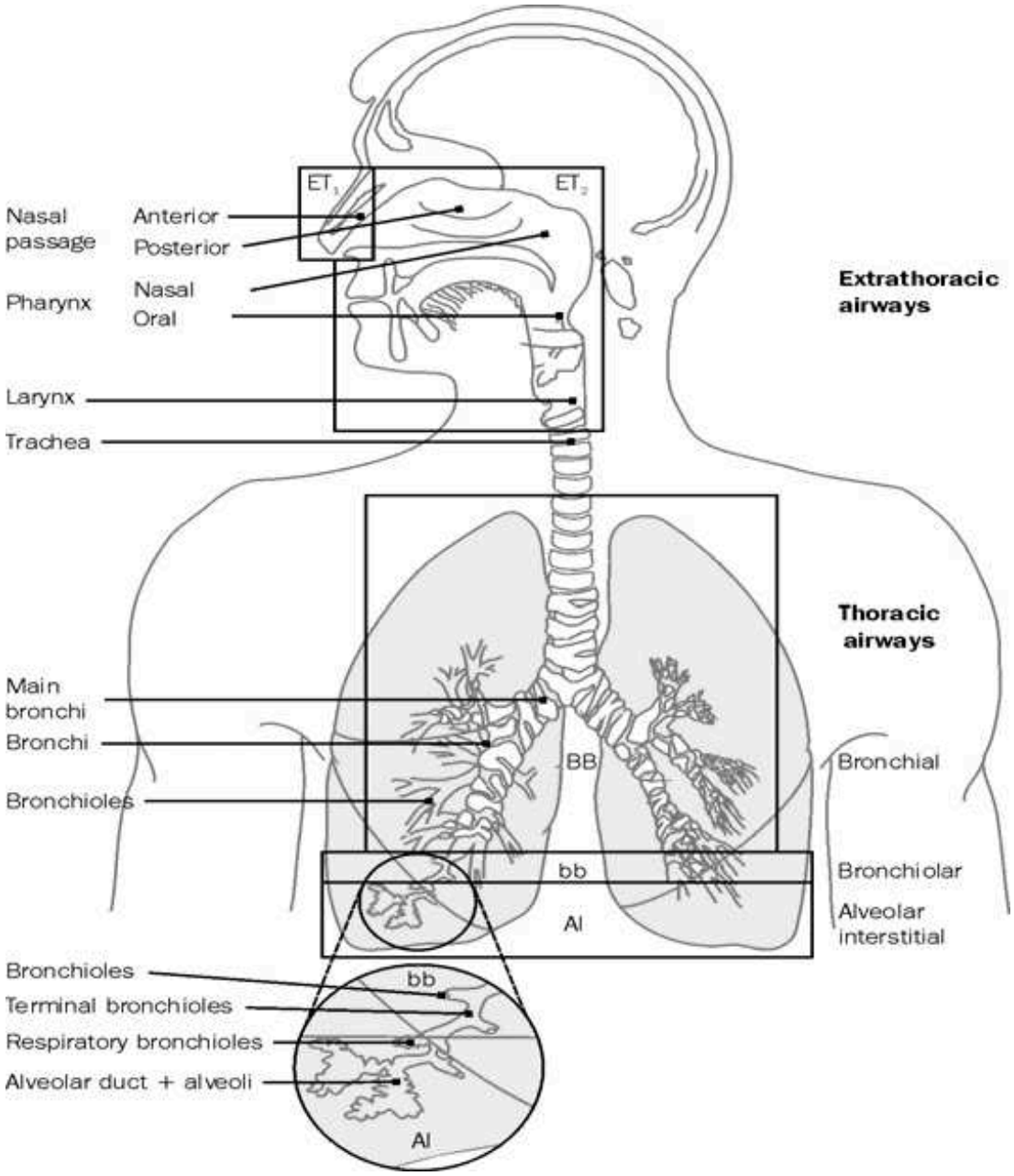

Fig 1.21: The ICRP Human Respiratory Tract Model. Reproduced from Health implications of Dounreay fuel fragments: Estimates of doses and risks, Figure 4.1.

What is Health Physics?

The first issue of the Health Physics Journal, volume 1 issue 1, published in January 1958, includes an article that describes the science of health physics in part but also focuses on the role

of the health physicist. In this article, Walter D. Claus states, “The health physicist may find themselves participating in roles such as assisting in the education of workers and of the general public in fostering a better understanding of the hazards (and lack thereof) of radiation” (Claus, 1958).

The science of health physics is indeed charged with providing access to the benefits of nuclear science while protecting all living things from the potential hazards of radiation. I argue that *fostering a better understanding of the hazards of radioactivity, and lack thereof,* may include providing data, regardless of the results or the available source term, at times when the general public is concerned with their well-being from potential exposure to radioactivity.

Past research indicates that resuspension of radioactive particles in the presence of high winds or fire is possible. I hypothesize that such particles may be captured by way of air sampling with a cascade impactor to determine their potential deposition location within the human respiratory tract. This research will test the possibility of using a 3D-printed cascade impactor in radioactive aerosol analysis by collecting air samples of naturally occurring radon and its progeny.

CHAPTER 2: LITERATURE REVIEW

The literature selected for review is summarized below. Due to the nature of the work conducted at the Rocky Flats Technical Plant, environmental issues realized during the life of plant operations, and the site's location relative to now populated areas, both the site and all its potential exposure concerns have been significantly scrutinized. As a result, the interested reader can find a considerable amount of literature on these topics. The material discussed in this section is of particular interest to this thesis. The relevant information of each reviewed document is summarized below.

Rocky Flats

A Model for a Comprehensive Assessment of Exposure and Lifetime Cancer Incidence Risk from Plutonium Released from the Rocky Flats Plant, 1953 – 1989, 2002

This paper discusses the use of a computer-based model to calculate ambient air concentrations, surface deposition, and risk estimate determinations of the incremental lifetime cancer incidence from plutonium inhalation released by the Rocky Flats Technical Plant between 1953 and 1989. This computer model relies on the source term studies, atmospheric transport models, cancer risk characterization, and environmental monitoring data collected during Phase II of the Historical Public Exposures Studies on Rocky Flats. Phase II of the public exposures study provided an in-depth investigation of the potential doses and risks to the general public from historical releases of plutonium from Rocky Flats. While Phase I consisted of an extensive investigation of plant operations and environmental releases that identified primary materials of concern, release points and events, quantities of radioactive material released, transport pathways,

and preliminary dose estimates to offsite personnel, Phase II reevaluated this data and provided information in greater detail.

Specific events of concern that resulted in the highest levels of radioactivity being released to the environment were those summarized in the introduction of this thesis: the 1957 fire, the 1969 fire, and the barrel leakage at the 903 Area. These events were included as source term computer model inputs. Routine plant operations at plutonium processing buildings also contributed to environmental activity releases and were also included as model source term inputs. Exhausted air from these buildings passed through HEPA filters with a pore size of 0.3 μm, and particle sizes of routine releases were assumed not to exceed 1.0 μm. Regardless, it was determined that minimal activity was released from routine operations and that the leakage at the 903 Area resulted in the most significant spread of radioactive contamination on- and off-site.

Computer model simulations of soil deposition and ambient air concentrations were validated by reviewing and comparing previous soil sampling studies and ambient air monitoring records. It is worth noting, however, that sampling studies and records are of samples obtained from the 0 – 3 cm layer. Final site remediation ensured that activity levels in the top three feet of soil were <50 pCi/g and <3,000 pCi/g in soil depths of three to six feet (DOE - Government Accountability Office, 2006).

Ultimately, this study determined that the maximum incremental lifetime cancer risk of incidence is in the range of 10^{-4}. In other words, there is a 1 in 10,000 chance, or 0.010 %, increase in incidence of cancer. A significant point is that this number is a worst-possible-case scenario. It is the increase in cancer risk specific to an adult male worker who lived in the model domain for the entire operating period of the Rocky Flats Technical Plant, including being in the plume path of the 1957 fire. The 0.010% increase in cancer incidence at the 95^{th} percentile to the laborer

extended south of the RFTP to the intersection of Colorado 58 and Interstate 70. At the 5th percentile to the laborer, the maximum incremental cancer incidence was 1 in 10 million, or a 0.00001% increased risk of developing cancer.

The paper discussed above was included to demonstrate the minimal risk of cancer incidence even at worst-case conditions from inhalation exposure to plutonium from the Rocky Flats Technical Plant. It is worth noting that studies by the American Cancer Society (2024) state that the average American male has a 40.9% lifetime risk of developing cancer and a 20.2% lifetime risk of dying from cancer, while the average American female has a 39.1% lifetime risk of developing cancer and a 17.7% lifetime risk of dying from cancer. The International Commission on Radiological Protection (ICRP) recommendations state that the detriment-adjusted nominal risk coefficients for cancer are 5.5 10^{-2} Sv^{-1} for the whole population based on cancer incidence data (ICRP 103, 2007). That is, the unexposed population has a 5.5% increased risk of cancer incidence for every one sievert of radiation exposure received over their lifetime.

Fires and Radioactivity

Resuspension and Atmospheric Transport of Radionuclides due to Wildfires near the Chernobyl Nuclear Power Plant in 2015: An Impact Assessment

This paper uses an atmospheric dispersion model to simulate the atmospheric transport and deposition of the radioactive plume released by wildfires that occurred in the Chernobyl Exclusion Zone (CEZ) in April and August 2015. This study used deposition measurements previously measured by Ukrainian authorities that were stored in the Norwegian Institute for Air Research (NILU) repository database (https://radio.nilu.no). Using known data of radionuclides that contaminated the Chernobyl site; ^{137}Cs, ^{90}Sr, ^{238}Pu, ^{239}Pu, ^{240}Pu, and ^{241}Am; radionuclide

deposition through eastern Europe was modeled. Results for the April 2015 and August 2015 fires are included in Figure 2.1 and Figure 2.2, respectively.

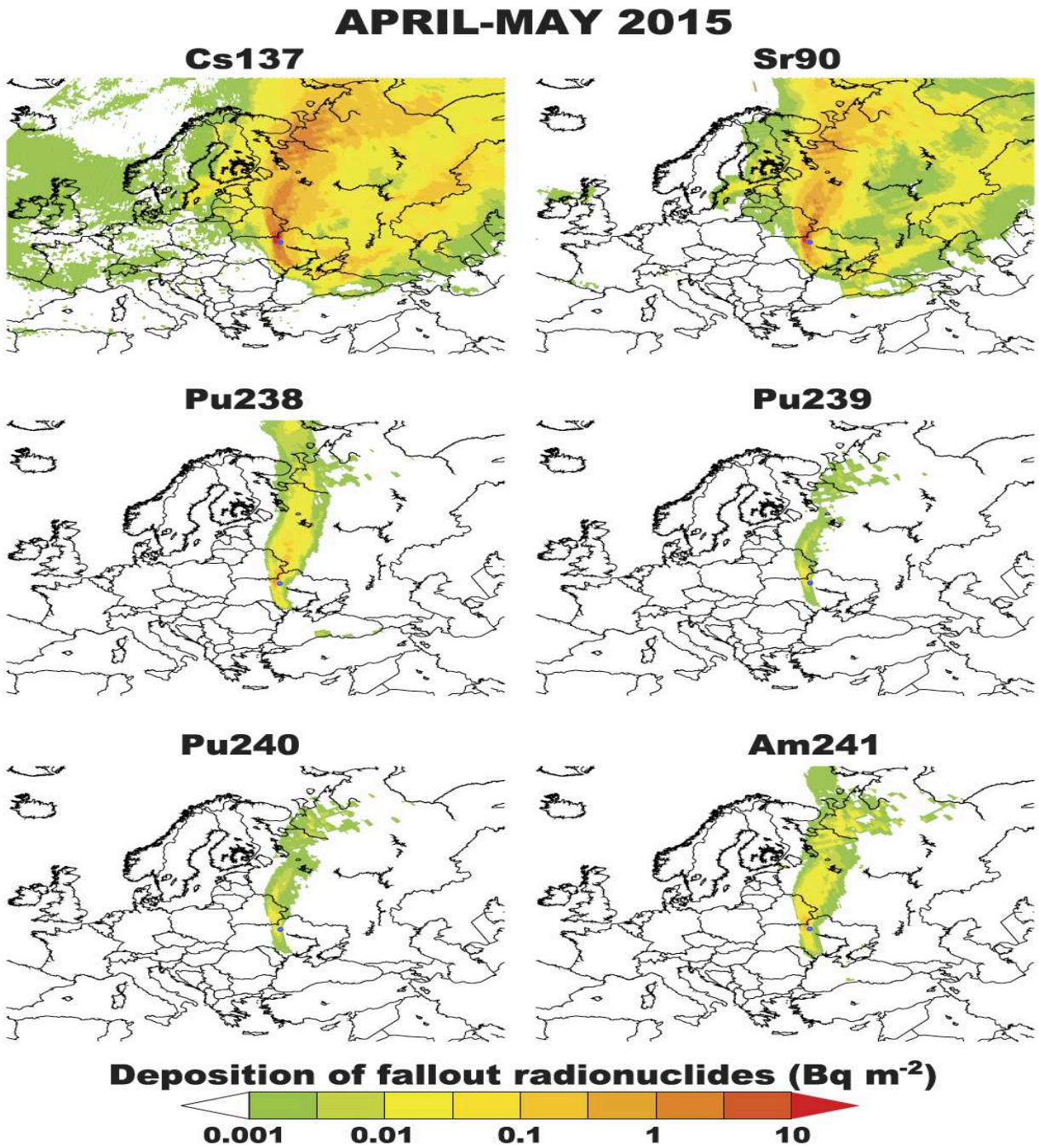

Fig 2.1: Radionuclide Deposition over Europe from Spring 2015 Fire at CEZ. Reproduced from Resuspension and atmospheric transport of radionuclides due to wildfires near the Chernobyl Nuclear Power Plant in 2015: An impact assessment, N. Evangeliou, et al., 2016.

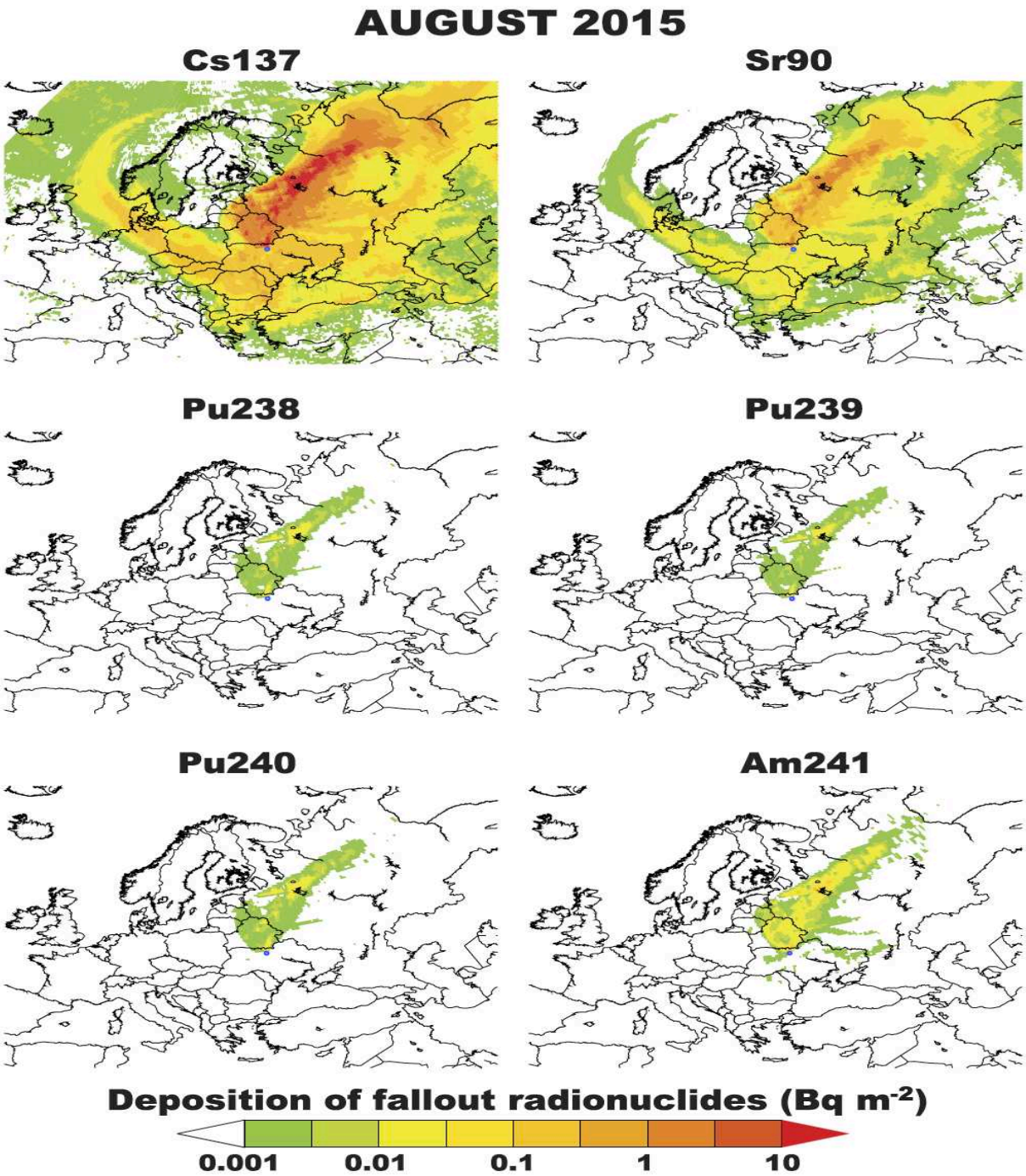

Fig 2.2: Radionuclide Deposition over Europe from Summer 2015 Fire at CEZ. Reproduced from Resuspension and atmospheric transport of radionuclides due to wildfires near the Chernobyl Nuclear Power Plant in 2015: An impact assessment, N. Evangeliou, et al., 2016.

Regarding studies at Rocky Flats, it is worth noting that no mention is given to any environmental remediation following the disaster at the Chernobyl Nuclear Power Plant that

occurred in April 1986. Actions taken to limit or prevent the spread of contamination from the CEZ are beyond the scope of this thesis and were not further investigated. Additionally, the reviewed paper states that only 20 – 30% of required fire preventative measures in the CEZ are completed annually due to a lack of funding and a significant reduction in forest road networks that are available for vehicle access. Department of Energy – Office of Legacy Management has a strenuous fire-mitigation plan at Rocky Flats National Wildlife Refuge that includes routine mowing of weeds and grasses, application of herbicide to control the abundance of fire-fueling weeds, and annual grading of access roads to provide fire breaks and easy access to remote areas for first responders (DOE – Office of Legacy Management, 2024). Ultimately, the reviewed paper was included to demonstrate the feasibility of resuspended radionuclides from wildfires; however, a reasonable comparison to the resuspension of radionuclides due to a wildfire at Rocky Flats cannot be made due to significant differences in terrain and firefighting capability as well as likely differences in remediation following known spreads of contamination to the environment. With regard to personal exposure to radiation from the CEZ fires, however, it is important to note that even in the ground contamination that resulted from the worst-case scenario that was the Chernobyl accident, estimated effective doses in the CEZ were about 1mSv y^{-1} and significantly lower in the rest of Europe. For reference, 1mSv is only a fraction of the exposure that could be received from a medical computed tomography (CT) scan.

Exposure to Radionuclides in Smoke from Vegetation Fires

This study measured activity concentrations of the naturally occurring radionuclides of uranium, thorium, radium, lead, and polonium in wildfire smoke. Radionuclides such as uranium and thorium, along with daughters in their decay chain, can be found easily in the environment, presenting a naturally occurring source of radioactivity to be measured. For comparison,

radioactivity from several sources was analyzed during this study. Vegetation such as tree trunk wood and leaves were collected from various trees in the absence of fire and taken to a laboratory for radioactive analysis. Additionally, surface-air samples were taken for background measurements in the absence of smoke and fire. An Andersen cascade impactor was also used during air sampling to characterize activity in various particle sizes. Field samples were then collected in the vicinity of bush and forest fires to determine activity concentrations of the naturally occurring radionuclides previously mentioned. All the air samples in this study used microfiber glass filters for collection and subsequent analysis.

The results of this study are shown in Table 2.1. Radionuclide activity concentrations were determined through radiochemistry and alpha spectrometry analysis.

Table 2.1: Radionuclide concentrations (Bq kg^{-1} dry weight) in plants, ashes from combustion, and in smoke-free surface air in Viseu district, Portugal Summer 2011. Table reproduced, with permission, from *Exposure to radionuclides in smoke from vegetation fires*, Carvalho, F. P. et al. 2013.

Samples	^{238}U	^{235}U	^{234}U	^{230}Th	^{226}Ra	^{210}Pb	^{210}Po	^{232}Th
Cistus, bushes	0.56 ± 0.02	0.027 ± 0.003	0.56 ± 0.02	0.57 ± 0.03	2.1 ± 0.2	9.90 ± 0.35	12.0 ± 2.4	0.38 ± 0.02
Oak tree, trunk wood	24.5 ± 0.6	1.18 ± 0.04	24.2 ± 0.6	1.9 ± 0.1	4.9 ± 1.1	–	–	0.112 ± 0.008
Oak tree, trunk wood	22.6 ± 0.8	1.08 ± 0.05	21.8 ± 0.8	1.60 ± 0.07	5.4 ± 0.5	3.27 ± 0.16	5.51 ± 0.02	0.095 ± 0.007
Oak tree, leaves	1.68 ± 0.07	0.08 ± 0.01	1.56 ± 0.07	0.51 ± 0.04	7.4 ± 0.7	17.2 ± 0.4	30.8 ± 1.2	0.29 ± 0.02
Eucalyptus, trunk wood	0.114 ± 0.004	0.0050 ± 0.0006	0.115 ± 0.004	0.023 ± 0.002	0.96 ± 0.13	0.98 ± 0.03	1.68 ± 0.05	0.016 ± 0.001
Eucalyptus, bark	0.29 ± 0.01	0.014 ± 0.003	0.30 ± 0.01	0.089 ± 0.008	26.0 ± 2.4	1.88 ± 0.09	2.60 ± 0.06	0.049 ± 0.007
Eucalyptus, leaves	4.4 ± 0.1	0.21 ± 0.01	4.1 ± 0.1	0.20 ± 0.02	37.3 ± 2.6	10.3 ± 0.4	49.4 ± 2.3	0.08 ± 0.01
Acacia tree, trunk wood	0.020 ± 0.001	0.0014 ± 0.0004	0.018 ± 0.001	0.017 ± 0.001	1.5 ± 0.1	2.04 ± 0.05	4.05 ± 0.15	0.008 ± 0.001
Acacia tree, leaves	13.0 ± 0.3	0.58 ± 0.02	12.8 ± 0.3	5.3 ± 0.3	30.8 ± 1.6	20.27 ± 0.47	8.61 ± 0.33	0.16 ± 0.02
Pine tree, trunk wood	0.105 ± 0.006	0.006 ± 0.002	0.112 ± 0.006	0.067 ± 0.006	1.14 ± 0.06	1.98 ± 0.09	0.97 ± 0.03	0.065 ± 0.006
Pine tree, trunk wood	0.103 ± 0.013	0.0050 ± 0.0047	0.106 ± 0.013	0.014 ± 0.003	0.92 ± 0.09	1.43 ± 0.13	1.53 ± 0.06	0.009 ± 0.003
Pine tree, bark	0.42 ± 0.02	0.019 ± 0.003	0.42 ± 0.02	–	2.7 ± 0.5	2.80 ± 0.08	2.87 ± 0.06	–
Pine tree, leaves (needles)	1.99 ± 0.07	0.13 ± 0.01	1.91 ± 0.07	2.1 ± 0.1	4.9 ± 0.3	10.36 ± 0.31	3.10 ± 0.08	1.10 ± 0.08
Ashes from ground after forest fire	135 ± 4	6.2 ± 0.3	146 ± 4	259 ± 20	477 ± 54	402 ± 6	1115 ± 66	55.7 ± 4.5
Fly ashes (in surface air collected on filter F#6)	347 ± 19	18.0 ± 3.9	372 ± 20	209 ± 13	6144 ± 2908	2070 ± 88	7255 ± 285	203 ± 13
Fly ashes (in surface air collected on filter F#11)	224 ± 12	9.8 ± 2.6	227 ± 12	261 ± 14	5763 ± 1489	923 ± 53	3604 ± 148	95.7 ± 7.1
Aerosol (surface air in absence of fire smoke)	71.0 ± 3.7	2.8 ± 1.0	71.8 ± 3.7	42.4 ± 2.6	–	5895 ± 218	111 ± 7	42.1 ± 2.7

Table 2.1 shows a clear and significant increase of measured radioactivity in fly ash (smoke particles) relative to the concentration measured in local vegetation and background air samples. Repeated smoke sampling near several wildfires indicated a consistent trend of increasing radionuclide concentrations in air with increasing amounts of smoke. Ultimately, this study determined that prolonged breathing of smoke near vegetation fires may increase the inhalation of

radioactivity by 40 times that inhaled by a chronic smoker; this was, however, determined to be mostly from ^{210}Po, a ^{222}Rn daughter that decays by alpha emission.

Similar to the preceding subchapter, this study demonstrates the feasibility of radionuclides to become airborne in the presence of fire. Specific physical properties of radionuclides should indeed be considered. Radionuclides that are nutrient analogues will concentrate in plant life and other vegetation leading to higher airborne concentrations in the event of a wildfire. In the case of this study, ^{210}Po and ^{210}Pb can partly be accumulated by root uptake. In addition to any external deposition, this likely contributed to higher concentrations in smoke.

Of additional interest to this thesis is the use of an Andersen cascade impactor for smoke sampling, which showed the radionuclide size distribution in several classes of aerosol particles. Refractory elements, such as ^{238}U, had a higher activity concentration in filters that captured larger particles relative to that seen in filters with the smallest particles. Conversely, ^{210}Po activity concentrations were highest in small particle distributions and lowest in large particles. Although not identified by spectroscopy, alpha-emitting radon progeny are hypothesized to have contributed to the highest activities of the final filter for research conducted for this thesis; see Chapter 4 (Results) for further discussion.

Radioactivity in smoke particulates from prescribed burns at the Savannah River Site and at selected southeastern United States forests

This paper similarly presents a radiological analysis of fly ash and smoke-free air, albeit from prescribed burns, at the Savannah River Site near Aiken, South Carolina. The Savannah River Site (SRS) currently focuses on environmental cleanup, nuclear materials management, and research and development activities. However, established as a DOE site in 1951, its mission was initially focused on the production of plutonium and tritium used in the manufacture of nuclear weapons until about 1991.

Of particular interest, this study performed air samples during various controlled burns at SRS over four years. Controlled burns are performed for various reasons, such as wildfire mitigation control; however, in this case, they were performed to maintain habitat for indigenous bird species in addition to reducing hazardous fuel buildup. The objectives of this study were to characterize concentrations of natural and manmade radionuclide isotopes in smoke during prescribed burns at SRS and at several off-site locations, as well as in reference air during non-burn days. Field samples were collected on glass fiber filters and subsequently analyzed.

The results of this study indicated that radionuclide activity concentrations differed on burn and non-burn days, with burn days consistently having higher radionuclide activity. Fire activity contributed to increasing concentrations for both manmade and natural radionuclides; specifically, of interest to research at Rocky Flats, this study showed that controlled burns at SRS resulted in a five-fold increase, relative to off-site samples, and a six-fold increase, relative to on-site non-burn days, of ^{238}Pu median concentrations. Indicating that this radionuclide is not only present at SRS, but that fire will increase its availability in air. The presence of $^{239,\ 240}$Pu were also reported as having increased activity on burn days, however, this isotope of plutonium is ubiquitous in the global atmosphere due to historical nuclear fallout. This study also included a public health assessment, and it is worth noting that it concluded that any dose received from SRS controlled burns contributes to a very small percentage of radiation dose received from other radiation sources.

Cascade Impactors and Particle Characterization

Characterization of Plutonium Aerosol Collected During an Accident

A study was conducted to characterize radioactivity, particle size distribution, and dissolution rate of plutonium aerosols collected on fixed air filter samplers (FASs) and continuous

air monitors (CAMs) collected during the 16 March 2000 release of an undetermined amount of $^{238}PuO_2$ in a room within the plutonium facility at Los Alamos National Laboratory. Eight workers were present, and 30 FASs and four CAMs were operating in the room at the time of the incident. Of specific interest to this thesis, one of two methods used to determine aerodynamic particle size, was resuspension and aerosolization of particles collected on air filters followed by size determination using a Lovelace Multi-jet Cascade Impactor. Sections of air filters were resuspended by placing them in vials containing ethyl alcohol and then subjecting them to ultrasonic agitation. The ethyl alcohol solution and a Lovelace nebulizer were then used to generate an aerosol. The aerosol was then passed through a radial diluter and activated carbon chamber with an ^{85}Kr discharge tube before being passed through the cascade impactor. The data obtained via this method determined the particle size distribution to have an activity median aerodynamic diameter (AMAD) of 4.8 μm at a standard deviation of 1.5. An advantage to this method is that it provides a direct measurement of aerodynamic particle size, which is needed for dose estimates without the need for assumptions on particle shape and density. However, the efficiency of the resuspension and sampling process was determined to be low (< 1% of activity on the filter).

In addition to other plutonium characteristics determined by this study, the particle size of inhaled radionuclides is an essential part of performing an accurate dose assessment. As described above, however, the process of determining particle size after the fact can be cumbersome, inefficient, and possibly provide inaccurate data. Providing an easy and readily available method to collect an air sample with an already distributed particle-size fraction could streamline the dose assessment process.

CHAPTER 3: MATERIALS & METHODS

Building a 3D Printed Cascade Impactor Prototype

The materials used for printing and building the cascade impactor are summarized in Table 3.1.

Table 3.1: Cascade Impactor Materials.

Materials	Model / Version
Shapr3D Computer Aided Design (CAD) modeling software for iPad	App version 5.531.0.6320
Raise3D 3D Printer	Model Pro3
1.75 mm polylactic acid (PLA) 3D filament	n/a
1/8-inch male iron pipe (MIP) to 3/8-inch female iron pipe (FIP) fitting	n/a
3/8-inch MIP to quick-disconnect fitting	n/a
(6) 1-7/8 inch outside diameter (O.D.) x 1-3/4 inch inside diameter (I.D.) - #65 O-ring	n/a

A base model for an Andersen cascade impactor was downloaded from the grabCAD website (https://grabcad.com/library/anderson-cascade-impactor-1). Files were uploaded into the Shapr3D iPad application to allow for modifications that were specific to this research. The goal was to build a cascade impactor in which the impact tray could hold a 47 mm air filter that could then be measured for radioactivity using counting equipment available at Colorado State University. A file for a nearly completed cascade impactor was primarily used. A pieced-together computer model could however not be printed. As a result, each piece of this CAD model was separated so that it was given its own file. Figure 3.1 shows an image of the original downloaded CAD file on the left and a copy in an exploded view to the right. Figures 3.2 through 3.9 show the image of each separate file after it was modified for use in this experiment. Although the impact tray was also separated, an image is not shown below.

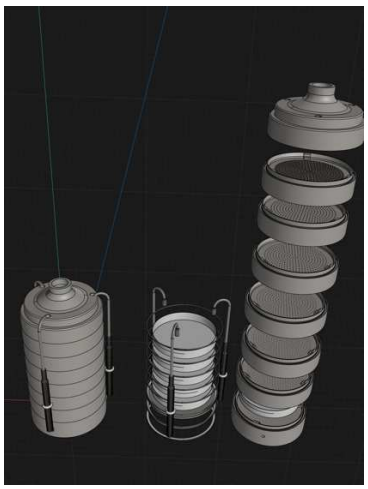

Fig 3.1: Original model

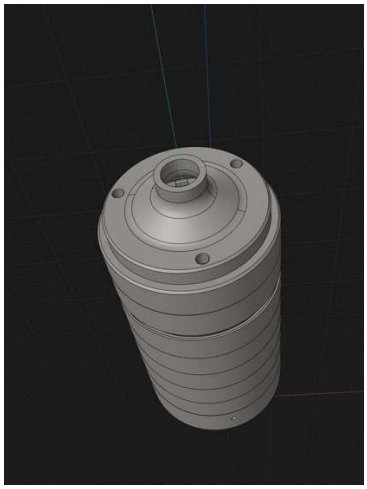

Fig 3.2: Modified model

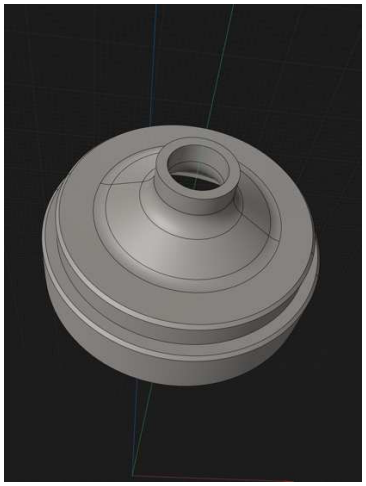

Fig 3.3: Inlet cone

Fig 3.4: Modified stage 0

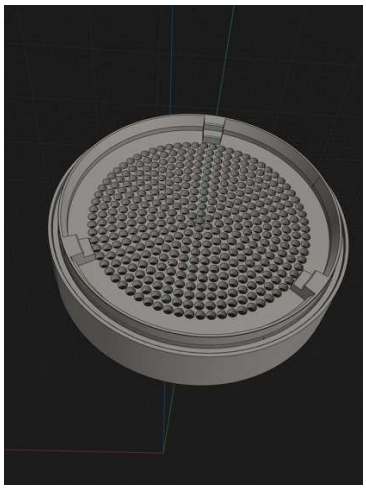

Fig 3.5: Modified stage 1

Fig 3.6: Modified stage 2

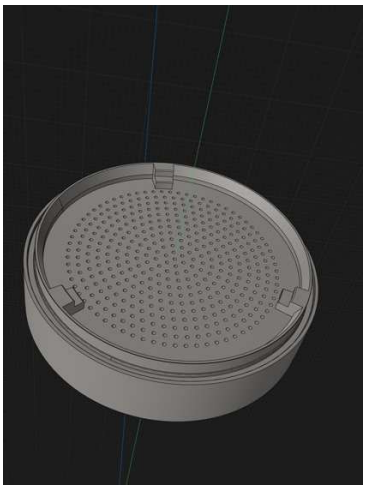

Fig 3.7: Modified stage 3

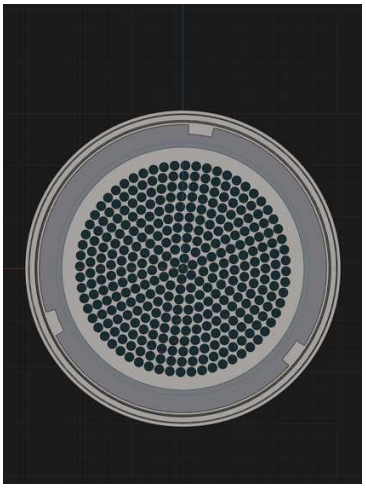

Fig 3.8: Modified final stage

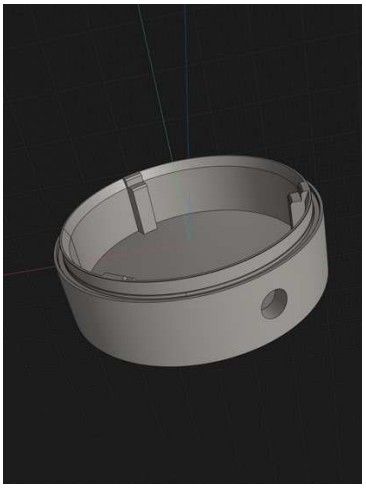

Fig 3.9: Modified base/outlet

Prototype printing of the original CAD files resulted in a cascade impactor that was 12 cm in diameter; this was significantly larger than the desired size. Shapr3D was used to scale the model down by a factor of 0.5. Each piece of the cascade impactor was again separated into individual files. Scaling by 0.5 gave the ideal size, where the impact tray used to hold the substrate could perfectly hold a 47 mm filter. The holes in each impactor stage were then re-scaled to achieve a hole diameter similar to the dimensions of a vendor-manufactured cascade impactor. Hole diameters were tested to confirm the design diameters using a microscope with a slide micrometer and a calibrated pin gauge. An Orthoplan microscope, six-watt LED spotlight, and Jenoptik ProgRes Gryphax Avior microscope high-definition camera were used to magnify and capture impactor stage images during the measurement process. During this process, imperfections of holes within each stage were noted. This is discussed further and demonstrated in chapter 5 of this thesis. Microscope and pin gauge measurements also differed from the design parameters, and an average of the measured hole diameters was used. Due to imperfections of each hole in the printing process, five holes were measured in each stage using the microscope. Hole parameters for each stage are found in Table 3.2.

Table 3.2: 3D Printed Cascade Impactor Parameters.

3D Printed Cascade Impactor Stage	Number of Holes	Design Hole Diameter (mm)	Average Measured Hole Diameter (mm)
Stage 0	91	2.534	2.435 ± 0.084
1st Stage	400	1.81	1.613 ± 0.168
2nd Stage	400	0.923	0.723 ± 0.025
3rd Stage	400	0.724	0.533 ± 0.047

A 4th stage was attempted. However, the small diameter of each hole was beyond the capability of the Raise3D printer, and the holes were not actually printed. It is also worth noting that each stage was printed in an “upside down” orientation so that the smooth surface of the stage was at the inlet. Printing in the original orientation resulted in the inlet having a rough surface, which could have affected particle flow through each stage.

The final collection stage was modified from a duplicate of the 1st stage CAD file, so no impact tray was used. Its borders were extended inward so that a 47 mm glass fiber filter would fit directly over the hole pattern. The hole pattern for the final stage maintained the same parameters of the 1st stage to ensure maximum airflow. This final collection stage would serve to capture any remaining particles that had not been collected in prior stages.

Once each stage was printed, six #65 rubber O-rings were fitted to each stage. The outlet port of the vacuum chamber, where the vacuum pump was to be attached, was mechanically modified after the fact. A 5/16-inch drill bit was used to enlarge the outlet port. Then, a 1/8-inch tap was used to machine threads. Polytetrafluoroethylene (PTFE) tape, commonly known as Teflon tape, was wrapped around the male threads of the 1/8-inch MIP to 3/8-inch FIP fitting and then threaded into the outlet port. Fittings were gathered such that either a male quick-disconnect fitting could be attached to the cascade impactor, which could then be directly mounted to the vacuum pump suction, or Tygon tubing could be used to marry the vacuum pump and cascade impactor via a barbed male hose adaptor. Tygon tubing between the pump and impactor allows for the impactor to be placed at some distance from the pump, as the sampling situation deems necessary. For example, if desired to sample in the breathing zone, approximately one meter from the ground, elevating the pump to this height may not be practical. This experiment used a barbed fitting on the 3D-printed model and Tygon tubing to attach each cascade impactor to their respective vacuum pump. This was done for consistency in sampling between impactors as the commercial cascade impactor could not be mounted directly to its vacuum pump. Rubber bands were used to compress the stages together in an attempt to minimize air leakage.

Flow through the 3D-printed model with its respective vacuum pump was checked with a Mesa Labs BGI tetraCal volumetric air flow calibrator. Airflow through the 3D-printed model

indicated a flow rate of 15.08 L/min. A crude leak test was performed by compressing the stages of the 3D-printed cascade impactor by hand. Airflow through the calibrator immediately showed an increase in flow rate; indicating leakage through one or all of the stages of the impactor proving that compression by rubber bands was insufficient. To remediate this, masking tape, commonly called painter's tape, was used at the seam of each stage. This proved to give the same flow rate shown when manually compressing the impactor by hand. The final flow rate was measured at 17.43 L/min.

Commercial Andersen Cascade Impactor

The commercial Andersen cascade impactor (ACI) had no vendor label and could not be tied to specific design parameters. An image of this model is included as Figure 3.10 and 3.11. Hole diameters were checked using the calibrated pin gauge to find vendor specifications that best matched the ACI. Design parameters for this ACI can be found in Table 3.3. The final stage (not listed below) was the final entry point into the vacuum chamber. A sample filter was used to cover this hole to capture any particles not captured in prior stages. By design, there is no impact plate on the first stage of the ACI; thus, no filter was used on this stage.

Fig 3.10: Commercial ACI (assembled)

Fig 3.11: Commercial ACI

Table 3.3: Commercial Andersen Cascade Impactor Design Parameters.

Andersen Cascade Impactor Stage	Number of Holes	Design Hole Diameter (mm)	Particle Size Range (microns)
1st Stage	400	1.18	7.0 and above
2nd Stage	400	0.91	4.7 – 7.0
3rd Stage	400	0.71	3.3 – 4.7
4th Stage	400	0.53	2.1 – 3.3
5th Stage	400	0.34	1.1 – 2.1
6th Stage	400	0.25	0.65 – 1.1

The design flow rate for an ACI is 28.3 L/min. Our ACI was connected to the same Mesa Labs airflow calibrator and its vacuum pump, a separate pump from that used for the 3D-printed impactor. Airflow through the ACI was adjusted to 28.29 L/min.

Conducting Air Samples and their Radiological Assessment

Although the 3D-printed cascade impactor is intended to one day be used for capturing dust particles with plutonium attached to them or plutonium particles by itself, should they be present, designing an experiment to capture airborne plutonium could not be safely accomplished. Naturally occurring sources were instead used to test the efficacy of a 3D-printed cascade impactor's ability to capture radioactive nuclides. Radon (Rn) is a radioactive gas that forms naturally when uranium, thorium, or radium decay in rocks, soil, and groundwater (U.S. Environmental Protection Agency, 2023). Of particular concern are the progeny of ^{222}Rn, specifically the particulate isotopes of polonium (Po), ^{218}Po and ^{214}Po, which give off highly energetic alphas in their decay. For this experiment, two methods were used to collect radon progeny on the air filters of each cascade impactor. One involved collecting air from a radon generator, a container with uranium-rich rocks, and the other was taking an environmental sample outside, at the southside of the Molecular, Radiological, and Biosciences (MRB) building on the Colorado State University campus. In both cases, air filters were either counted by a simple gross alpha/beta counter or in a gas proportional counter. The materials used for air sampling can be

found in Table 3.4. A simple schematic of the sampling setup is shown in Figure 3.11. This figure shows the setup to collect air from the radon generator or for an environmental sample.

Table 3.4: Materials Used in Air Sampling.

Materials	**Model / Version**
Hydrophilic, binderless, glass fiber filter paper (47 mm)	HI-Q Environmental Products Company. Part No. FP5211-47
(2) Dayton Electric Manufacturing 1/6th Horsepower, 60 Hz, 115 V, Vacuum Pumps	Model No. 4Z334
2 ft of 1-1/4 inch I.D. x 1-5/8 inch O.D. Tygon tubing, ACI to radon generator	n/a
2 ft of 5/8 inch I.D. x 7/8 inch O.D. Tygon tubing, 3D-printed impactor to radon generator	n/a
(2) 1.5 ft of 1/2 inch I.D. x 5/8 inch Tygon tubing, each impactor to pump	n/a
Ludlum Measurements Inc. Alpha Beta Sample Counter	Model 3030E
Mirion Gas Proportional Counter	Model LB4200

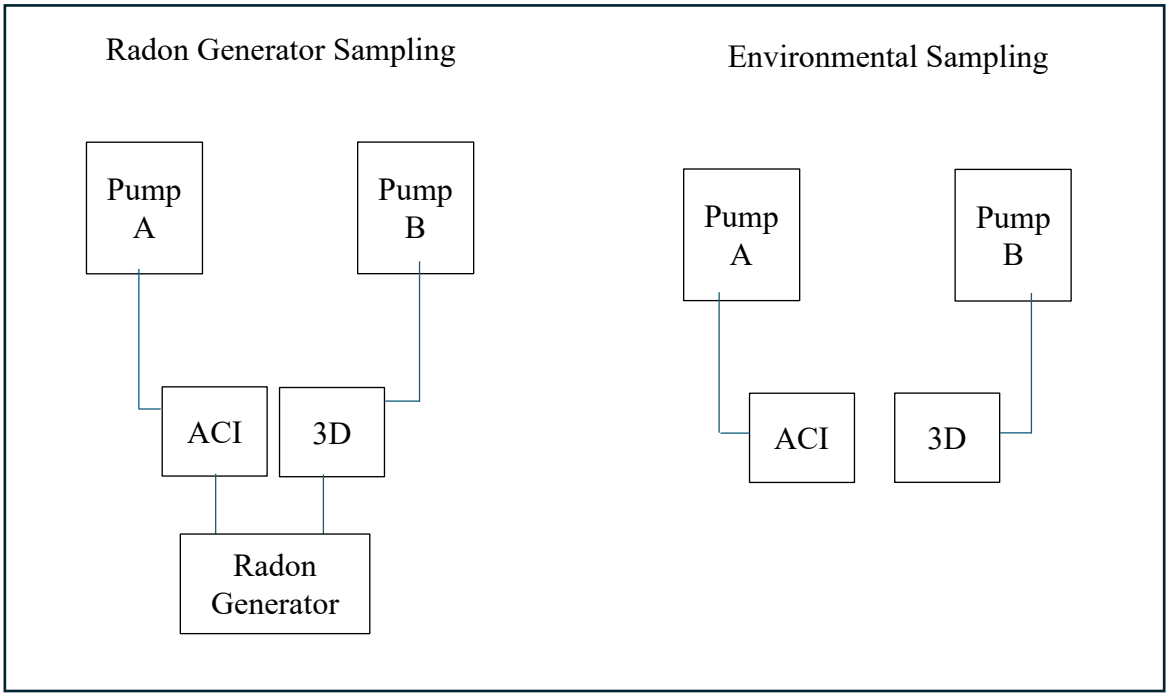

Fig 3.11: Simple air sampling schematic. Tygon tubing was used to connect a vacuum pump to a cascade impactor. If used for sampling from the radon generator, size respective Tygon tubing was used to connect the generator to the inlet of each impactor. No additional Tygon was used for environmental sampling.

As an initial test to see if both cascade impactors could capture radon progeny, each was connected to its respective pump with 1.5 feet of Tygon tubing. Approximately 2 feet of Tygon

tubing, size respective to the inlet of each cascade impactor, was attached to the air inlet of each impactor. The other end was inserted into the radon generator as per Figure 3.11. A radiological air sampling procedure used by Vista Technologies on DOD development projects was obtained from the Nuclear Regulatory Commission (NRC) website (Vista Technologies, NRC, 1999). This was used as a template for the first sampling test. Once the tubing was inserted into the radon generator, the pumps were started in tandem, and a five-minute air sample was drawn. After five minutes, both pumps were secured, and the air samples were allowed to sit for 40 minutes. During the 40-minute wait time, a five-minute background count was completed with the Ludlum 3030E. After 40 minutes, samples were counted, starting with the first stage of each impactor, then the second, and so on. Only one filter could be counted at a time using the Ludlum 3030E.

Subsequent sampling was conducted not in accordance with any procedure in particular. Longer sampling times were used in an attempt to collect more radon progeny. Environmental air sampling was conducted next. The sampling setup was moved outside to the south entrance of the MRB building and set up for environmental sampling per Figure 3.11. Pumps were again turned on in tandem and allowed to draw air for 60 minutes. During this sampling time, quality control checks and a five-minute background count were conducted with a Mirion Model LB4200 gas proportional counter (GPC). The goal during this part of the experiment was to observe the decay curve of the short-lived radon progeny. As such, no wait time was used after samples were collected, as multiple rounds of counting were carried out for each filter. After the 60-minute sample time, each filter was counted with the Mirion GPC. Only one of two counting drawers that fit our 47 mm filters was used for this experiment, and up to four samples could be counted at once. A procedure was used to count for alphas and then betas, each for five minutes. Once all the air filters for both cascade impactors were counted, three additional rounds of counting were

performed. This allowed each filter to be counted four times over approximately two hours. Next, a 60-minute air sample was drawn from the radon generator. Similar to the environmental sampling procedure, filters were counted for alphas and then betas, each for five minutes, using the Mirion Model LB4200 GPC. Again, all filters were counted four times over approximately two hours.

CHAPTER 4: RESULTS

3D Printed Cascade Impactor

Each stage of the 3D-printed cascade impactor is shown in Figures 4.1 – 4.5. A stage together with an impact tray and filter is shown in Figure 4.6. The completely assembled impactor as used for sampling is shown in Figure 4.7. An unused stage 3, printed in the original orientation and not upside-down, is shown in Figure 4.8. This figure demonstrates a rough surface expected to have inhibited particle flow had it been left as the inlet side. An unused printed stage shows an attempt at printing smaller holes in what would have been a subsequent stage, Figure 4.9. Clearly, holes were not actually printed.

Fig 4.1: Stage 0**.**

Fig 4.2: Stage 1**.**

Fig 4.3: Stage 2.

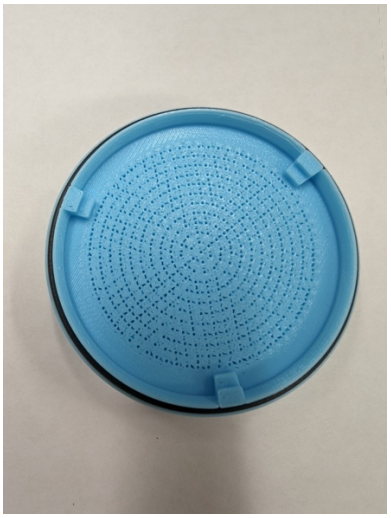

Fig 4.4: Stage 3.

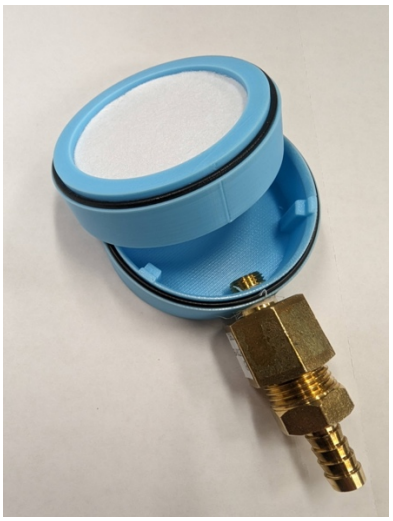

Fig 4.5: Final Stage with Vacuum Chamber.

Fig 4.6: Stage with Impact Tray.

Fig 4.7: Impactor as used for Sampling.

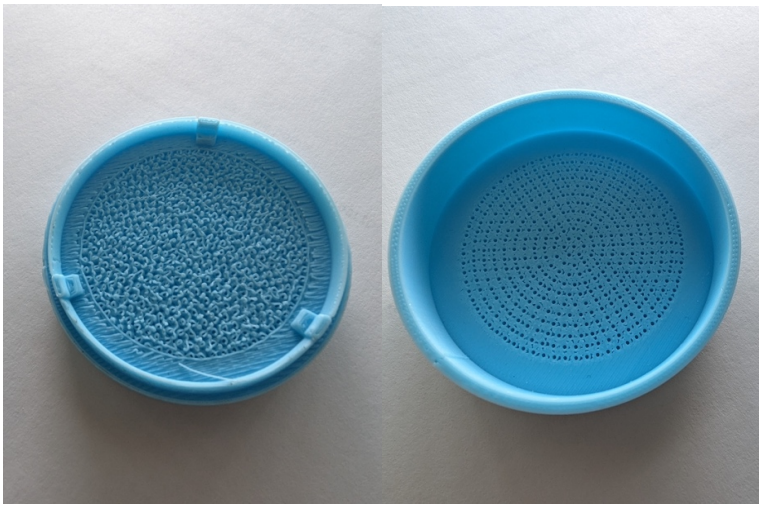

Fig 4.8: Stage Printed in the Original Orientation

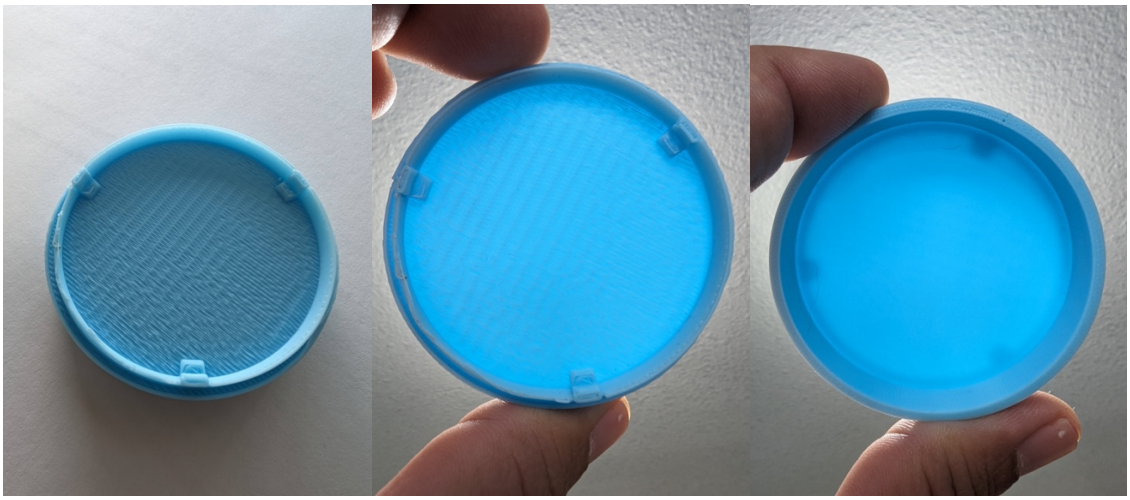

Fig 4.9: Failed Attempt at Stage with Smaller Holes

Air Sampling & Counting

Environmental samples for the ACI and 3D-printed cascade impactor were collected at approximately the same outdoor conditions and the exact geographical location. Temperature was 52 degrees Fahrenheit, pressure at 29.89 inches Hg, humidity at 18.6 %, and wind at approximately 4 MPH from the NE.

Radon Generator & Ludlum 3030E

The results of the initial test, a five-minute sample taken from the radon generator followed by a 40-minute wait, are shown in Table 4.1. Each filter, including the background filter, was counted for five minutes. The documented time is the start time, and all samples were counted individually using the Ludlum 3030E. Alpha and beta total counts were converted to counts per second (CPS) and then to units of activity, becquerel (Bq), using equations 1 and 2.

$$disintegrations\ per\ second\ (dps) = \frac{CPS\ sample - CPS\ background}{Detector\ Efficiency} \quad (1)$$

$$1\ Bq = 1\ dps \quad (2)$$

Stages 2 through 6 for the ACI corresponds to filters 1 through 5. Stage 1 of the ACI did not have an impact tray or filter. Similarly, stages 1 through 3 correspond to filters 1 through 3 of the 3D-printed impactor. Stage 1 of the ACI corresponds to stage 0 of the 3D printed cascade impactor; therefore, no impact tray or filter were used. In both impactors, the final stage corresponds to the final filter utilized to collect all particulates not previously collected and to prevent particulate matter from entering the vacuum pump.

Table 4.1: Radon Generator Samples Counted with Ludlum 3030E

BACKGROUND AND EFFICIENCY									
TIME	ALPHA TOTAL COUNTS	ALPHA CPS	BETA TOTAL COUNTS	BETA CPS		DETECTOR ALPHA EFF	DETECTOR BETA EFF		
1418	2	0.007	368	1.227		0.385	0.195		
COMMERCIAL ACI									
FILTER	TIME	ALPHA TOTAL COUNTS PER LITER	ALPHA CPS-L	ALPHA NET (CPS-L)	ALPHA ACTIVITY (Bq/L)	BETA TOTAL COUNTS PER LITER	BETA CPS-L	BETA NET (CPS-L)	BETA ACTIVITY (Bq/L)
1	1515	0.03535	0.00012	-0.00655	-0.01701	2.32591	0.00775	-1.21891	-6.25084
2	1526	0.06363	0.00021	-0.00645	-0.01677	2.22694	0.00742	-1.21924	-6.25253
3	1537	0.02828	0.00009	-0.00657	-0.01707	2.72888	0.00910	-1.21757	-6.24395
4	1548	0.04242	0.00014	-0.00653	-0.01695	2.57335	0.00858	-1.21809	-6.24661
5	1554	0.05656	0.00019	-0.00648	-0.01683	2.63697	0.00879	-1.21788	-6.24552
FINAL	1559	0.10604	0.00035	-0.00631	-0.01640	2.52386	0.00841	-1.21825	-6.24746
3D-PRINTED CASCADE IMPACTOR									
FILTER	TIME	ALPHA TOTAL COUNTS PER LITER	ALPHA CPS-L	ALPHA NET (CPS-L)	ALPHA ACTIVITY (Bq/L)	BETA TOTAL COUNTS PER LITER	BETA CPS-L	BETA NET (CPS-L)	BETA ACTIVITY (Bq/L)
1	1510	0.16064	0.00054	-0.00613	-0.01593	4.49799	0.01499	-1.21167	-6.21371
2	1520	0.40161	0.00134	-0.00533	-0.01384	4.09639	0.01365	-1.21301	-6.22057
3	1532	0.29834	0.00099	-0.00567	-0.01473	4.33735	0.01446	-1.21221	-6.21646
FINAL	1543	0.22949	0.00076	-0.00590	-0.01533	0.40161	0.00134	-1.22533	-6.28373

Environmental Air Sampling & Mirion LB4200

The environmental sampling results for the commercial ACI and the 3D-printed cascade impactor are summarized in Table 4.2 and Table 4.3, respectively. Each round of counting, after round 1, represents a subsequent count of the same filter. All filters from the commercial ACI were counted with either detector 1 or 2 from tray B of the Mirion LB4200 (detector B1 or B2). Similarly, all filters from the 3D-printed cascade impactor were counted with either detector 3 or 4 from tray B of the Mirion LB4200 (detector B3 or B4). Counting results were selected to output in counts per minute (CPM) and were subsequently converted to activity in becquerels using equations 1 and 2. Detector efficiencies used to convert counts to activity are listed in their respective data tables. The alpha and beta activity decay curves for all filters in each impactor are shown in Figures 4.10 – 4.13. These figures are separated by radiation type and the applicable

impactor that collected them. To compare the activity collected by each stage, Figures 4.14 – 4.21 are included. Similarly, these figures were also separated by radiation type; however, samples were compared by their respective location within the cascade impactor. Stages 4 and 5 of the ACI were not used in this comparison since their small hole size did not correspond with any stage in the 3D-printed model. In both cases, the final filter was used to capture any particulate matter that flowed through all other stages; thus, these filters were compared. With the exception of the final filters, compared filters from each impactor were counted at the same time, thus representing the same time interval since sample collection. Some bias exists in the final filter comparison as they do not represent the exact same activity decay time frame. Since specific radionuclides were not identified in this experiment, no activity decay corrections were calculated.

Table 4.2: Environmental Sampling – ACI

BACKGROUND AND EFFICIENCY											
TIME	ALPHA CPM	ALPHA CPS	BETA CPM	BETA CPS	DETECTOR	ALPHA EFF	ALPHA U(E) (+/-)	BETA Eff	BETA U(E) (+/-)	(ALPHA EFF)^2	(BETA EFF)^2
1031	0	0.0	4.4	0.07	B1	0.345	0.013	0.515	0.019	0.119	0.265
1031	0	0.0	4.4	0.07	B2	0.352	0.013	0.525	0.020	0.124	0.276
ROUND 1											
FILTER	TIME	ALPHA CPM-L	ALPHA CPS-L	ALPHA NET (CPS-L)	ALPHA ACTIVITY (Bq/L)	BETA CPM-L	BETA CPS-L	BETA NET (CPS-L)	BETA ACTIVITY (Bq/L)	ALPHA UNC	BETA UNC
1	1135	0.00059	0.00001	0.00001	0.00003	0.00306	0.00005	-0.07328	-0.14230	0.0000004	0.0000255
2	1135	0.00094	0.00002	0.00002	0.00004	0.00082	0.00001	-0.07332	-0.13966	0.0000005	0.0000250
3	1149	0.00012	0.00000	0.00000	0.00001	0.00271	0.00005	-0.07329	-0.14231	0.0000002	0.0000255
4	1149	0.00047	0.00001	0.00001	0.00002	0.00141	0.00002	-0.07331	-0.13964	0.0000004	0.0000250
5	1203	0.00094	0.00002	0.00002	0.00005	0.00177	0.00003	-0.07330	-0.14234	0.0000006	0.0000255
FINAL	1203	0.00648	0.00011	0.00011	0.00031	0.01850	0.00031	-0.07303	-0.13910	0.0000014	0.0000249
ROUND 2											
FILTER	TIME	ALPHA CPM-L	ALPHA CPS-L	ALPHA NET (CPS-L)	ALPHA ACTIVITY (Bq/L)	BETA CPM-L	BETA CPS-L	BETA NET (CPS-L)	BETA ACTIVITY (Bq/L)	ALPHA UNC	BETA UNC
1	1215	0.00047	0.00001	0.00001	0.00002	0.00236	0.00004	-0.07329	-0.14232	0.0000004	0.0000255
2	1215	0.00047	0.00001	0.00001	0.00002	0.00118	0.00002	-0.07331	-0.13965	0.0000004	0.0000250
3	1228	0.00047	0.00001	0.00001	0.00002	0.00224	0.00004	-0.07330	-0.14232	0.0000004	0.0000255
4	1228	0.00012	0.00000	0.00000	0.00001	0.00247	0.00004	-0.07329	-0.13960	0.0000002	0.0000250
5	1241	0.00059	0.00001	0.00001	0.00003	0.00236	0.00004	-0.07329	-0.14232	0.0000004	0.0000255
FINAL	1241	0.00318	0.00005	0.00005	0.00015	0.00825	0.00014	-0.07320	-0.13942	0.0000010	0.0000250
ROUND 3											
FILTER	TIME	ALPHA CPM-L	ALPHA CPS-L	ALPHA NET (CPS-L)	ALPHA ACTIVITY (Bq/L)	BETA CPM-L	BETA CPS-L	BETA NET (CPS-L)	BETA ACTIVITY (Bq/L)	ALPHA UNC	BETA UNC
1	1253	0.00024	0.00000	0.00000	0.00001	0.00165	0.00003	-0.07331	-0.14234	0.0000003	0.0000255
2	1253	0.00071	0.00001	0.00001	0.00003	0.00189	0.00003	-0.07330	-0.13962	0.0000005	0.0000250
3	1305	0.00012	0.00000	0.00000	0.00001	0.00295	0.00005	-0.07328	-0.14230	0.0000002	0.0000255
4	1305	0.00024	0.00000	0.00000	0.00001	0.00377	0.00006	-0.07327	-0.13956	0.0000003	0.0000250
5	1318	0.00035	0.00001	0.00001	0.00002	0.00330	0.00005	-0.07328	-0.14229	0.0000003	0.0000255
FINAL	1318	0.00118	0.00002	0.00002	0.00006	0.00860	0.00014	-0.07319	-0.13941	0.0000006	0.0000250
ROUND 4											
FILTER	TIME	ALPHA CPM-L	ALPHA CPS-L	ALPHA NET (CPS-L)	ALPHA ACTIVITY (Bq/L)	BETA CPM-L	BETA CPS-L	BETA NET (CPS-L)	BETA ACTIVITY (Bq/L)	ALPHA UNC	BETA UNC
1	1331	0.00024	0.00000	0.00000	0.00001	0.00259	0.00004	-0.07329	-0.14231	0.0000003	0.0000255
2	1331	0.00024	0.00000	0.00000	0.00001	0.00295	0.00005	-0.07328	-0.13959	0.0000003	0.0000250
3	1343	0.00047	0.00001	0.00001	0.00002	0.00330	0.00005	-0.07328	-0.14229	0.0000004	0.0000255
4	1343	0.00082	0.00001	0.00001	0.00004	0.00130	0.00002	-0.07331	-0.13964	0.0000005	0.0000250
5	1356	0.00106	0.00002	0.00002	0.00005	0.00412	0.00007	-0.07326	-0.14226	0.0000006	0.0000255
FINAL	1356	0.00153	0.00003	0.00003	0.00007	0.00353	0.00006	-0.07327	-0.13957	0.0000007	0.0000250

Table 4.3: Environmental Sampling – 3D-Printed Cascade Impactor

BACKGROUND AND EFFICIENCY											
TIME	ALPHA CPM	ALPHA CPS	BETA CPM	BETA CPS	DETCETOR	ALPHA EFF	ALPHA U(E) (+/-)	BETA EFF	BETA U(E) (+/-)	$(\text{ALPHA EFF})^2$	$(\text{BETA EFF})^2$
1031	0	0.0	3.4	0.06	B3	0.346	0.013	0.511	0.019	0.120	0.261
1031	0	0.0	3.2	0.05	B4	0.353	0.013	0.518	0.019	0.125	0.268
ROUND 1											
FILTER	TIME	ALPHA CPM-L	ALPHA CPS-L	ALPHA NET (CPS-L)	ALPHA ACTIVITY (Bq/L)	BETA CPM-L	BETA CPS-L	BETA NET (CPS-L)	BETA ACTIVITY (Bq/L)	ALPHA UNC	BETA UNC
1	1135	0.00115	0.00002	0.00002	0.00006	0.00516	0.00009	-0.05658	-0.11073	0.000001	0.000037
2	1135	0.00038	0.00001	0.00001	0.00002	0.00210	0.00004	-0.05330	-0.10289	0.000001	0.000035
3	1149	0.00019	0.00000	0.00000	0.00001	0.00344	0.00006	-0.05661	-0.11078	0.000000	0.000037
FINAL	1149	0.00727	0.00012	0.00012	0.00034	0.03098	0.00052	-0.05282	-0.10196	0.000002	0.000035
ROUND 2											
FILTER	TIME	ALPHA CPM-L	ALPHA CPS-L	ALPHA NET (CPS-L)	ALPHA ACTIVITY (Bq/L)	BETA CPM-L	BETA CPS-L	BETA NET (CPS-L)	BETA ACTIVITY (Bq/L)	ALPHA UNC	BETA UNC
1	1215	0.00096	0.00002	0.00002	0.00005	0.00516	0.00009	-0.05658	-0.11073	0.000001	0.000037
2	1215	0.00057	0.00001	0.00001	0.00003	0.00363	0.00006	-0.05327	-0.10284	0.000001	0.000035
3	1228	0.00057	0.00001	0.00001	0.00003	0.00306	0.00005	-0.05662	-0.11079	0.000001	0.000037
FINAL	1228	0.00363	0.00006	0.00006	0.00017	0.01281	0.00021	-0.05312	-0.10255	0.000002	0.000035
ROUND 3											
FILTER	TIME	ALPHA CPM-L	ALPHA CPS-L	ALPHA NET (CPS-L)	ALPHA ACTIVITY (Bq/L)	BETA CPM-L	BETA CPS-L	BETA NET (CPS-L)	BETA ACTIVITY (Bq/L)	ALPHA UNC	BETA UNC
1	1253	0.00096	0.00002	0.00002	0.00005	0.00421	0.00007	-0.05660	-0.11076	0.000001	0.000037
2	1253	0.00115	0.00002	0.00002	0.00005	0.00229	0.00004	-0.05330	-0.10289	0.000001	0.000035
3	1305	0.00134	0.00002	0.00002	0.00006	0.00287	0.00005	-0.05662	-0.11080	0.000001	0.000037
FINAL	1305	0.00363	0.00006	0.00006	0.00017	0.00727	0.00012	-0.05321	-0.10273	0.000002	0.000035
ROUND 4											
FILTER	TIME	ALPHA CPM-L	ALPHA CPS-L	ALPHA NET (CPS-L)	ALPHA ACTIVITY (Bq/L)	BETA CPM-L	BETA CPS-L	BETA NET (CPS-L)	BETA ACTIVITY (Bq/L)	ALPHA UNC	BETA UNC
1	1331	0.00115	0.00002	0.00002	0.00006	0.00516	0.00009	-0.05658	-0.11073	0.000001	0.000037
2	1331	0.00115	0.00002	0.00002	0.00005	0.00402	0.00007	-0.05327	-0.10283	0.000001	0.000035
3	1343	0.00172	0.00003	0.00003	0.00008	0.00478	0.00008	-0.05659	-0.11074	0.000001	0.000037
FINAL	1343	0.00153	0.00003	0.00003	0.00007	0.00784	0.00013	-0.05320	-0.10271	0.000001	0.000035

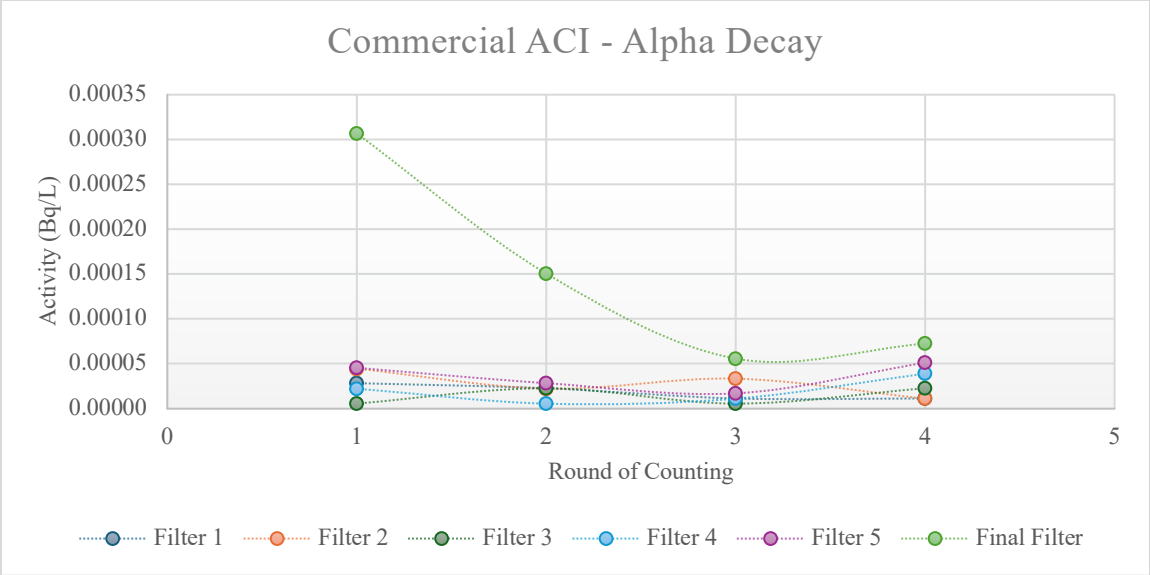

Fig 4.10: Environmental Sampling Alpha Decay Curves

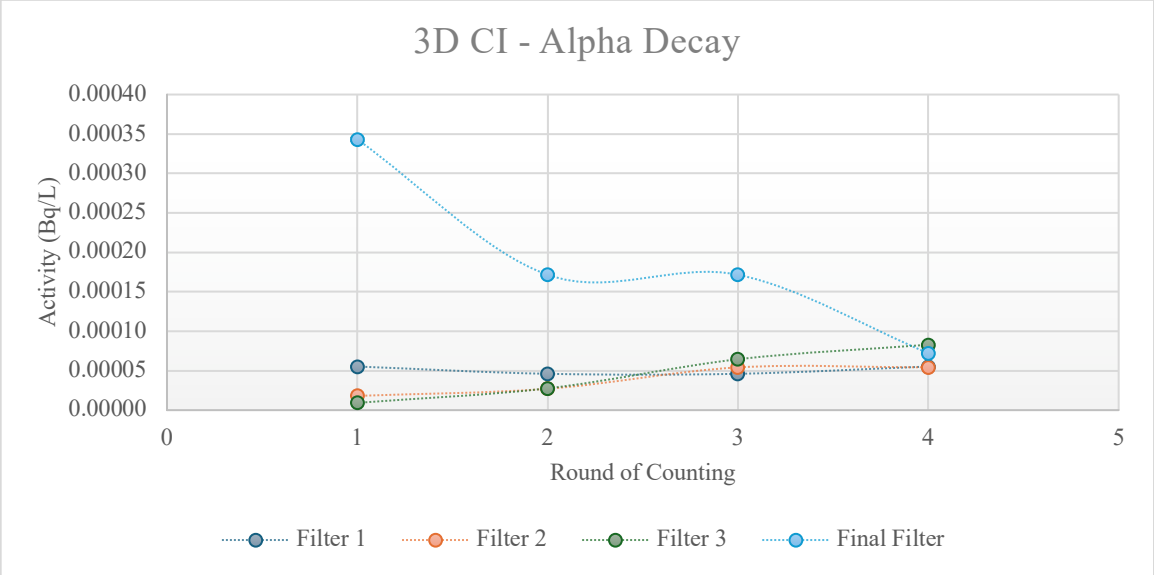

Fig 4.11: Environmental Sampling Alpha Decay Curves

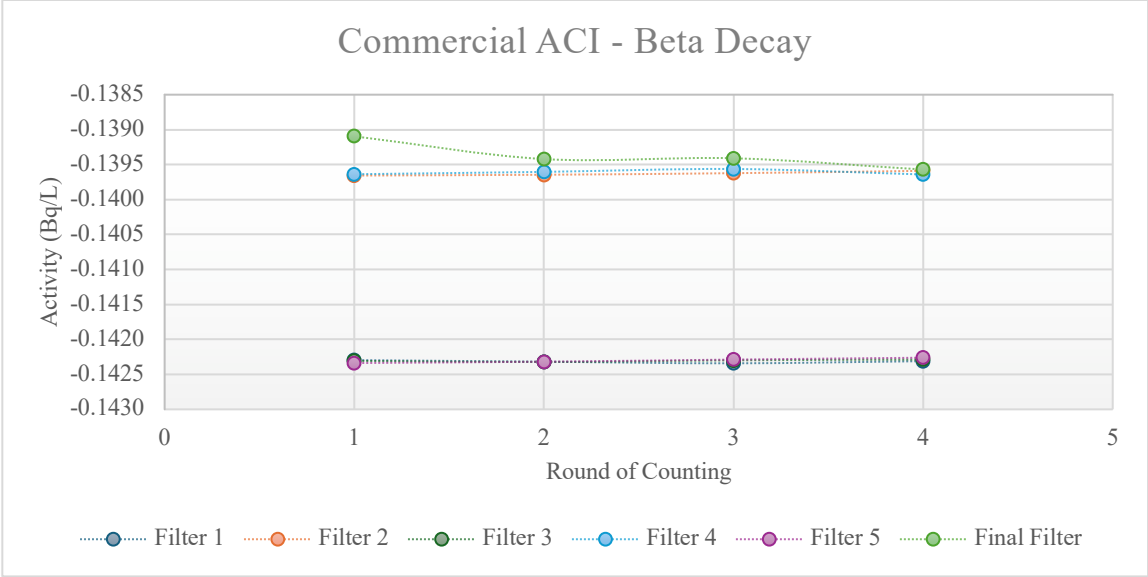

Fig 4.12: Environmental Sampling Beta Decay Curves

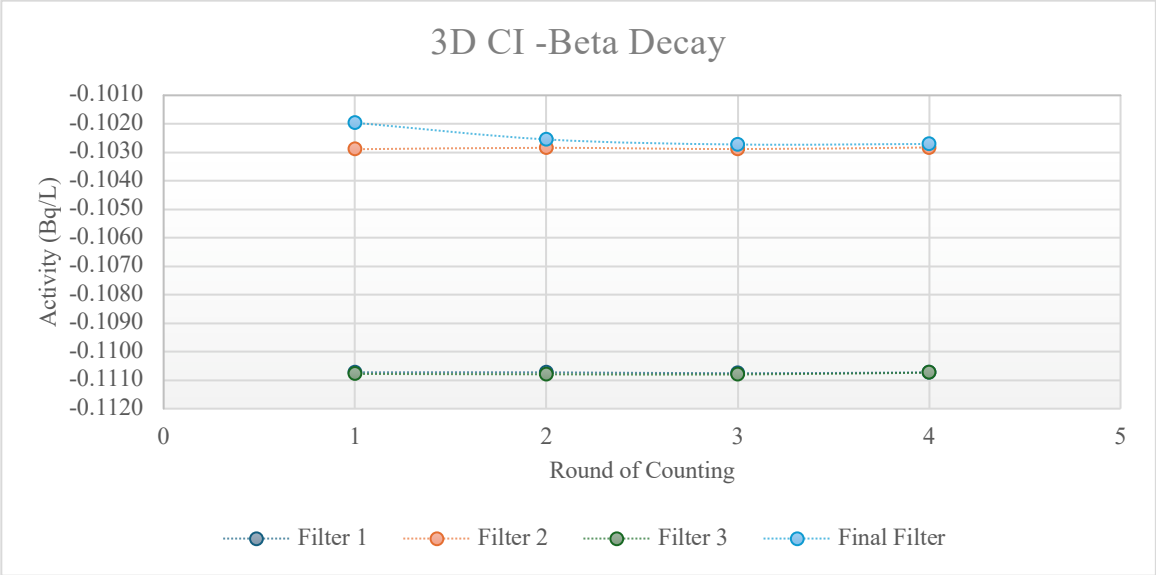

Fig 4.13: Environmental Sampling Beta Decay Curves

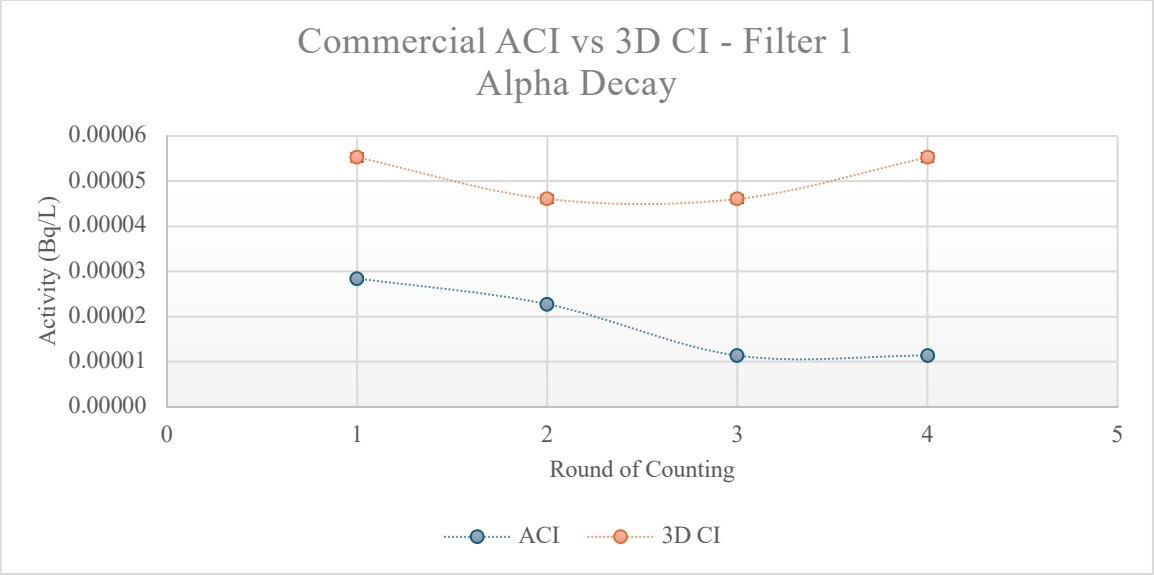

Fig 4.14: Environmental Sampling Filter 1 Alpha Activity Decay Curves

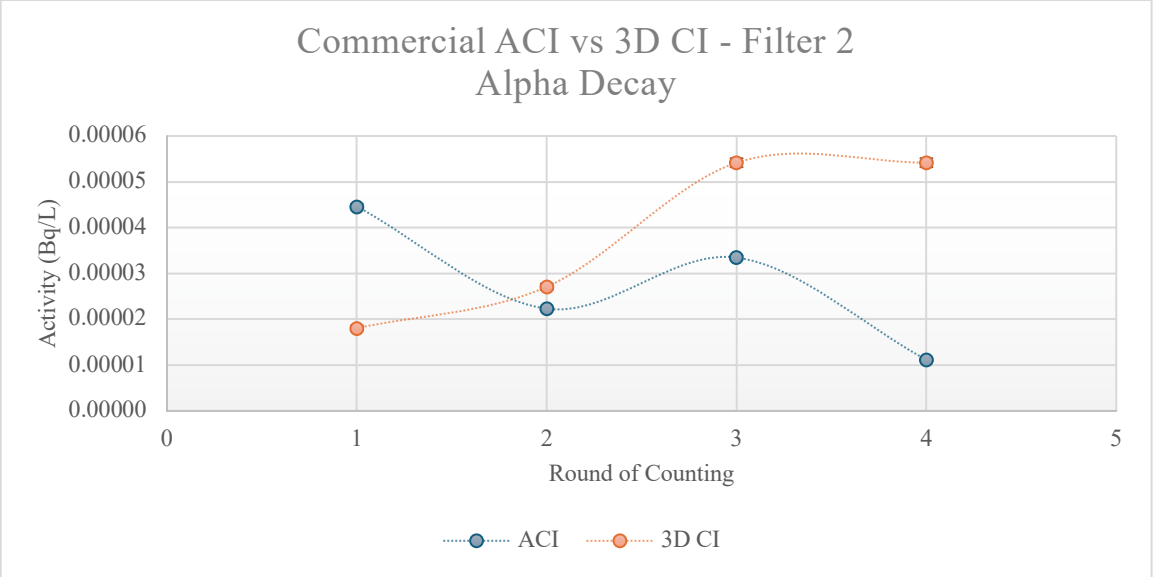

Fig 4.15: Environmental Sampling Filter 2 Alpha Activity Decay Curves

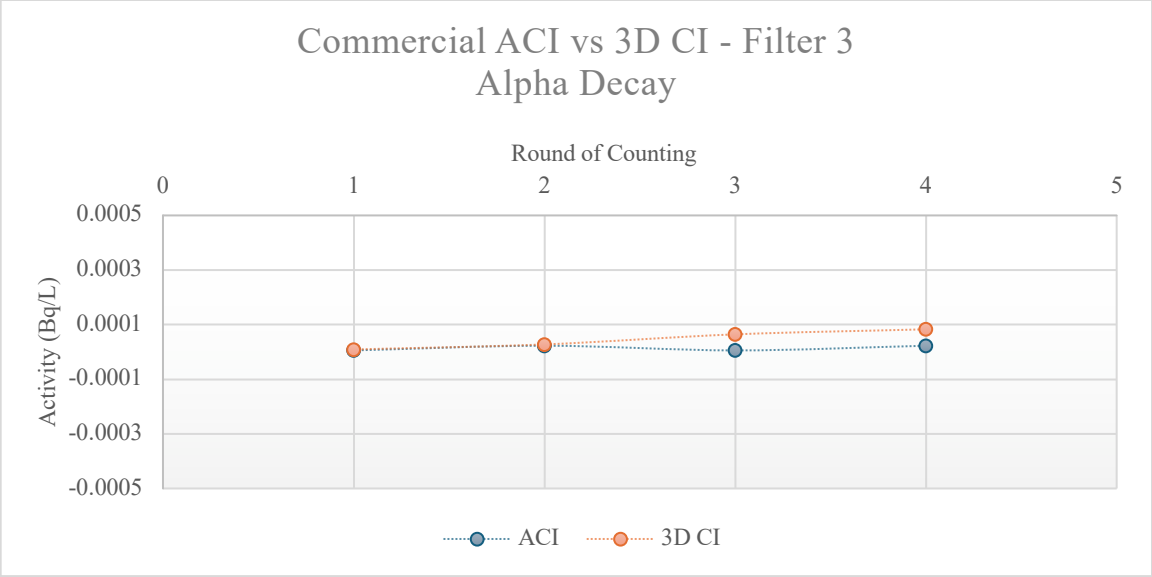

Fig 4.16: Environmental Sampling Filter 3 Alpha Activity Decay Curves

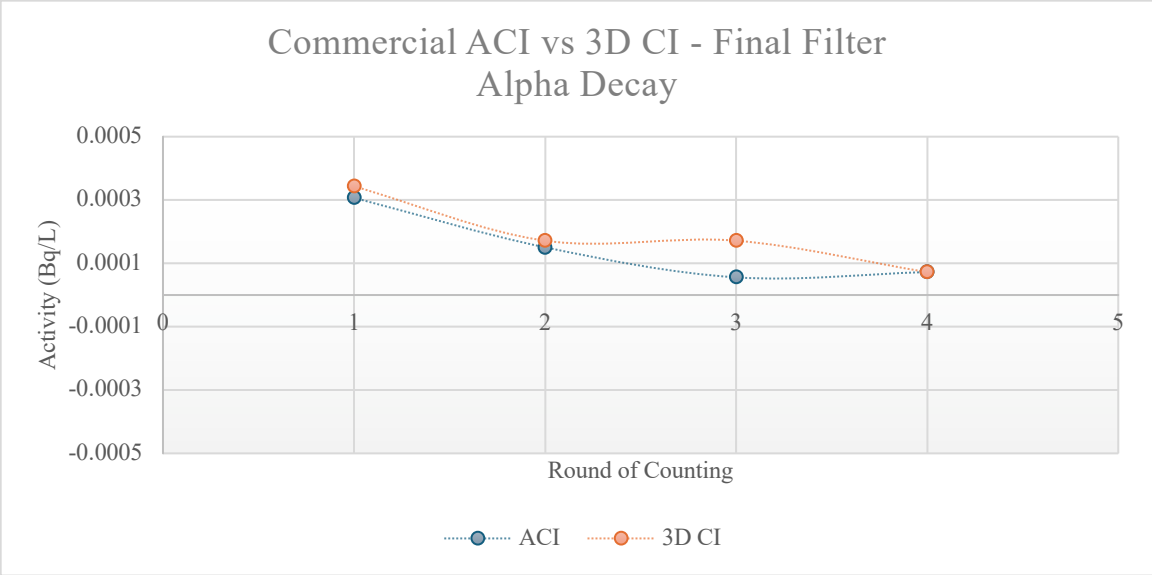

Fig 4.17: Environmental Sampling Final Filter Alpha Activity Decay Curves

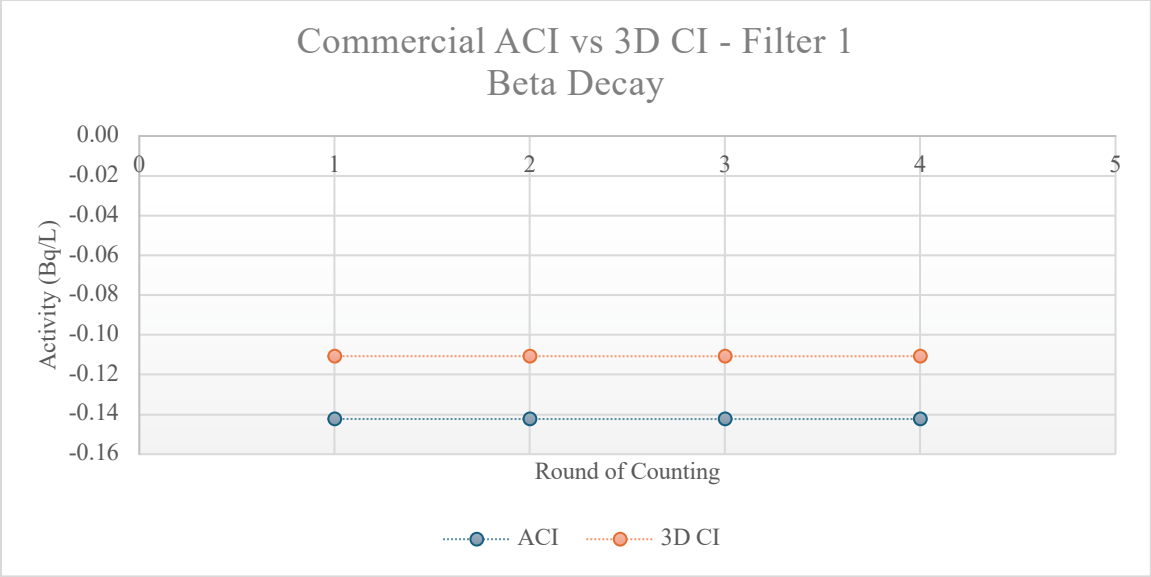

Fig 4.18: Environmental Sampling Filter 1 Beta Activity Decay Curves

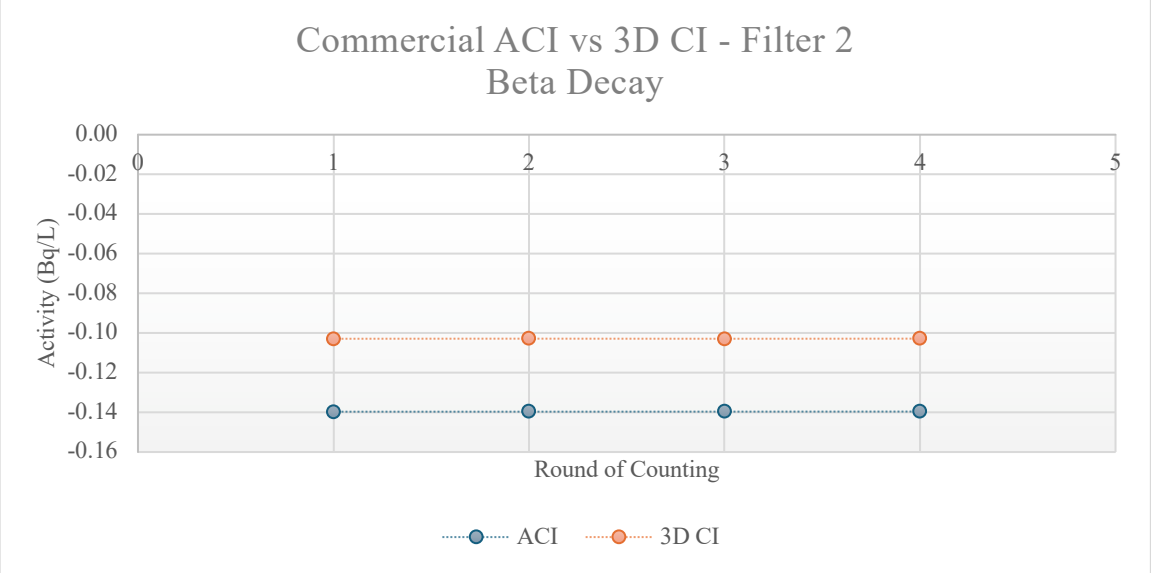

Fig 4.19: Environmental Sampling Filter 2 Beta Activity Decay Curves

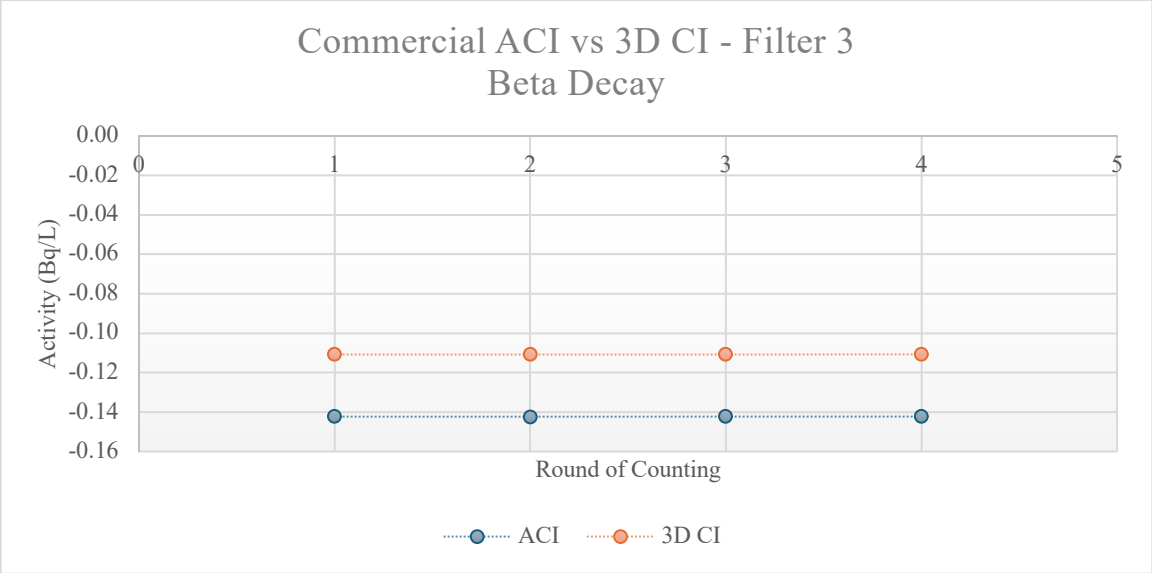

Fig 4.20: Environmental Sampling Filter 3 Beta Activity Decay Curves

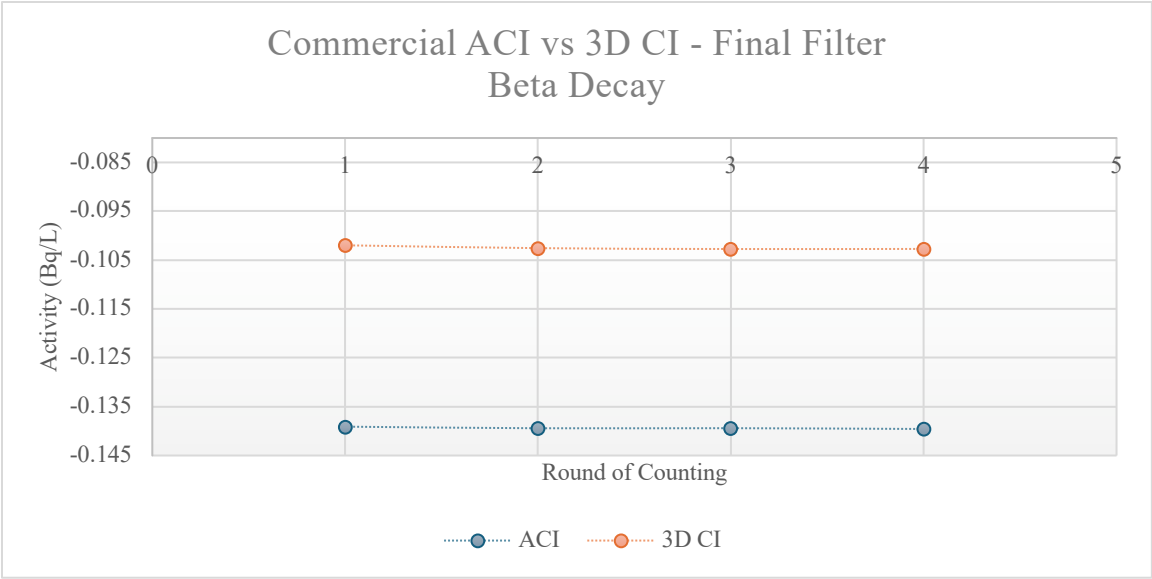

Fig 4.21: Environmental Sampling Final Filter Beta Activity Decay Curves

Radon Generator Sampling & Mirion LB4200

Radon generator sampling in this part of the experiment was completed exactly as discussed above for the 60-minute environmental sampling. Results are per Tables 4.4 and 4.5 and Figures 4.22 – 4.33.

Table 4.4: Radon Generator Sampling – Commercial ACI

BACKGROUND AND EFFICIENCY											
TIME	ALPHA CPM	ALPHA CPS	BETA CPM	BETA CPS	DETECTOR	ALPHA EFF	ALPHA U(E) (+/-)	BETA EFF	BETA U(E) (+/-)	(ALPHA EFF)^2	(BETA EFF)^2
1031	0	0.00	4.4	0.07	B1	0.35	0.01	0.52	0.02	0.12	0.27
1031	0	0.00	4.4	0.07	B2	0.35	0.01	0.53	0.02	0.12	0.28
ROUND 1											
FILTER	TIME	ALPHA CPM-L	ALPHA CPS-L	ALPHA NET (CPS-L)	ALPHA ACTIVITY (Bq/L)	BETA CPM-L	BETA CPS-L	BETA NET (CPS-L)	BETA ACTIVITY (Bq/L)	ALPHA UNC	BETA UNC
1	1411	0.00189	0.00003	0.00003	0.00009	0.00636	0.00011	-0.07323	-0.14219	0.0000008	0.0000255
2	1411	0.00212	0.00004	0.00004	0.00010	0.00483	0.00008	-0.07325	-0.13953	0.0000008	0.0000250
3	1424	0.00094	0.00002	0.00002	0.00005	0.00283	0.00005	-0.07329	-0.14230	0.0000006	0.0000255
4	1424	0.00082	0.00001	0.00001	0.00004	0.00342	0.00006	-0.07328	-0.13957	0.0000005	0.0000250
5	1437	0.00047	0.00001	0.00001	0.00002	0.00389	0.00006	-0.07327	-0.14227	0.0000004	0.0000255
FINAL	1437	0.00071	0.00001	0.00001	0.00003	0.00283	0.00005	-0.07329	-0.13959	0.0000005	0.0000250
ROUND 2											
FILTER	TIME	ALPHA CPM-L	ALPHA CPS-L	ALPHA NET (CPS-L)	ALPHA ACTIVITY (Bq/L)	BETA CPM-L	BETA CPS-L	BETA NET (CPS-L)	BETA ACTIVITY (Bq/L)	ALPHA UNC	BETA UNC
1	1449	0.00130	0.00002	0.00002	0.00006	0.00719	0.00012	-0.07321	-0.14216	0.0000006	0.0000255
2	1449	0.00118	0.00002	0.00002	0.00006	0.00330	0.00005	-0.07328	-0.13958	0.0000006	0.0000250
3	1501	0.00106	0.00002	0.00002	0.00005	0.00283	0.00005	-0.07329	-0.14230	0.0000006	0.0000255
4	1501	0.00047	0.00001	0.00001	0.00002	0.00306	0.00005	-0.07328	-0.13959	0.0000004	0.0000250
5	1513	0.00012	0.00000	0.00000	0.00001	0.00342	0.00006	-0.07328	-0.14228	0.0000002	0.0000255
FINAL	1513	0.00059	0.00001	0.00001	0.00003	0.00212	0.00004	-0.07330	-0.13962	0.0000004	0.0000250
ROUND 3											
FILTER	TIME	ALPHA CPM-L	ALPHA CPS-L	ALPHA NET (CPS-L)	ALPHA ACTIVITY (Bq/L)	BETA CPM-L	BETA CPS-L	BETA NET (CPS-L)	BETA ACTIVITY (Bq/L)	ALPHA UNC	BETA UNC
1	1525	0.00082	0.00001	0.00001	0.00004	0.00424	0.00007	-0.07326	-0.14226	0.0000005	0.0000255
2	1525	0.00071	0.00001	0.00001	0.00003	0.00460	0.00008	-0.07326	-0.13954	0.0000005	0.0000250
3	1537	0.00059	0.00001	0.00001	0.00003	0.00271	0.00005	-0.07329	-0.14231	0.0000004	0.0000255
4	1537	0.00094	0.00002	0.00002	0.00004	0.00236	0.00004	-0.07329	-0.13961	0.0000005	0.0000250
5	1549	0.00071	0.00001	0.00001	0.00003	0.00212	0.00004	-0.07330	-0.14233	0.0000005	0.0000255
FINAL	1549	0.00035	0.00001	0.00001	0.00002	0.00283	0.00005	-0.07329	-0.13959	0.0000003	0.0000250
ROUND 4											
FILTER	TIME	ALPHA CPM-L	ALPHA CPS-L	ALPHA NET (CPS-L)	ALPHA ACTIVITY (Bq/L)	BETA CPM-L	BETA CPS-L	BETA NET (CPS-L)	BETA ACTIVITY (Bq/L)	ALPHA UNC	BETA UNC
1	1601	0.00035	0.00001	0.00001	0.00002	0.00306	0.00005	-0.07328	-0.14230	0.0000003	0.0000255
2	1601	0.00094	0.00002	0.00002	0.00004	0.00295	0.00005	-0.07328	-0.13959	0.0000005	0.0000250

3	1614	0.00035	0.00001	0.00001	0.00002	0.00330	0.00005	-0.07328	-0.14229	0.0000003	0.0000255
4	1614	0.00047	0.00001	0.00001	0.00002	0.00247	0.00004	-0.07329	-0.13960	0.0000004	0.0000250
5	1626	0.00082	0.00001	0.00001	0.00004	0.00259	0.00004	-0.07329	-0.14231	0.0000005	0.0000255
FINAL	1626	0.00047	0.00001	0.00001	0.00002	0.00330	0.00005	-0.07328	-0.13958	0.0000004	0.0000250

Table 4.5: Radon Generator Sampling – 3D-Printed Cascade Impactor

BACKGROUND AND EFFICIENCY											
TIME	ALPHA CPM	ALPHA CPS	BETA CPM	BETA CPS	DETECTOR	ALPHA EFF	ALPHA U(E) (+/-)	BETA EFF	BETA U(E) (+/-)	$(\text{ALPHA EFF})^2$	$(\text{BETA EFF})^2$
1031	0	0.00	3.40	0.06	B3	0.35	0.01	0.51	0.02	0.12	0.26
1031	0	0.00	3.20	0.05	B4	0.35	0.01	0.52	0.02	0.12	0.27
ROUND 1											
FILTER	TIME	ALPHA CPM-L	ALPHA CPS-L	ALPHA NET (CPS-L)	ALPHA ACTIVITY (Bq/L)	BETA CPM-L	BETA CPS-L	BETA NET (CPS-L)	BETA ACTIVITY (Bq/L)	ALPHA UNC	BETA UNC
1	1411	0.00153	0.00003	0.00003	0.00007	0.00440	0.00007	-0.05659	-0.11075	0.0000011	0.0000366
2	1411	0.00076	0.00001	0.00001	0.00004	0.00325	0.00005	-0.05328	-0.10286	0.0000008	0.0000350
3	1424	0.00038	0.00001	0.00001	0.00002	0.00306	0.00005	-0.05662	-0.11079	0.0000006	0.0000366
FINAL	1424	0.00287	0.00005	0.00005	0.00014	0.00880	0.00015	-0.05319	-0.10268	0.0000015	0.0000349
ROUND 2											
FILTER	TIME	ALPHA CPM-L	ALPHA CPS-L	ALPHA NET (CPS-L)	ALPHA ACTIVITY (Bq/L)	BETA CPM-L	BETA CPS-L	BETA NET (CPS-L)	BETA ACTIVITY (Bq/L)	ALPHA UNC	BETA UNC
1	1449	0.00153	0.00003	0.00003	0.00007	0.00765	0.00013	-0.05654	-0.11064	0.0000011	0.0000365
2	1449	0.00057	0.00001	0.00001	0.00003	0.00229	0.00004	-0.05330	-0.10289	0.0000007	0.0000350
3	1501	0.00057	0.00001	0.00001	0.00003	0.00421	0.00007	-0.05660	-0.11076	0.0000007	0.0000366
FINAL	1501	0.00115	0.00002	0.00002	0.00005	0.00918	0.00015	-0.05318	-0.10266	0.0000010	0.0000349
ROUND 3											
FILTER	TIME	ALPHA CPM-L	ALPHA CPS-L	ALPHA NET (CPS-L)	ALPHA ACTIVITY (Bq/L)	BETA CPM-L	BETA CPS-L	BETA NET (CPS-L)	BETA ACTIVITY (Bq/L)	ALPHA UNC	BETA UNC
1	1525	0.00249	0.00004	0.00004	0.00012	0.00478	0.00008	-0.05659	-0.11074	0.0000015	0.0000366
2	1525	0.00019	0.00000	0.00000	0.00001	0.00344	0.00006	-0.05328	-0.10285	0.0000004	0.0000350
3	1537	0.00096	0.00002	0.00002	0.00005	0.00612	0.00010	-0.05656	-0.11069	0.0000009	0.0000365
FINAL	1537	0.00191	0.00003	0.00003	0.00009	0.00631	0.00011	-0.05323	-0.10276	0.0000012	0.0000350
ROUND 4											
FILTER	TIME	ALPHA CPM-L	ALPHA CPS-L	ALPHA NET (CPS-L)	ALPHA ACTIVITY (Bq/L)	BETA CPM-L	BETA CPS-L	BETA NET (CPS-L)	BETA ACTIVITY (Bq/L)	ALPHA UNC	BETA UNC
1	1601	0.00191	0.00003	0.00003	0.00009	0.00535	0.00009	-0.05658	-0.11072	0.0000013	0.0000366
2	1601	0.00115	0.00002	0.00002	0.00005	0.00440	0.00007	-0.05326	-0.10282	0.0000010	0.0000350
3	1614	0.00134	0.00002	0.00002	0.00006	0.00268	0.00004	-0.05662	-0.11081	0.0000011	0.0000366
FINAL	1614	0.00038	0.00001	0.00001	0.00002	0.00421	0.00007	-0.05326	-0.10282	0.0000006	0.0000350

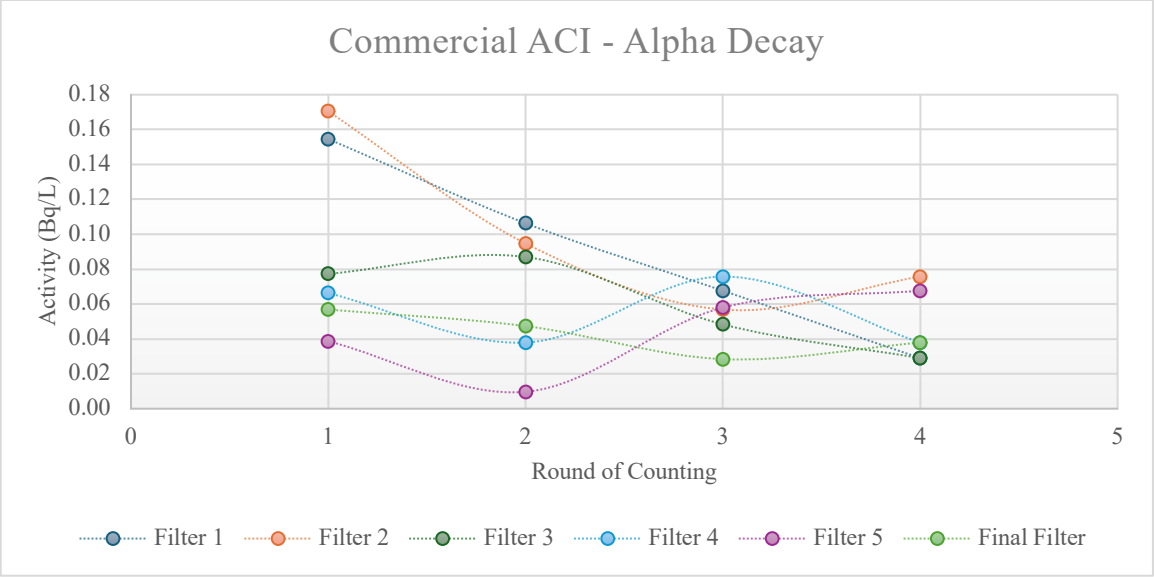

Fig 4.22: Radon Generator Alpha Decay Curves

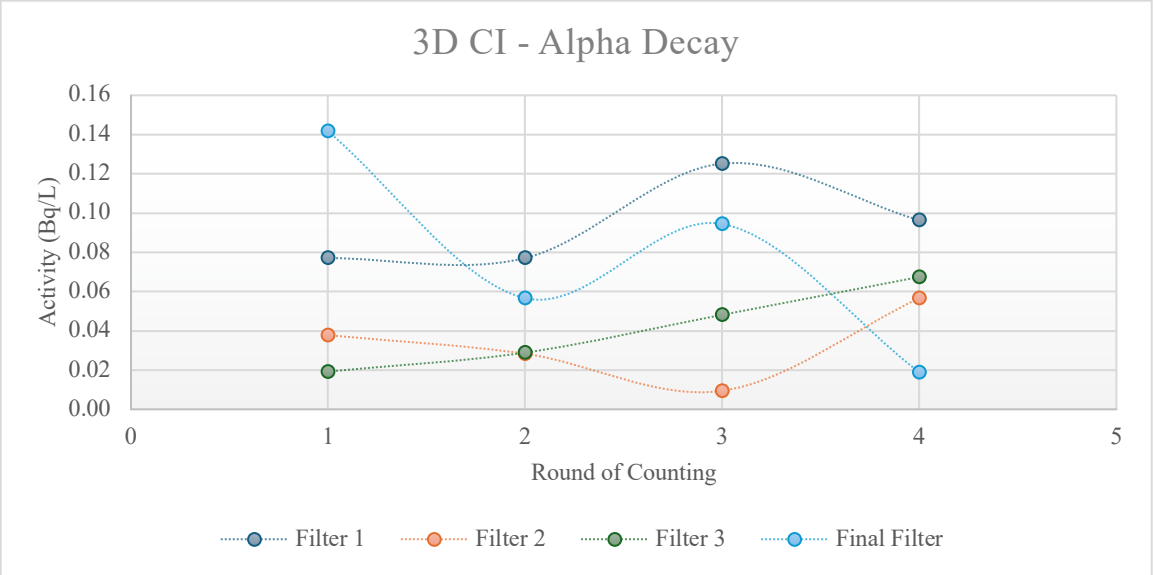

Fig 4.23: Radon Generator Alpha Decay Curves

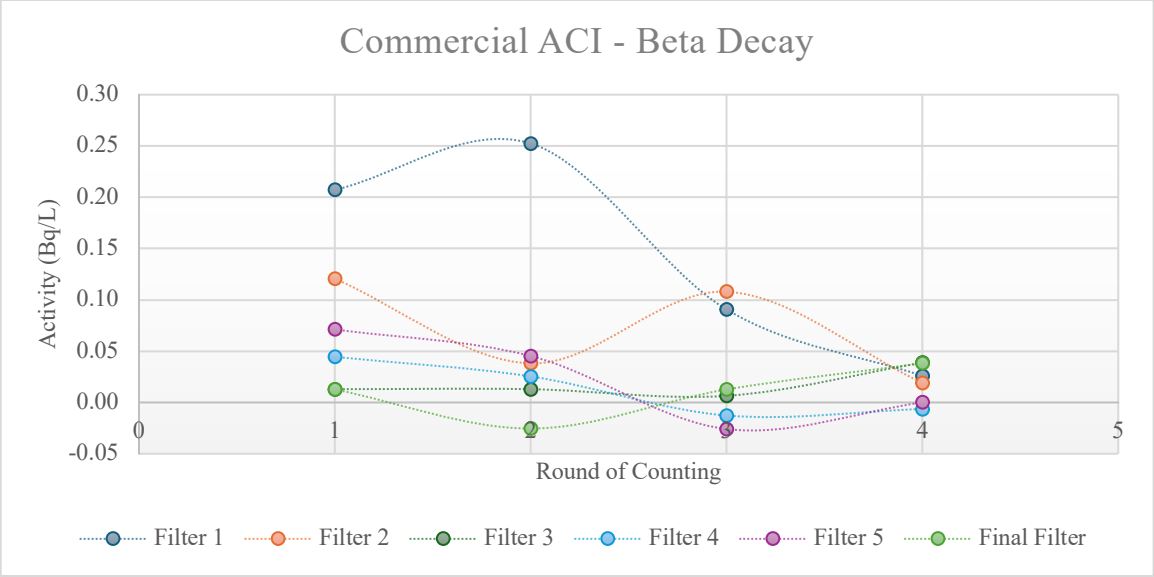

Fig 4.24: Radon Generator Beta Decay Curves

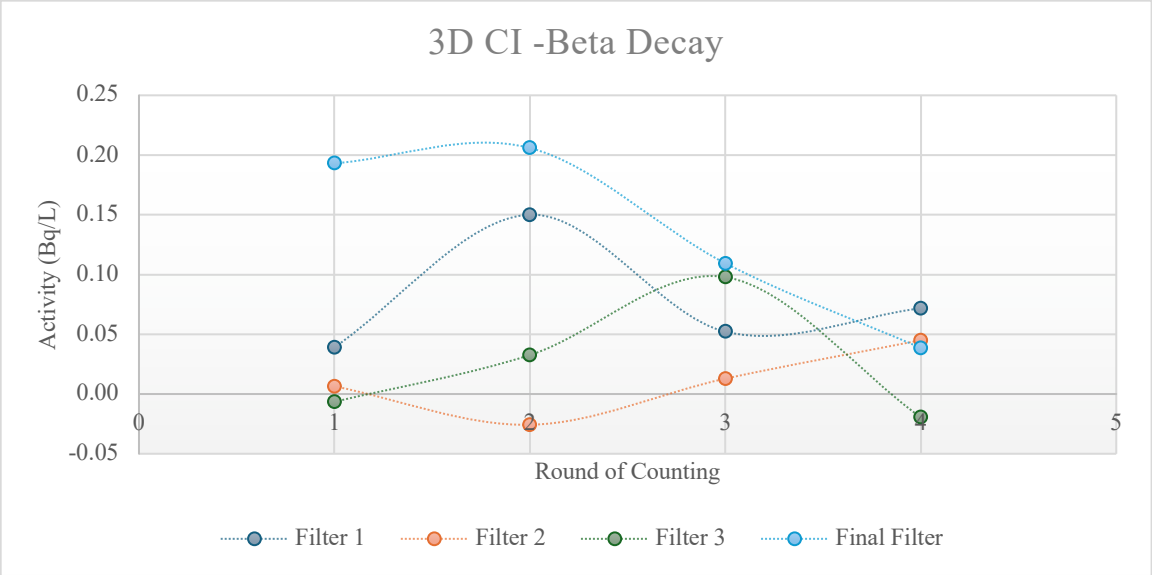

Fig 4.25: Radon Generator Beta Decay Curves

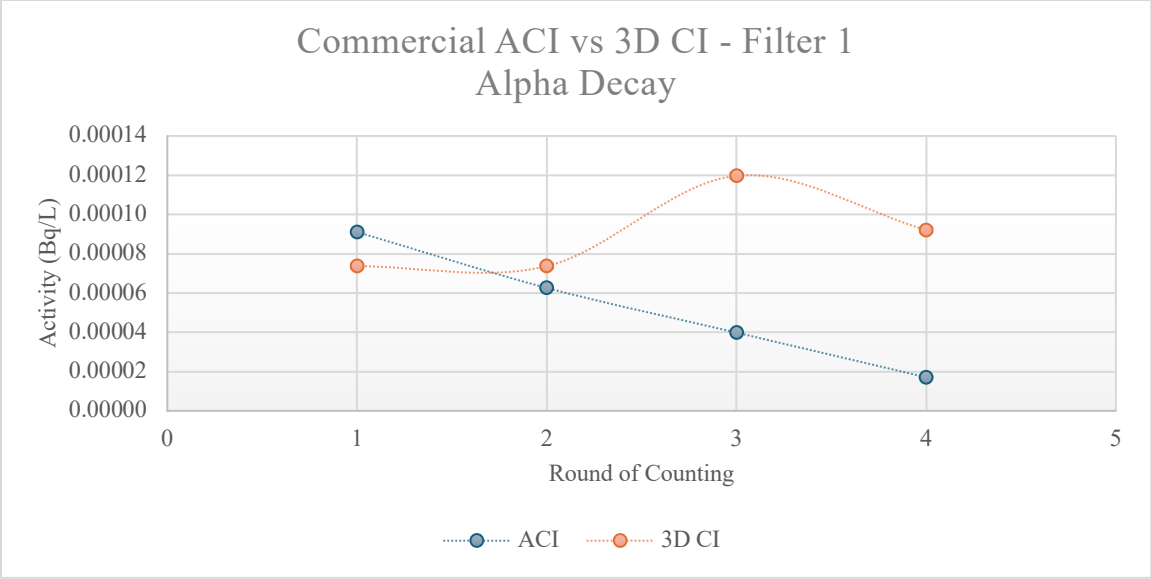

Fig 4.26: Radon Generator Filter 1 Alpha Activity Decay Curves

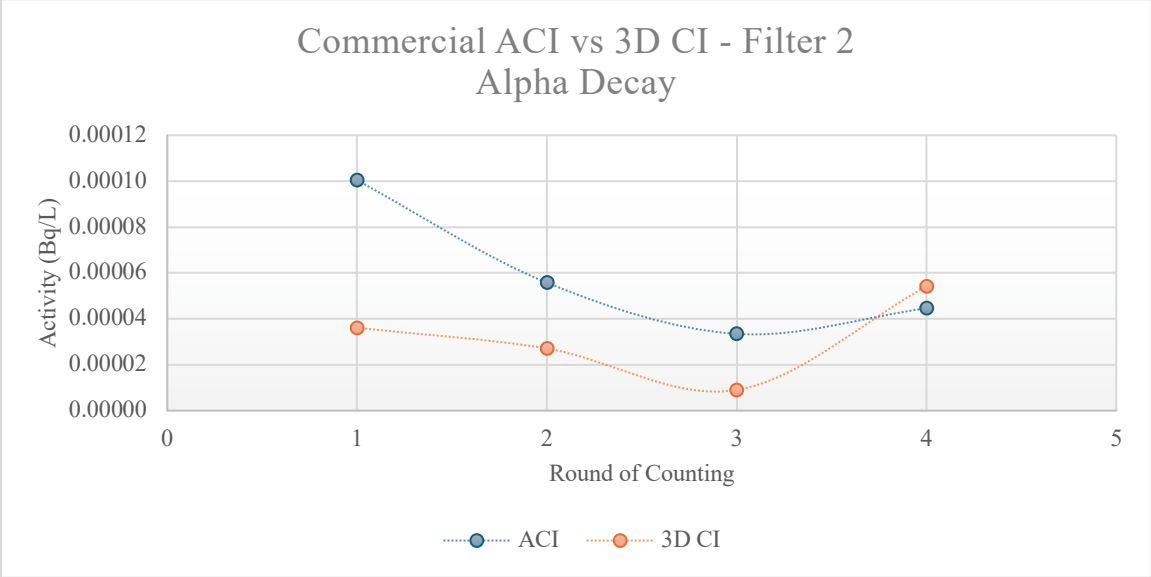

Fig 4.27: Radon Generator Filter 2 Alpha Activity Decay Curves

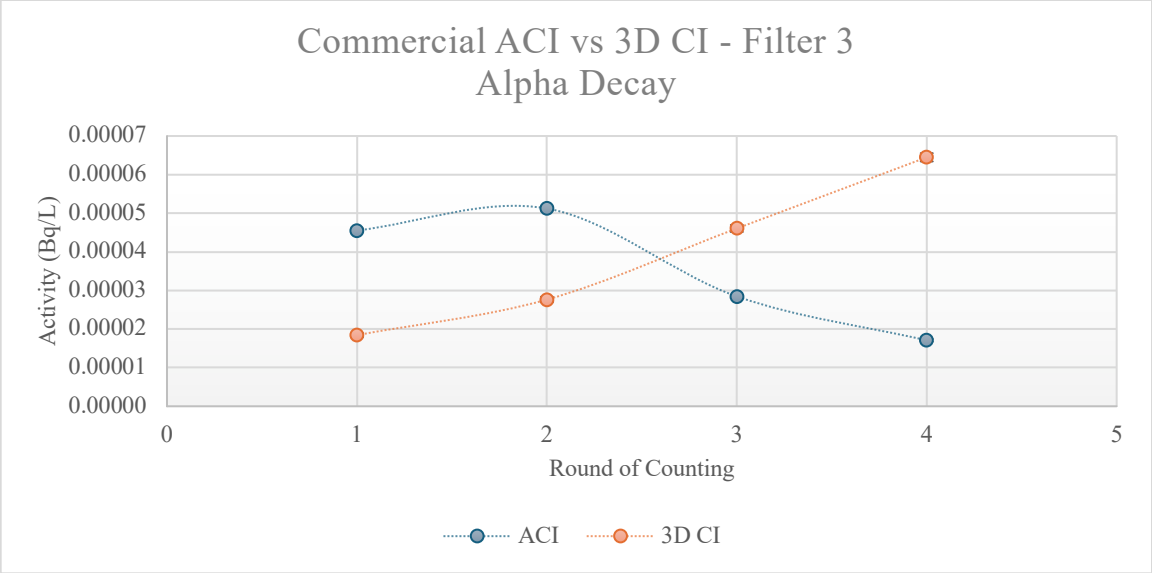

Fig 4.28: Radon Generator Filter 3 Alpha Activity Decay Curves

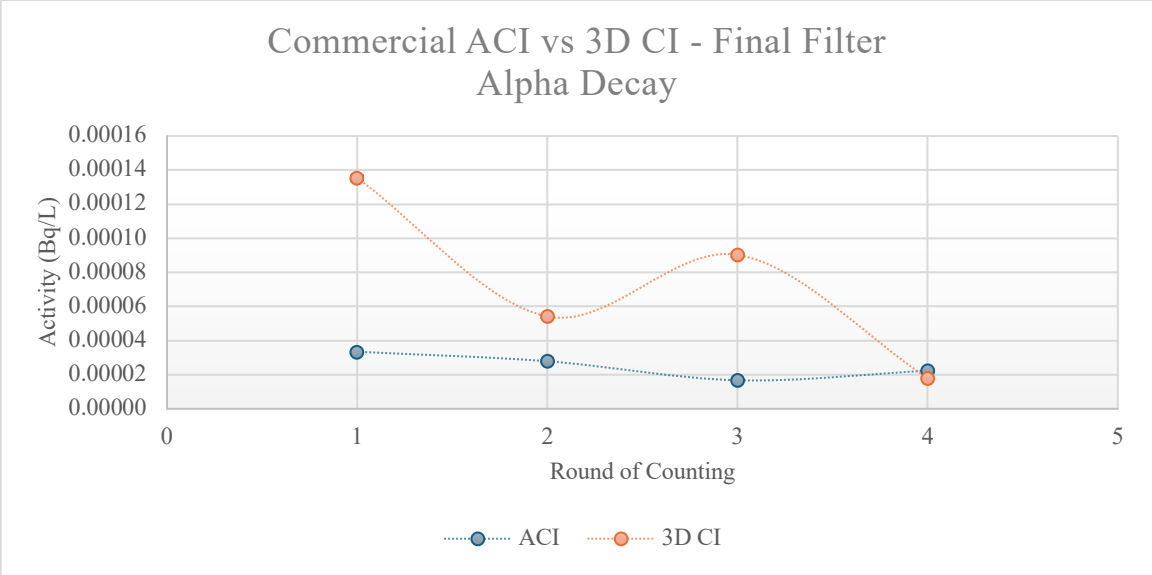

Fig 4.29: Radon Generator Final Filter Alpha Activity Decay Curves

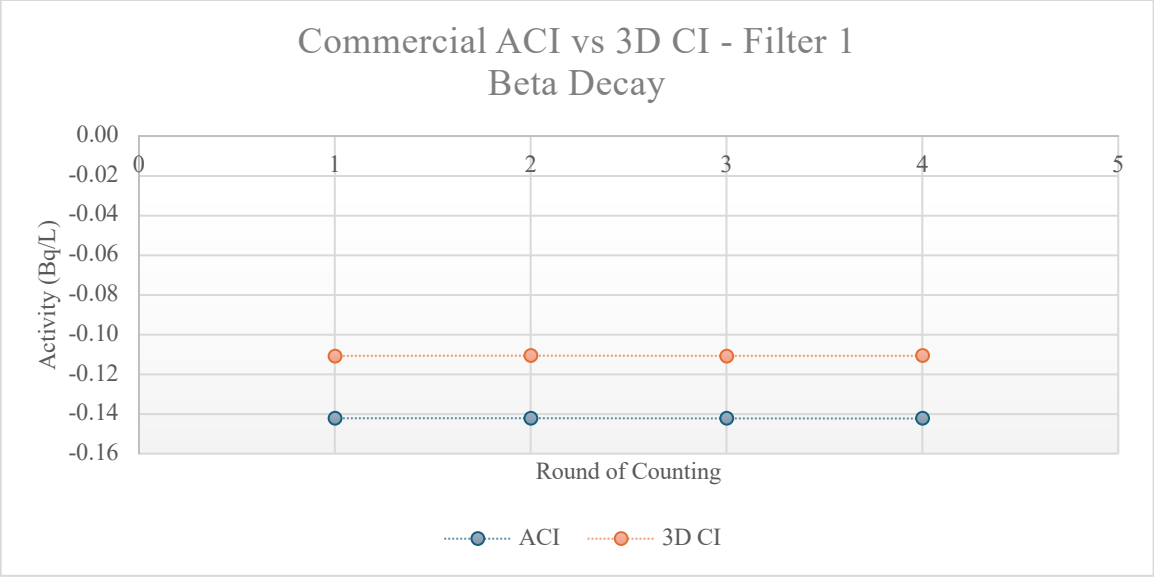

Fig 4.30: Radon Generator Filter 1 Beta Activity Decay Curves

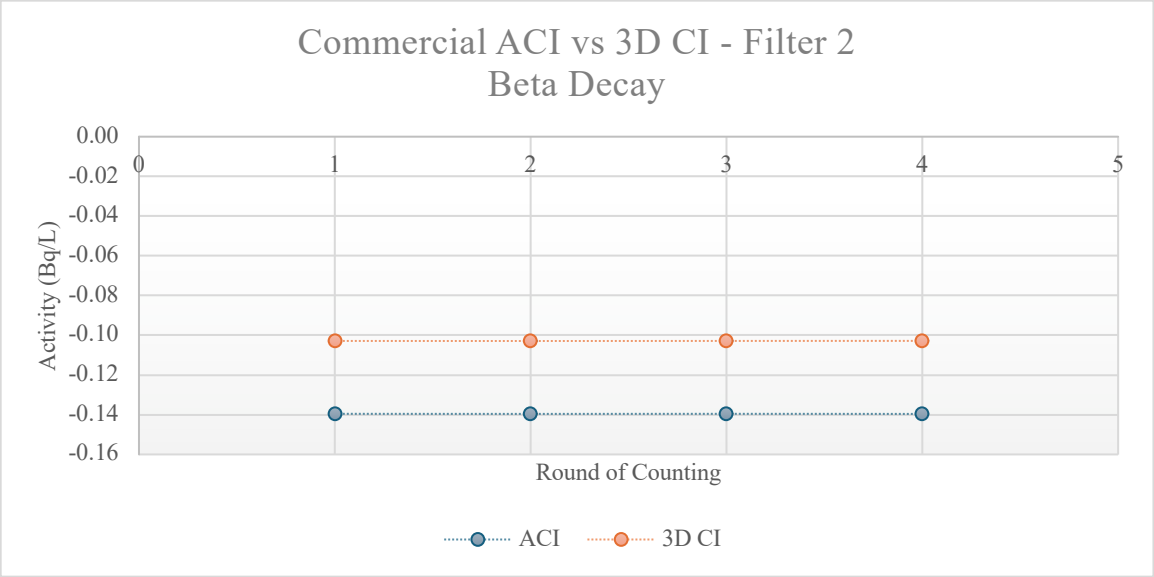

Fig 4.31: Radon Generator Filter 2 Beta Activity Decay Curves

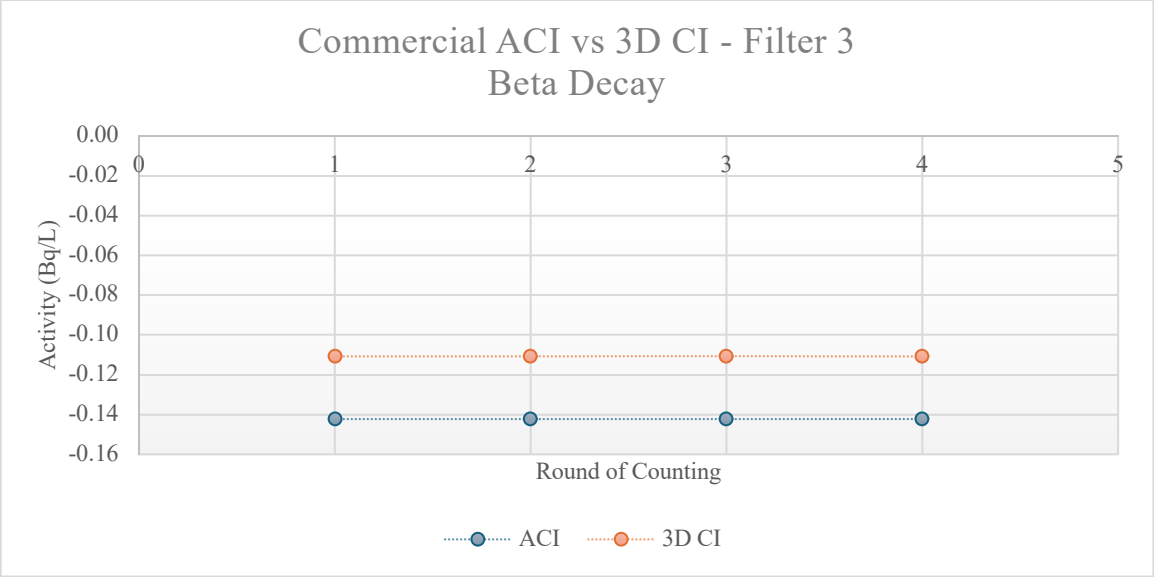

Fig 4.32: Radon Generator Filter 3 Beta Activity Decay Curves

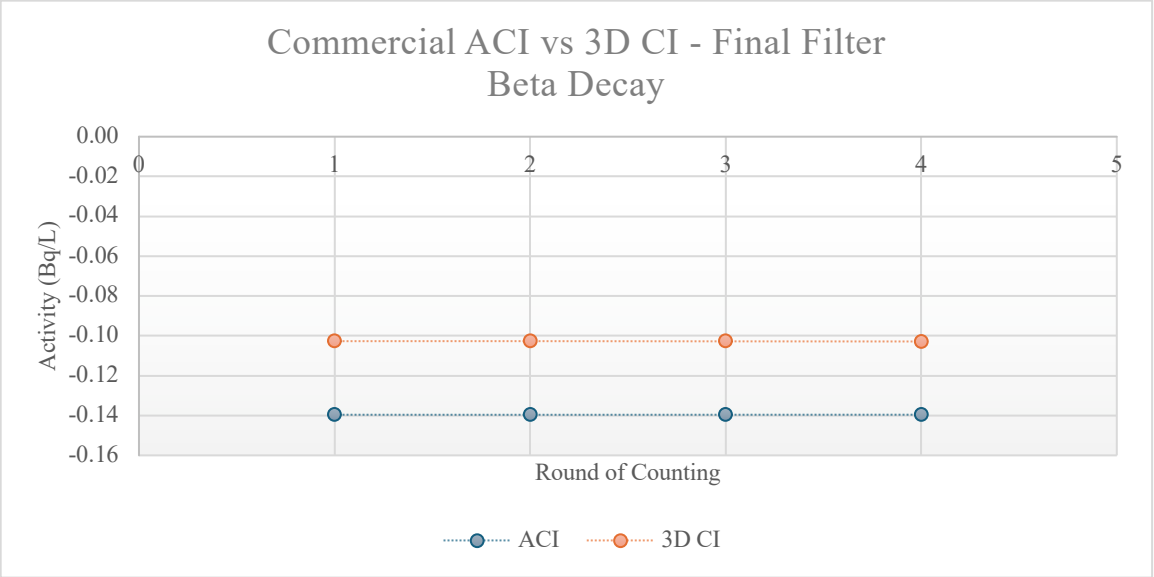

Fig 4.33: Radon Generator Final Filter Beta Activity Decay Curves

A comparison to show the activity fraction collected by each stage is shown in Table 4.6. Since many of the filters showed beta activity to be less than background, only alpha activity was compared. Alpha activity in becquerels was summed for each cascade impactor at each round of sampling. The alpha activity observed on each filter was then divided by the total alpha activity

summed for each impactor during each round of counting. Filter 6 of the ACI is the final filter of this impactor and corresponds to filter 4, the final filter, of the 3D-printed cascade impactor.

Table 4.6: Alpha Activity Fraction by Filter

ALPHA ACTIVITY FRACTION BY FILTER					
ACI			3D CI		
FILTER	ACTIVITY FRACTION	TOTAL ACT (Bq/L)	FILTER	ACTIVITY FRACTION	TOTAL ACT (Bq/L)
LUDLUM 3030E					
1	17%	-0.10102	1	27%	-0.060
2	17%		2	23%	
3	17%		3	25%	
4	17%				
5	17%				
6	16%		4	26%	
GPC ENVIRONMENTAL					
ROUND 1					
1	6%	0.76974	1	13%	0.44515
2	10%		2	4%	
3	1%		3	2%	
4	5%				
5	10%				
6	68%		4	81%	
ROUND 2					
1	9%	0.42863	1	17%	0.28481
2	9%		2	10%	
3	9%		3	10%	
4	2%				
5	11%				
6	60%		4	63%	
ROUND 3					
1	8%	0.22843	1	14%	0.35168
2	25%		2	16%	
3	4%		3	19%	
4	8%				
5	13%				
6	41%		4	51%	
ROUND 4					
1	5%	0.35326	1	21%	0.27671
2	5%		2	20%	
3	11%		3	31%	
4	19%				
5	25%				
6	35%		4	27%	
GPC RADON GENERATOR					
ROUND 1					
1	27%	0.56409	1	28%	0.27575
2	30%		2	14%	
3	14%		3	7%	
4	12%				
5	7%				
6	10%		4	51%	
ROUND 2					
1	28%	0.38282	1	40%	0.19096
2	25%		2	15%	
3	23%		3	15%	
4	10%				
5	3%				
6	12%		4	30%	
ROUND 3					
1	20%	0.33490	1	45%	0.27728

2	17%		2	3%	
3	14%		3	17%	
4	23%				
5	17%				
6	8%		4	34%	
ROUND 4					
1	10%	0.27712	1	40%	0.23932
2	27%		2	24%	
3	10%		3	28%	
4	14%				
5	24%				
6	14%		4	8%	

CHAPTER 5: DISCUSSION

This project set out to use 3D printer technology to create a functional, cost-effective, and lightweight cascade impactor that any interested person could print. While cascade impactors themselves have a variety of uses, the idea behind this research was born with a particular use in mind. If proven effective, a build-it-yourself cascade impactor and a visit to the local hardware store could yield an at-home sampling setup that can sample and separate airborne particulate by size, albeit methods to determine the presence of radioactivity would need to be resolved and planned ahead of time. If used to collect air samples downwind of the Rocky Flats Technical Plant during a wildfire or high-wind event, a setup similar to that described in this research could not only be used to determine the presence of airborne radionuclides, but a functional and well-characterized cascade impactor would indicate approximate particle size. In addition to other radionuclide characteristics, the particle size of inhaled radionuclides is an essential variable needed to perform an accurate dose assessment. Sampling near RFTP, however, is only one of many potential uses. Regardless of its use, this discussion will focus on the efficacy of a 3D-printed cascade impactor in separating particle size fractions relative to the capability of a commercial Andersen cascade impactor.

Impactor Design and Fabrication

A close look at various stages of the 3D-printed prototype under a microscope during the hole verification process hinted at the inability of the available 3D printer to print a functional cascade impactor. Commercial cascade impactors are machined to provide a smooth metal surface through each stage to maximize particle capture at each impact plate. The Raise3D model Pro3 produced a significant number of imperfections. This is evidenced by inconsistent hole diameters

within each stage and an inability to print smooth surfaces in each hole. This is clearly shown in Figures 5.1 – 5.4. An attempt to smooth out each hole was not considered due to the fragility, small diameter, and number of holes in each stage.

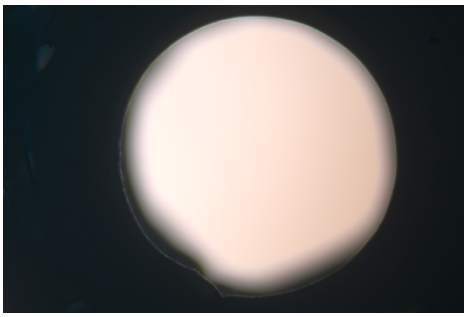

Fig 5.1: Close-up of Stage 0

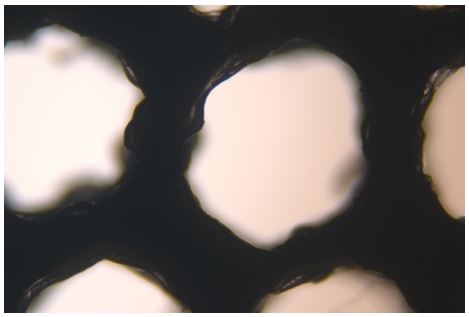

Fig 5.2: Close-up of Stage 1

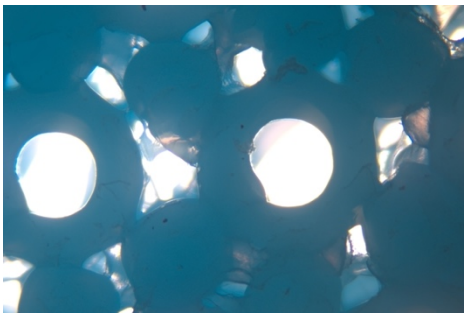

Fig 5.3: Close-up of Stage 2

Fig 5.4: Close-up of Stage 3

In addition to the rough edges of Figure 5.2, Figures 5.3 and 5.4 show oblong penetrations adjacent to each hole. These were not part of the design but a function of the print quality when attempting to print hole diameters of less than 1 mm and are believed to be print limitations on available 3D printer technology. Although secondary and tertiary prints improved the overall quality of each stage, explicitly printing "upside-down" to achieve a smooth stage inlet, resolution seems to be a limiting factor.

Overall, most of the deformities and imperfections discussed are suspected to have resulted from heat creep, a term that describes the melting of plastic filaments used in 3D printing during the printing process. This is common in fused filament fabrication (FFF) printers such as the Raise3D model Pro3 printer. To address problems with print quality, consideration should be given

to the quality of the printer used as well as the possibility of using commercial 3D printing services, such as Xometry. Expertise in 3D printing, as well as a more expensive printer, could avoid issues such as heat creep and overall issues with print resolution.

Particle Characterization

Several methods exist to characterize particle distribution in cascade impactors. The radioactive content of specific radionuclides for each impact plate and/or the change in weight of particulate collected at each stage can be compared (L'Annunziata, 2012). Only gross alpha and beta analysis was performed in this study; therefore, specific radionuclide identification was not possible. Additionally, a comparison by differences in mass collected was not performed. Relatively simple comparisons in decay curves and activity fractions in each filter were instead used as a starting point to determine the efficacy of a 3D-printed cascade impactor.

Trend analysis of alpha and beta decay curves for all filters indicated similar behavior in environmental sampling but mostly inconsistent trends when using the radon generator. The radon generator produced higher activities in most filters; still, in both sampling scenarios, activity was very low. In nearly all cases, sample collection produced less than one CPM, equating to less than one becquerel of activity on all filters counted. As a result, it is hypothesized that the outlying data points that gave the appearance of erratic data can be attributed to fluctuations in naturally occurring background radiation. The filter three comparison of environmental sampling identified the most consistent unbiased relationship in decay curves for alpha activity, Figure 4.16. Similarly, comparisons of activity fraction in like stages between the commercial ACI and 3D-printed prototype mainly yielded inconsistent results; again, fluctuations in background radiation are the suspected cause. In some cases, however, specifically during environmental sampling, large fractions of the activity were collected in the final filter for both impactors and smaller fractions

in all preceding stages. Radon generator sampling in the commercial ACI indicated a more significant fraction of activity in the early stages and a much smaller fraction captured by the final filter. Although similar results were observed in radon generator samples using the 3D-printed cascade impactor, changes between impactors were inconsistent. This is, in part, hypothesized to be due to aerosol collection in the additional stages, stages 4 and 5, in the commercial impactor that the 3D-printed model did not have.

It is important to note that radioactive aerosols are formed from the attachment of radionuclides to sub-micron airborne particles, such as dust, already present in air. Due to the construction of the radon generator, uranium-rich rocks in a plastic container, minimal amounts of airborne particles were available for the formation of radon-generated radioactive aerosols. It is hypothesized that gas deposition on the collection filters contributed to higher collection efficiencies in early stages of both cascade impactors during radon generator sampling.

Conclusion

Significant imperfections of a printed prototype indicate that a stage-to-stage comparison between a commercial and a 3D-printed cascade impactor cannot be justified. Additionally, it is unlikely that current technology is capable of printing the exact same impactor with each subsequent print. The determination of a similar decay curve between stages of both impactors in some instances as well as similar trends in activity fraction by filter, however, indicate that a functional 3D-printed cascade impactor is feasible. Individually, each printed cascade impactor would require proper characterization to determine the particle size fraction that each stage captures. In summary, the evidence outlined in this study suggests that a functional cascade impactor can be fabricated by 3D printing. Still, additional studies would be necessary to characterize particle size distribution properly.

Future Work

Design improvements were considered after the fact. For example, constructing mechanical means to hold together and compress the completed 3D-printed prototype would have eliminated the need to use painter's tape to minimize interstage leakage. Although it is unlikely that functional springs could be printed, thereby providing compression similar to that of a commercial ACI, the edges of the prototype could have been extended to allow for a clamp or nut-and-bolt assembly to compress the stages mechanically.

Following specific methods outlined by L'Annunziata (2012) could provide additional insight into characterizing a specific 3D-printed impactor. However, multiple impactors should be considered to determine if a single design and 3D printer could provide comparable data in subsequent prints. Such a study could determine that characterizing a prototype from a single design would produce the same characterized model.

The modified CAD files used in this study have been uploaded to a web-based open source library for use in future studies. These files may be accessed via the link below.

https://grabcad.com/library/modified-andersen-cascade-impactor-1

REFERENCES

Aguilar, J. (2022, February 8). Concerns raised about a Marshall-style wildfire on former Rocky Flats nuclear site. *The Denver Post.* https://www.denver7.com/news/marshall-fire/concerns-raised-about-a-marshall-style-wildfire-on-former-rocky-flats-nuclear-weapons-site

Anna, D. H. (2011). *The Occupational Environment – Its Evaluation, Control, and Management*. American Industrial Hygiene Association.

Benjamin, S. G., James, E. P., Szoke, E. J., Schlatter, P. T., & Brown, J. M. (2023). The 30 December 2021 Colorado Front Range Windstorm and Marshall Fire: Evolution of surface and 3D structure, NWP guidance, NWS forecasts, and decision support. *Weather and Forecasting*, *38*(12), 2551–2573. https://doi.org/10.1175/waf-d-23-0086.1

Carvalho, F. P., et al. (2013). Exposure to radionuclides in smoke from vegetation fires. *Science of The Total Environment*, *472*, 421–424. https://doi.org/10.1016/j.scitotenv.2013.11.073

Cheng, Y. S. (2004). Characterization of plutonium aerosol collected during an accident. *Health Physics*, *87*(6), 596–605. https://doi.org/10.1097/01.hp.0000138577.21388.a7

Claus, W. D. (1958). What is Health Physics? *Health Physics*, *1*(1), 56–61. https://doi.org/10.1097/00004032-195801000-00009

Cochran, T. B. (1996). *Overview of Rocky Flats Operations.*

Colorado Department of Public Health and Environment. (2023). *Rocky Flats - Historical Public Exposure Studies*. https://cdphe.colorado.gov/hm/rf-historical-public-exposure-studies

Colorado Department of Public Health and Environment – Hazardous Materials & Waste Management Division. (2024). *How was air quality measured? Is air quality currently monitored?* https://cdphe.colorado.gov/hm/rocky-flats-faq

Colorado Department of Public Health and Environment, Radiological Assessments Corporation. (1999, August). *Development of the Rocky Flats Plant 903 Area Plutonium Source Term. Final Report, Rev 1*.

Colorado Department of Public Safety – Division of Fire Prevention and Control. (2024). *Historical Wildfire Information*. https://dfpc.colorado.gov/sections/wildfire-information-center/historical-wildfire-information

Commodore, A. A., et al. (2012). Radioactivity in smoke particulates from prescribed burns at the Savannah River Site and at selected Southeastern United States forests. *Atmospheric Environment*, *54*, 643–656. https://doi.org/10.1016/j.atmosenv.2012.01.050

Department of Energy Government Accountability Office. (2006, July 10). *Nuclear cleanup of Rocky Flats: Doe can use lessons learned to improve oversight of other sites' cleanup activities*. GAO Report number GAO-06-352. https://www.gao.gov/assets/a250766.html

Department of Energy Office of Environment, Health, Safety, and Security - Office of Health and Safety. *The September 1957 Rocky Flats Fire: A Guide to Records Series of the Department of Energy.* https://ehss.energy.gov/ohre/new/findingaids/epidemiologic/rockyfire/intro.html

Department of Energy – Office of Legacy Management. (2020). *Rocky Flats History.* https://www.energy.gov/lm/articles/rocky-flats-site-colorado-history-documents

Evangeliou, N., Zibtsev, S., Myroniuk, V., Zhurba, M., Hamburger, T., Stohl, A., Balkanski, Y., Paugam, R., Mousseau, T. A., Møller, A. P., & Kireev, S. I. (2016). Resuspension and

atmospheric transport of radionuclides due to wildfires near the Chernobyl Nuclear Power Plant in 2015: An impact assessment. *Scientific Reports*, *6*(1). https://doi.org/10.1038/srep26062

Harrison, J.D., Fell, T., Phipps, A.W., Smith, T., Ellender, M., Ham, G., Hodgson, A., Wilkins, B.T. (2005). Health Implications of Dounreay Fuel Fragments: Estimates of Doses and Risks. Health Protection Agency, Radiation Protection Division.

Hatch, T. F. (1961). Distribution and Deposition of Inhaled Particles in Respiratory Tract. *Bacteriological Reviews, American Society for Microbiology Journals*, 25(3). https://doi.org/10.1128/br.25.3.237-240.1961

Hinds, W. C. (1982). *Aerosol Technology – Properties, Behavior, and Measurement of Airborne Particles.* John Wiley & Sons, Inc.

ICRP. (1979). Limits for Intakes of Radionuclides by Workers. ICRP Publication 30.

ICRP. (1994). Human Respiratory Tract Model for Radiological Protection. ICRP Publication 66.

ICRP. (2007). The 2007 Recommendations of the International Commission on Radiological Protection. ICRP Publication 103.

Johnson, T. E. (2017). *Introduction to Health Physics*. 5ed. McGraw Hill.

Kumar, V. (2018). *Anderson Cascade Impactor*. Free CAD Designs, Files & 3D Models | The GrabCAD Community Library. https://grabcad.com/library/anderson-cascade-impactor-1

L'Annunziata, M. F. (2012). *Handbook of Radioactive Analysis*. 3ed. Elsevier Inc.

National Archives. (2023). *Records of the Energy Research and Development Administration [ERDA]*. https://www.archives.gov/research/guide-fed-records/groups/430.html

National Park Service. (1998). *Historic American Engineering Record, Rocky Flats Plant, sheets 1 – 17.* https://www.loc.gov/pictures/resource/hhh.co0471.sheet.00002a/?co=hh

Nayak S., Ghugare P., and Vaidhun B. (2020). Evaluation of Aerodynamic Particle Size Distribution of Drugs Used in Inhalation Therapy: A Concise Review. *International Journal of Research*, 8(7), 264-271. https://doi.org/10.29121/granthaalayah.v8.i7.2020.579

NILU. (2020). *NILU Radioactivity Data Inventory*. https://radio.nilu.no/

Oak Ridge Associated Universities (ORAU) Team National Institute for Occupational Health (NIOSH). (2004, January 6). *Dose Reconstruction Project Technical Basis Document for the Rocky Flats Plant – Occupational Environmental Dose.* Document Number: ORAUT-TKBS-0011-4. https://www.cdc.gov/niosh/ocas/pdfs/arch/rocky4.pdf

Office of the Deputy Assistant Secretary of Defense for Nuclear Matters. (2020). *Nuclear Matters Handbook*.

Rademacher, S. E., Hubbell, J. L., & Cicotte, G. R. (2007). *Boeing Michigan Aeronautical Research Center (BOMARC) Missile Shelters and Bunkers Scoping Survey Workplan*. https://doi.org/10.21236/ada471460

Reed, B. C. (2014). *The History and Science of the Manhattan Project*. Springer.

Rhodes, R. (1968). *The Making of the Atomic Bomb*. Simon & Schuster, Inc.

Rocky Flats Stewardship Council. (2022, February 7). *Virtual Meeting via WebEx*. https://static1.squarespace.com/static/641cd3744417ce6ff13df850/t/64b3ff1526c7c9774f0d9c83/1689517845447/RFSC_minutes_2_7_22+FINAL.pdf

Rood, A. S., Grogan, H. A., & Till, J. E. (2002). A model for a comprehensive assessment of exposure and lifetime cancer incidence risk from plutonium released from the Rocky Flats Plant, 1953–1989. *Health Physics*, *82*(2), 182–212. https://doi.org/10.1097/00004032-200202000-00005

U.S. Department of Energy – Office of Legacy Management. (2023, August). *Rocky Flats Site, Colorado; A CERCLA/RCRA Site Fact Sheet.* https://www.energy.gov/lm/articles/rocky-flats-site-colorado-fact-sheet

U.S. Department of Energy – Office of Legacy Management. (2024). *Rocky Flats Wildland Fire Information.* https://www.energy.gov/lm/rocky-flats-wildland-fire-information

U.S. Environmental Protection Agency. (2023). *What is Radon?* https://www.epa.gov/radon/what-radon

U.S. Fish & Wildlife Service. (2023). *Rocky Flats National Wildlife Refuge*. https://www.fws.gov/refuge/rocky-flats/visit-us

Vista Technologies, NRC.(1999, January 1). *Procedure-16 Air Radiological Sampling.* https://www.nrc.gov/docs/ML9934/ML993470082.pdf

Wildfire worries dominate discussion of Rocky Flats refuge. (2022, February 12). *The Associated Press.* https://kdvr.com/news/local/rocky-flats-wildfire-meeting/

Young, Q. (2022, February 24). Fear of a Marshall Fire at Rocky Flats is real. *Colorado Newsline*. https://coloradonewsline.com/2022/02/24/fear-of-a-marshall-fire-at-rocky-flats-is-real/

Zaffos, J. (2015, January 31). Plan for a burn at Rocky Flats stirs lingering fears. *High Country News*. https://www.hcn.org/articles/nuclear-fallout-for-proposed-burn/

APPENDIX: PERMISSIONS

Many figures used in this thesis were copied from a variety of documents. Those obtained from government documents and those in the public domain were cited accordingly. Those figures which required permission for use include “with permission” or “used with permission” in the figure heading. Documents granting permission for applicable figures are included in this appendix.

Subject: RE: Request for use of Figures in Master's Thesis
Date: Thursday, March 28, 2024 at 6:56:06 AM Mountain Daylight Time
From: NIOSH OCAS (CDC)
To: Alcantar,Rich

**** Caution: EXTERNAL Sender ****

Rich,

As long as the figures are cited (referenced) appropriately, there is no issue with using any of the figures or information in the document entitled Technical Basis Document for the Rocky Flats Plant – Occupational Environmental Dose" document number: ORAUT-TKBS-0011-4. We wish you the best of luck on your Thesis.

From: Alcantar,Rich <Rich.Alcantar@colostate.edu>
Sent: Wednesday, March 27, 2024 11:53 AM
To: NIOSH OCAS (CDC) <ocas@cdc.gov>; NIOSH OCAS (CDC) <ocas@cdc.gov>
Subject: Request for use of Figures in Master's Thesis

Good day,

I am writing in regards to requesting the use of figures used in NIOSH Dose Reconstruction Project "Technical Basis Document for the Rocky Flats Plant – Occupational Environmental Dose" document number: ORAUT-TKBS-0011-4; specifically, Figures 4A-4 and 4A-7.

Figures are intended to be used in a master's thesis titled DEVELOPING METHODS TO SAMPLE POTENTIAL RESUSPENSION OF RADIOACTIVE CONTAMINANTS NEAR THE FORMER ROCKY FLATS TECHNICAL that I am authoring.

Best,
Rich Alcantar
Lieutenant Junior Grade
Medical Service Corps, United States Navy
Masters Student, Radiological Health Sciences
Environmental & Radiological Health Sciences
Colorado State University

Subject: Re: Permission Request Form [#2317]
Date: Tuesday, April 23, 2024 at 8:04:18 AM Mountain Daylight Time
From: Gumbel, Erin
To: Alcantar,Rich
CC: permissions@ametsoc.org
Attachments: Signature_04182019142534.jpg

**** Caution: EXTERNAL Sender ****

Dear Mx. Alcantar,

Thank you for your email. This signed message constitutes permission to use the material requested below.

You may include Figure 6 from Benjamin et al's 2023 WAF article in your Colorado State thesis, "DEVELOPING A METHOD TO SAMPLE POTENTIAL RESUSPENSION OF RADIOACTIVE CONTAMINANTS NEAR THE FORMER ROCKY FLATS TECHNICAL PLANT," with the following conditions:

1. Include the complete bibliographic citation of the original source.
2. Include the following statement with that citation: **© American Meteorological Society. Used with permission.**

You may also need to credit the USGS for the underlying satellite image, based on this figure's caption.

Congratulations on completing your thesis! If you have any questions or need additional information, please feel free to contact me.

Please note: If the material in an AMS journal is credited to another source, the requester must obtain permission or license from that source directly. That material may not be used without permission or license from the copyright holder.

Best,

Ms. Erin Gumbel, she/her/hers
Senior Peer Review Support Associate
Senior Permissions Specialist
egumbel@ametsoc.org
617-226-3926

ELSEVIER LICENSE
TERMS AND CONDITIONS

Apr 17, 2024

This Agreement between RICHARD ALCANTAR ("You") and Elsevier ("Elsevier") consists of your license details and the terms and conditions provided by Elsevier and Copyright Clearance Center.

License Number	5771360939296
License date	Apr 17, 2024
Licensed Content Publisher	Elsevier
Licensed Content Publication	Science of The Total Environment
Licensed Content Title	Exposure to radionuclides in smoke from vegetation fires
Licensed Content Author	Fernando P. Carvalho,João M. Oliveira,Margarida Malta
Licensed Content Date	Feb 15, 2014
Licensed Content Volume	472
Licensed Content Issue	n/a
Licensed Content Pages	4
Start Page	421
End Page	424
Type of Use	reuse in a thesis/dissertation
Portion	figures/tables/illustrations
Number of figures/tables/illustrations	1
Format	print
Are you the author of this Elsevier article?	No
Will you be translating?	No
Title of new work	DEVELOPING A METHOD TO SAMPLE POTENTIAL RESUSPENSION OF RADIOACTIVE CONTAMINANTS NEAR THE FORMER ROCKY FLATS TECHNICAL PLANT
Institution name	Colorado State University
Expected presentation date	Apr 2024
Portions	Table 1: Radionuclide concentrations of various material
Requestor Location	RICHARD ALCANTAR 5948 Manistee Ave LOVELAND, CO 80538 United States Attn: RICHARD ALCANTAR
Publisher Tax ID	98-0397604
Total	**0.00 USD**
Terms and Conditions	